

A Survey for H₂O Megamasers in Active Galactic Nuclei – II. A Comparison of Detected and Undetected Galaxies

J. A. Braatz

Department of Astronomy, University of Maryland, College Park, MD 20742

A. S. Wilson

Department of Astronomy, University of Maryland, College Park, MD 20742
and

Space Telescope Science Institute, 3700 San Martin Drive, Baltimore, MD 21218

and

C. Henkel

Max-Planck-Institut für Radioastronomie, Auf dem Hügel 69, D-53121 Bonn, Germany

ABSTRACT

A survey for H₂O megamaser emission from 354 active galaxies has resulted in the detection of 10 new sources, making 16 known altogether. The galaxies surveyed include a distance-limited sample (covering Seyferts and LINERs with recession velocities < 7000 km s⁻¹) and a magnitude-limited sample (covering Seyferts and LINERs with m_B ≤ 14.5). In order to determine whether the H₂O-detected galaxies are “typical” AGN or have special properties which facilitate the production of powerful masers, we have accumulated a database of physical, morphological, and spectroscopic properties of the observed galaxies. The most significant finding is that H₂O megamasers are detected only in Seyfert 2 and LINER galaxies, not Seyfert 1s. This lack of detection in Seyfert 1s indicates that either they do not have molecular gas in their nuclei with physical conditions appropriate to produce 1.3 cm H₂O masers or the masers are beamed away from Earth, presumably in the plane of the putative molecular torus which hides the Seyfert 1 nucleus in Seyfert 2s. LINERs are detected at a similar rate to Seyfert 2s, constituting a strong argument that at least some nuclear LINERs are AGN rather than starbursts, since starbursts have not been detected as H₂O megamasers. We preferentially detect H₂O emission from the nearer galaxies and from those which are apparently brighter at mid- and far-infrared and centimeter radio wavelengths. There is also a possible trend for the H₂O-detected galaxies to be more intrinsically luminous in nuclear 6 cm radio emission than the undetected ones, though these data are incomplete. We find evidence that Seyfert 2s with very high (N_H > 10²⁴ cm⁻²) X-ray absorbing columns of gas are more often detected as H₂O maser emitters than Seyfert 2s with lower columns. It may be that the probability of detecting H₂O maser emission in Seyfert galaxies increases with increasing column of cool gas to the nucleus, from Seyfert 1s through NLXGs to Seyfert 2s.

Subject headings: galaxies: active — galaxies: nuclei — galaxies: Seyfert — ISM: molecules — masers — radio lines: galaxies

1. Introduction

Sub-milliarcsecond VLBI mapping of the H₂O maser emission in NGC 4258 shows that the masers originate in a thin disk or annulus with inner radius 0.13 pc and outer radius 0.28 pc (Miyoshi et al. 1995). The edge-on disk is in Keplerian rotation about the (presumed) nuclear black hole and central engine, and it has a significant warp. Parts of the disk are thus illuminated by the weak, obscured nuclear X-ray source reported by Makishima et al. (1994). Heating of molecular gas by X-ray absorption has been shown to give rise to an H₂O-enhanced layer in which collisional pumping can account for the observed maser luminosity in NGC 4258 (Neufeld & Maloney, 1995).

It is not clear whether the geometry of the nuclear gas in NGC 4258 is unique or common among AGN. If many AGN have similar nuclear disks which support powerful H₂O masers, then the small number of galaxies with detected H₂O megamasers would be just those for which the nuclear disk is viewed close to edge-on. In this case, the isotropic properties of the H₂O-detected and undetected galaxies would be indistinguishable. On the other hand, it may be that some special geometrical or physical conditions, which are present only in a subset of AGN, are required to produce powerful H₂O masers. The combination of a nuclear hard X-ray source and a thin, warped molecular disk, as seen in NGC 4258, is one possibility. Another is a nuclear hard X-ray source surrounded by a thick torus, with the maser emission originating from the heated inner edge of torus, as may be the case in NGC 1068 (Greenhill et al. 1996). We might then expect to find other observable manifestations of these special conditions in the galaxies detected as H₂O megamasers.

Braatz, Wilson & Henkel (1996, hereafter [Paper I]) presented the results of a large (354 galaxies) survey of active galaxies (Seyferts, LINERs and radio galaxies) for emission from H₂O in the 6₁₆ – 5₂₃ 1.3 cm line. Ten new H₂O megamasers¹ were discovered, bringing the total number of such galaxies known to 16. The present paper describes a study based on this survey, with the goal of determining whether the galaxies which are detected in H₂O emission are similar to the general AGN population or represent a special subset. To this end, a database of photometric, morphological and spectroscopic properties of all active galaxies observed for H₂O emission has

¹In Paper I and the present paper, we adopt the arbitrary definition of an H₂O megamaser as a galaxy emitting an isotropic luminosity of $> 20 L_{\odot}$ in the 6₁₆ – 5₂₃ line.

been compiled. The galaxies in the database include the 354 galaxies observed in Paper I, the five previously known H₂O megamasers (NGC 1068, NGC 3079, NGC 4258, NGC 4945 and the Circinus galaxy) and five galaxies observed by others (M31 and M81 by Huchtmeier, Eckart & Zensus 1988; M51 (NGC 5194) and Arp 220 by Henkel, Wouterloot & Bally 1986; and NGC 5195 by Claussen & Lo 1986), for a total of 364. Table 1 lists the most important entries in the database. The primary sources of data are: the Huchra (1993) and Véron-Cetty & Véron (1991) catalogs; the Third Reference Catalog of Bright Galaxies (RC3) (de Vaucouleurs et al. 1991); the NASA Extragalactic Database (NED); and the IRAS Faint Source Catalog (Moshir et al. 1989).

Section 2 describes the galaxy samples and statistical tests used. Section 3 compares the total galaxy properties of the H₂O-detected and undetected galaxies, while Section 4 is devoted to a similar comparison for the nuclear properties. Results and conclusions are summarized in Section 5.

2. The Galaxy Samples and Statistical Tests

For the purpose of statistical analyses, we will consider several subsets of the list of observed AGN. The first, which will be referred to as the “distance-limited sample”, consists of all observed Seyferts and LINERs with $cz \leq 7000 \text{ km s}^{-1}$. The second (“sensitivity-limited sample”) includes all objects in the distance-limited sample which have been observed with an absolute sensitivity to 1.3 cm H₂O emission of better than $2 L_{\odot} (\text{km s}^{-1})^{-1}$. This sample is useful because the absolute sensitivity varies greatly from galaxy to galaxy. The limit chosen is empirical, but ensures that all galaxies with a detected narrow-line megamaser are included in the sensitivity-limited sample. The third sample (“magnitude-limited sample”) includes all objects observed from Huchra’s catalog with an apparent B magnitude brighter than or equal to 14.5. In presenting the statistical results, these samples are also occasionally divided according to activity class, i.e. Seyfert 1, Seyfert 2 and LINER. A summary of the number of galaxies in each of the various samples is given in Table 2.

In the following sections the galaxies detected in H₂O 1.3 cm emission will be compared to the undetected galaxies graphically, and statistical tests will be applied to give a quantitative assessment of the significance of any differences found. All the histograms have a similar layout, as described in the caption to Figure 2. The number of galaxies plotted in each histogram can be found in Table 3.

In evaluating the plots and results of the statistical tests, it is helpful to bear in mind the following simplified situations. If all active galaxies had similar H₂O maser luminosities, then we would tend to detect the *nearer* ones. If the ratio of the maser luminosity to the luminosities in other wavebands is similar from galaxy to galaxy (i.e. the galaxies have similar spectral shapes, but widely differing intrinsic luminosities), then we would tend to detect the *apparently brighter* (in other wavebands) ones. In a dataset with a limited number of detections, it may be difficult to

distinguish between these possibilities, since the nearer galaxies tend to be the apparently brighter. We will also search for correlations between *absolute* maser and other waveband luminosities, especially for properties which may be physically associated with the H₂O maser production. Examples of such properties might be 1.3 cm radio continuum luminosity (a source of “seed” photons) and nuclear hard X-ray luminosity (the probable source of heating of the nuclear disk). Our hope is to identify which, if any, intrinsic properties are crucial for H₂O maser production in AGN.

2.1. Description of the Statistical Tests

In comparing the physical properties of the detected and undetected galaxies, we will apply several general, nonparametric tests. When an observation results in no detection but has an upper (or lower) limit, the resulting data point is referred to as a “censored” value. A measured or calculated data point is an “uncensored” value. For example, the inclinations of the galactic disks are all uncensored, whereas the IRAS flux at 12 μm (which has only an upper limit for many galaxies) is partially censored. The Kolmogorov-Smirnov (K-S) test is used to compare distributions which contain only uncensored data. The K-S test applies to unbinned data values, so it has a higher “resolution” than the binned data plotted in the histograms. In comparing censored data, the techniques of “survival analysis” (Feigelson & Nelson, 1985) have been applied via the ASURV software package. The five statistical tests from ASURV which are used to compare the distributions are: Gehan’s generalized Wilcoxon test with permutation variance, Gehan’s generalized Wilcoxon test with hypergeometric variance, the logrank test, the Peto-Peto test, and the Peto-Prentice test. These tests are generalizations of standard techniques based on ranking the data values and comparing the distributions of the ranks. They differ from one another primarily in the way that censored data points are weighted in the computation of the test statistic. All of the weightings are valid, and the prevailing wisdom says to consider all results and use caution when the reported statistical significances are vastly different. The Peto-Prentice test has been shown to be particularly effective when comparing samples with dissimilar sizes, as we have here for the H₂O-detected and undetected galaxies. The tests from the ASURV package are valid for uncensored data as well as censored, though for completely uncensored data the Peto-Peto test reduces to the logrank test and the Peto-Prentice method reduces to Gehan’s test.

The result of each statistical test is a significance value which describes the probability that one parent population would produce the two samples. In Table 3, these probabilities are listed for each parameter, mostly for the distance-limited sample. A probability of 0.05 or smaller is often taken to be indicative of a meaningful difference in the distributions. A probability of greater than 0.10 indicates there is little evidence that the parent distributions are different. Probability values of less than about 0.01 are not well defined for nonparametric tests involving small samples.

2.2. Distribution in Space

Figure 1 shows the location in Galactic coordinates for each source observed. The data are plotted in an Aitoff projection so that equal areas on the plot represent equal areas on the sky. The zone of avoidance through the Galactic plane is evident. Fewer than 6% of all the observed galaxies are found between Galactic latitudes -15° and 15° , an area which covers more than a quarter of the total sky. The distribution of observed galaxies is not dominated by individual clusters – for example, only 10 galaxies from the Virgo cluster are included.

A histogram of the recession velocity of observed galaxies is shown in Figure 2. The galaxies detected in H₂O emission tend towards smaller recession velocities (i.e. they are closer) than undetected galaxies in the distance- and magnitude-limited samples. The probability that the distributions of recession velocities of the H₂O-detected and undetected galaxies in the distance-limited sample are different is 91.4% from the K-S test, and $\geq 99\%$ from the other tests (Table 3). Thus there are certainly more galaxies with H₂O emission than we have found, but they are simply too distant to detect at our sensitivity. As might be expected, the distribution of detected galaxies does follow that of the sensitivity-limited sample.

2.3. Completeness

For galaxies within a few hundred Mpc ($z \lesssim 0.1$), evolutionary and cosmological effects are minimal, so it is reasonable to assume that Seyfert and LINER galaxies within this region are uniformly distributed in space. Given this presumed uniformity, it is clear that AGN catalogs are incomplete to the distance and magnitude limits chosen for our observations, and this incompleteness is reflected in our samples (any cosmological evolution with the number of active galaxies increasing towards larger distance strengthens this conclusion). Furthermore, a number of known AGNs were not observed because of telescope scheduling limitations. In addition to the 5 galaxies mentioned in Paper I which have either $cz < 7000 \text{ km s}^{-1}$ or $m_B < 14$, we did not observe 20 galaxies with $14.0 < m_B < 14.5$ from the Huchra catalog. Because we *have* observed 20 galaxies from this last range of magnitudes, we choose to use the limiting magnitude of 14.5 rather than 14 in our magnitude-limited sample.

A common test for sample completeness is the V/V_{max} test. This procedure was devised by Schmidt (1968) as a test for uniform spatial distribution in quasar samples. If it is known beforehand that a sample of objects is uniformly distributed in space, then the V/V_{max} test can be applied to check for completeness. The procedure works as follows: for each source in the sample, a sphere, S , is defined with a radius equal to the distance from the Earth to the source. The volume of S is given by $V = \frac{4}{3}\pi r^3$, where r is the distance to the source. A second sphere, S_{max} , is defined with a radius r_{max} equal to the maximum distance the source could have and

still be a member of the sample. For example, in a sample selected by the single criterion of being closer than the distance corresponding to a recessional velocity of 7000 km s⁻¹, the radius of S_{max} would be $r_{max} = 7000 \text{ km s}^{-1} / H_0$. For a sample selected only by having magnitude brighter than $m_B = 14.5$, the radius would be $r'_{max} = r \times 10^{(14.5-m_B)/5}$, where m_B is the apparent magnitude of the galaxy and r its distance. The values of V/V_{max} for a uniformly distributed sample of galaxies are expected to have a uniform distribution between 0 and 1, and the mean value $\langle V/V_{max} \rangle = 0.5$. Figure 3 shows the value of $\langle V/V_{max} \rangle$ as a function of recession velocity for the distance-limited sample, assuming that V_{max} is determined only by the recession velocity limit of 7000 km s⁻¹. Figure 4 shows $\langle V/V_{max} \rangle$ as a function of magnitude for the magnitude-limited sample, assuming that V_{max} is determined only by the magnitude limit of $m_B = 14.5$. The real situation is clearly more complex, with the degree of completeness of the two samples being limited by both magnitude and distance, which are not independent quantities, and other parameters discussed below. It is, nevertheless, clear that both samples are incomplete, with $\langle V/V_{max} \rangle = 0.25 \pm 0.02$ for the distance-limited sample and $\langle V/V_{max} \rangle = 0.27 \pm 0.02$ for the magnitude-limited sample. The drop-off from the expected galaxy counts at larger distances is also evident in Figure 2, in which the number of galaxies in each velocity bin would grow quadratically with increasing distance for a uniform and complete sample. Figures 3 and 4 also show the values of $\langle V/V_{max} \rangle$ for each AGN class individually. The degree of incompleteness is similar for Seyfert 1 and 2 galaxies, but the LINERs are not as well represented at large distances or at faint magnitudes. LINER nuclei have weaker emission lines than Seyferts, and the high quality, starlight-subtracted spectra required to distinguish this nuclear emission from that of the surrounding starlight are only available for nearby galaxies.

The completeness of the samples is primarily determined by the methods and sensitivities used in surveys for AGN. Other factors which contribute to incompleteness include (a) the increasing difficulty of detecting point-like Seyfert nuclei with increasing distance (starlight contamination increases with distance for a fixed aperture size), (b) obscuration in and near the Galactic plane (zone of avoidance), and (c) the difficulty of detecting Seyfert nuclei in highly inclined galaxies because of obscuration by the galactic disk. The last effect is well known (e.g. Keel 1980) and is illustrated for our samples in Figure 5, where the observed distribution of galactic inclinations for the distance-limited sample is compared to that for a group of randomly oriented thin disks. The distribution of thin disks is normalized such that the number of disks with inclinations $i < 45^\circ$ is equal to the number of galaxies in the distance-limited sample with $i < 45^\circ$. Disregarding incompleteness of the galaxies in the subset of the distance-limited sample with $i < 45^\circ$, we find that there are ~ 110 galaxies which are omitted from the distance-limited sample because of internal obscuration by the galactic disk. The figure shows an apparent underrepresentation of galaxies in the $10^\circ - 30^\circ$ range and an overabundance of galaxies in the $30^\circ - 40^\circ$ range, which may indicate a systematic error in the measurement of axial ratios, perhaps influenced by the presence of bars or disturbed systems.

3. Properties of the Galaxy

3.1. B Magnitude

Figures 6 and 7 show the distributions of apparent and absolute total (i.e. galaxy plus nucleus) B magnitudes for the H₂O-detected and undetected galaxies. The integrated m_B magnitudes are primarily taken from RC3 and are not corrected for galactic extinction. The detected galaxies tend to be brighter than the undetected ones in the distance- or magnitude-limited samples (with $\sim 90\%$ confidence – see Table 3). However, there is no difference between the distributions of the detected galaxies and those undetected in the sensitivity-limited sample. The difference in apparent brightness between the detected and undetected galaxies in the distance- and magnitude-limited samples is therefore best understood as a sensitivity issue, as discussed previously in connection with the recession velocities of the samples. When the Seyfert 1 galaxies (which are all undetected in H₂O maser emission – see Section 4.1) are left out of the calculation, the difference in the detected and undetected galaxies’ apparent brightness becomes slightly more significant (Table 3).

The absolute magnitudes (M_B) of the galaxies were calculated using “face-on” apparent magnitudes corrected for internal and Galactic extinction (from RC3). The distribution of detected galaxies is not unusual compared to the undetected ones (Figure 7), although the results given in Table 3 show a weak tendency for the maser-detected galaxies to be of lower luminosity. These calculations (but not the figure) include 51 galaxies from the distance-limited sample which do not have magnitude corrections available for internal and Galactic extinction, but do have upper limits to M_B determined from uncorrected apparent magnitudes. The absence of maser detections in Seyfert 1 galaxies does not account for the weak tendency of H₂O-detected galaxies to be intrinsically fainter than undetected ones. Table 3 shows the test results comparing detected galaxies with only undetected Seyfert 2’s and LINERs, and the marginal difference in the population persists at about the same confidence level ($\sim 88\%$) as when all undetected galaxies (including Seyfert 1’s) are included.

3.2. Morphological Type

The distribution of Hubble stage index is shown in Figure 8. The index, T , as described in RC3, gives a numerical assignment to the large-scale galactic morphology, from elliptical galaxies on the left ($T = -5$ or -4), to lenticulars ($-3 \leq T \leq -1$), and early- to late-type spirals ($0 \leq T \leq 7$) on the right. The values $T = 8$ and $T = 9$ are used to describe galaxies with only a hint of spiral structure, $T = 90$ represents irregular galaxies, and $T = 99$ is reserved for peculiar galaxies. The distribution of T among the detected galaxies is indistinguishable from that of the undetected ones (Table 3).

3.3. Inclination

The inclination i of each galactic disk was calculated from the axial ratio b/a according to $i = \sin^{-1} \sqrt{[1 - (b/a)^2]/0.96}$ (e.g. Whittle, 1992). During earlier stages of this survey, there was a trend for the detected megamasers to prefer highly inclined host galaxies (Braatz, Wilson & Henkel, 1995). A histogram of inclination angles for the current sample is shown in Figure 9. The addition of the recently discovered masers in IC 1481 and NGC 5347, which have modest inclinations, decreases the probability that the masers come from a more highly inclined parent distribution than the undetected galaxies. The probability that the detected galaxies have higher inclinations than the undetected ones is in the range 80% – 94 %, depending on which test is used (Table 3). Despite the marginal character of this difference, the substantial fraction of masers in inclined galaxies (7 of the 14 galaxies with detected megamasers and meaningful inclinations have $i > 67^\circ$) merits some discussion.

Maiolino & Rieke (1995, hereafter MR95) have analyzed a magnitude-limited sample of Seyfert galaxies to study, among other things, the relation of Seyfert type to disk inclination. MR95 give special consideration to intermediate Seyfert classifications (i.e. 1.2, 1.5, 1.8, 1.9). They provide evidence that Seyferts with the intermediate classifications 1.8 or 1.9 favor highly inclined galaxies, and they suggest that these nuclei may be type 1 Seyferts which are obscured by a 100 pc-scale torus in the galactic disk rather than the nuclear torus, which is probably randomly oriented with respect to the galactic disk (Ulvestad & Wilson 1984b; Wilson & Tsvetanov 1994). Indeed, three galaxies with detected H₂O megamasers are included in MR95's sample as type 1.9 Seyferts (NGC 2639, NGC 4258, and NGC 5506) and five other megamasers are included as type 2 Seyferts (in this paper we classify NGC 2639 and NGC 4258 as LINERs, not Seyferts). Because classifications into the intermediate types are not available or are contradictory for many of the galaxies in our sample, we have opted to list only the basic classification (i.e. type 1, 2, or LINER). The breakdown of inclinations by Seyfert types for the distance-limited sample is shown in Figure 10. Seyfert 1 galaxies are mildly underrepresented at high inclinations: $\frac{10}{43} = 23\%$ of Seyfert 1s with meaningful inclination values have $i > 70^\circ$, compared to $\frac{33}{105} = 31\%$ of Seyfert 2s and $\frac{20}{54} = 37\%$ of LINERs. To determine the impact of this effect on the statistical results, we have also compared the inclinations of the H₂O-detected galaxies to only Seyfert 2 and LINER undetected galaxies. The results are essentially the same as when the undetected Seyfert 1 galaxies are included (Table 3).

If the total gain in extragalactic H₂O maser sources were *dominated* by amplification in gas associated with the 100 pc-scale torus of MR95 or other molecular clouds in the galactic disk, we might expect the total or peak observed maser power to be correlated with the galaxy inclination. Figure 11 shows the isotropic total maser luminosity of each detected source plotted as a function of the galactic inclination. The maser luminosities are taken from Table 2 of Paper I and are plotted with a nominal uncertainty of 25%. Measured luminosities are subject to calibration uncertainties, intrinsic variability, and especially the unknown beaming factor which corrects the

inferred “isotropic luminosity” to the true luminosity. Clearly the plot should be interpreted cautiously; regardless, it shows no trends. The peak luminosities, obtained from the peak fluxes given in Table 2 of Paper I, are plotted against the inclination in Figure 12, with nominal 50% uncertainties. Again, no correlation is evident.

A compelling argument against maser amplification in the disk of the galaxy has been that the masers are very compact and associated only with the nucleus (e.g. Claussen & Lo 1986; Haschick et al. 1990). If maser amplification occurred in the disk of the host galaxy, both extended and compact nuclear radio continuum emission could be amplified, so the observed maser emission would tend to trace the nuclear 1.3 cm radio continuum structure. Recently, Gallimore et al. (1996) have discovered weak H₂O maser components in NGC 1068 located $\sim 0.3''$ (20 pc) from the “true” nucleus, and coincident with the brightest 1.3 cm radio continuum peak. It seems unlikely that these masers receive significant amplification from disk gas since NGC 1068 is fairly face-on ($i \simeq 29^\circ$). Gallimore et al. (1996) suggest that the nonnuclear masers are associated with a shock front which excites the ambient molecular gas.

In conclusion, if the possible trend for detected H₂O megamasers to occur preferentially in highly inclined galaxies is confirmed by larger samples, amplification by gas coplanar with the galaxy disk would be implied. The 100 pc-scale torus proposed by MR95 is one candidate, although it is not clear whether such a large structure could be heated to the temperatures of > 300 K at which water is abundant (Neufeld, Lepp & Maloney 1995). An alternative source of amplification could be a molecular cloud, heated by starlight, along the line of sight to the nucleus (Haschick & Baan 1990).

3.4. Mid- and Far-Infrared Properties

The Infrared Astronomical Satellite (IRAS) mapped 98% of the celestial sphere at wavelengths of 12, 25, 60, and 100 μm . Active galaxies are known to be powerful IR sources, and in many cases the mid-IR emission of an AGN dominates its energy output and is an excellent indicator of its bolometric luminosity. Still, the detailed processes which determine the IR properties of AGN are poorly understood. The emission at mid-IR wavelengths (12 and 25 μm) are strongly related to the active nucleus, and are believed to result from reprocessing of more energetic photons by dust near the central engine. The far-IR emission (60 and 100 μm), on the other hand, can be a tracer of dust heated in star forming regions. Ongoing star formation is often seen in active galaxies and so may contribute to the far-IR luminosity. Henkel, Wouterloot & Bally (1986) have found that the presence of extragalactic H₂O masers appears to be correlated with the 100 μm flux densities and the S(60)/S(100) and S(12)/S(25) color temperatures in a sample of bright IRAS galaxies. However, only two (NGC 1068 and NGC 3079) are megamasers, with the rest being associated with galaxies undergoing active star formation.

Histograms of flux and power for all 4 IRAS bands are shown in Figures 13 – 20. Most of the H₂O-detected galaxies fall within the normal range of IR flux, though a few are unusually bright. The statistical difference between detected and undetected galaxies in apparent IR brightness at 12 μm and 25 μm is the most significant of all total galaxy properties compared, with the detected galaxies being brighter at > 99% confidence level (Table 3). The maser-detected galaxies are brighter at 60 and 100 μm as well, though the significance is marginal at 100 μm . In IR power, the distribution of the detected galaxies closely follows that of the undetected ones in the magnitude- and distance-limited samples. Thus, the higher apparent IR brightness of the detected galaxies may result, at least in part, from them being nearer than the undetected galaxies.

Because the IRAS properties of Seyfert 1s, Seyfert 2s and LINERs are different (e.g. Miley, Neugebauer & Soifer 1985), it is instructive to see IR properties differentiated by AGN class. The IRAS fluxes at 25 μm and 60 μm for the distance-limited sample are shown in Figure 21 with different AGN classes plotted with different symbols. The LINERs are noticeably “cooler”, on average, than the Seyfert galaxies at these wavelengths (in the distance-limited sample, $\langle \frac{S(25)}{S(60)} \rangle = 0.14 \pm 0.02$ for LINERs, 0.33 ± 0.03 for Seyfert 2s, and 0.37 ± 0.04 for Seyfert 1s). The detected galaxies tend to follow the run of their class, but three Seyfert 2s (NGC 4945, NGC 1068, and the Circinus galaxy) and two LINERs (NGC 3079 and NGC 4258) are unusually bright. This is consistent with the conclusion above that the detected H₂O masers tend to be the apparently brightest galaxies at all IRAS bands.

A color-color diagram is shown in Figure 22 for the distance-limited sample, with the ratio $S(12)/S(25)$ plotted on the abscissa and the ratio $S(60)/S(100)$ on the ordinate. The far-IR color is particularly sensitive to the presence of foreground Galactic “cirrus” emission, which can cause artificially small values of $S(60)/S(100)$. The H₂O detected galaxies are all in areas relatively free of the cirrus emission. The entire sample follows a pattern in which galaxies with cooler mid-IR colors have warmer far-IR colors. Normal galaxies follow this pattern as well (e.g. Helou 1986). The AGN classes can be statistically separated in this figure, with the Seyfert 2s being the coolest at short IR wavelengths, the LINERs being the coolest at long wavelengths, and the Seyfert 1s spread through the middle ground. (For galaxies in the distance-limited sample, $\langle \frac{S(12)}{S(25)} \rangle$ is 0.61 ± 0.08 , 0.39 ± 0.02 and 0.75 ± 0.05 , and $\langle \frac{S(60)}{S(100)} \rangle$ is 0.53 ± 0.04 , 0.66 ± 0.03 and 0.35 ± 0.02 for Seyfert 1, Seyfert 2 and LINER galaxies, respectively.) The maser-detected galaxies again follow their class and are unremarkable for the most part. However, two detected galaxies (ESO 103-G35 and Mrk 1210) stand out as having very warm far-IR colors. Both of these galaxies are weak 60 μm and 100 μm sources with uncertainties in $\log S(60)/S(100)$ much larger than the other sources plotted. For ESO 103-G35 $\log S(60)/S(100) = 0.34 \pm 0.13$, and for Mrk 1210 $\log S(60)/S(100) = 0.16 \pm 0.08$. Notwithstanding these uncertainties, the colors are reliably warmer than the other plotted galaxies. Warm colors in the far-IR are sometimes used to identify galaxies with ongoing starbursts or an AGN, with the infrared emission originating in dust heated by hot stars or the AGN (e.g. Rowan-Robinson and Crawford 1989). The mid-IR colors of ESO 103-G35 and Mrk 1210 are not unusual for the Seyfert 2 population. A histogram showing the distribution

of the S(60)/S(100) ratio is shown in Figure 23. The maser-detected galaxies tend to have larger S(60)/S(100) ratios than the undetected galaxies at a significance level of $\sim 98\%$ (Table 3). When the detected and undetected distributions of only Seyfert 2 and LINER galaxies are considered, the significance level remains at $\sim 98\%$ (Table 3). The difference in far-IR color is thus not influenced by the absence of H₂O maser detections in Seyfert 1 galaxies. However, the significance level is reduced (78%) and the effect marginal when only the Seyfert 2s are included.

In Figure 24, the ratio S(25)/S(60) is plotted against the power in the 25 μm band for the distance-limited sample. The general trend for both H₂O-detected and undetected galaxies is for the color to become warmer as the IR power increases. The LINERs again tend to be intrinsically weaker and cooler than the Seyferts. The color of the maser-detected galaxies shows considerable dispersion, with two being particularly warm (Mrk 1210 and ESO 103-G35 – the same galaxies as were unusually warm in the S(60)/S(100) ratio) and two being unusually cool (NGC 3079 and NGC 4945). The megamaser galaxy NGC 1052 is the warmest of all observed LINERs. Nevertheless, the detected galaxies, as a group, are not strongly associated with warm S(25)/S(60) IRAS ratios (Table 3). A histogram showing the distribution of S(25)/S(60) for the detected and undetected galaxies in the distance-limited sample is shown in Figure 25. In summary, the galaxies detected as H₂O masers tend to be the apparently brightest at mid- and far-infrared wavelengths and to have unusually warm far-infrared colors.

4. Nuclear properties

4.1. AGN Class

The most striking trend from our survey is that no Seyfert 1s were detected. Ten of the masers are found in Seyfert 2 galaxies and six are in LINERs (including the galaxy TXFS 2226-184 (Koekemoer et al. 1995), which is not a member of the samples discussed in this paper). The fraction of H₂O-detected LINERs in the distance-limited sample – 0.075 ($\frac{5}{67}$) – and magnitude-limited sample – 0.079 ($\frac{5}{63}$) – is similar to that of Seyfert 2s – 0.071 ($\frac{10}{141}$) and 0.071 ($\frac{8}{112}$), respectively. However, the LINERs in our sample tend to be closer than the Seyfert 2s. The fraction of detected Seyfert 2s in the sensitivity-limited sample – 0.14 ($\frac{10}{73}$) – is thus somewhat larger than, but comparable to, that of LINERs – 0.096 ($\frac{5}{52}$).

The detected fraction of Seyfert 2s and LINERs together are 0.072 ± 0.019 ($\frac{15}{208}$), 0.074 ± 0.021 ($\frac{13}{175}$) and 0.069 ± 0.018 ($\frac{15}{215}$) in the distance-limited, magnitude-limited, and combined distance- and magnitude-limited samples, respectively. If Seyfert 1s have the same detection probabilities, the random chances of detecting 0 out of the 57 (distance-limited), 54 (magnitude-limited), and 70 (combined distance- and magnitude-limited) samples are only $0.014^{+0.030}_{-0.010}$, $0.015^{+0.035}_{-0.011}$, and $0.006^{+0.018}_{-0.005}$, respectively. This difference in detection rates cannot be ascribed to a larger mean

distance to the Seyfert 1s, which are located at the same mean distance (53.0 ± 3.2 Mpc) as the Seyfert 2s (52.9 ± 1.9 Mpc) for the distance-limited sample, though the LINERs in the distance-limited sample are nearer (37.3 ± 3.0 Mpc), as mentioned earlier. These statistics show that the incidence of detectable H₂O megamasers in Seyfert 1 galaxies is much smaller than in Seyfert 2s and LINERs.

The absence of detections in Seyfert 1 galaxies indicates either that these galaxies do not have molecular gas with appropriate conditions to mase, or that the masers in these galaxies are beamed away from our line of sight. The first possibility would violate the strongest version of the unified scheme, in which the populations of Seyfert 1s and 2s are identical except for angle of view. It might, however, be consistent with scenarios in which Seyfert 2s evolve into 1s or vice versa (e.g. Miller 1995). Turning to the second possibility, Seyfert 2 galaxies are thought to contain Seyfert 1 nuclei obscured by a pc-scale thick disk or torus (e.g. Antonucci 1993). A reasonable scenario is that the masers originate in gas associated with the torus and are beamed in its plane. VLBA observations of NGC 4258 (Miyoshi et al. 1995) show that the masers are found in a thin edge-on disk, so if other H₂O megamasers have a similar structure, our detection of only type 2 Seyferts indicates that the thick torus and thin disk tend to be coplanar. One possibility is that the thick torus and thin disk occupy the same radial range from the nucleus, with the gas density in the thick torus increasing towards the central plane. Another possibility is that the thin disk is nearer to the nucleus than the torus. The thin disk might then flare out with increasing distance from the nucleus and gradually transform into a thick disk. Recent high resolution observations of NGC 1068 (Greenhill et al. 1996) suggest that some maser emission is associated with the inner edge of the torus.

4.2. Nuclear V Magnitude

It is difficult to make statistical conclusions based on optical photometric properties of AGN because there is no data set available which measures only the nonstellar nuclear component of the V band emission. Both Huchra and Véron-Cetty & Véron list V magnitudes which are taken with small aperture measurements (i.e. $\lesssim 15''$) when available. For a given aperture size and nuclear luminosity, the fractional unwanted contribution from stars in the host galaxy is a function of the galaxy's distance. The accumulation of data from a number of different surveys with varying apertures also complicates the picture. Nonetheless, it is useful to check the distribution of nuclear magnitudes using the available data. The magnitudes were taken from the Huchra catalog when given there, otherwise the values were taken from the Véron-Cetty & Véron catalog.

Figures 26 and 27 show the distributions of apparent and absolute “nuclear” V magnitude. There is no significant difference between the maser-detected and undetected galaxies.

4.3. Radio Flux and Luminosity

The radio emission from Seyfert and LINER galaxies is, in general, weak and often dominated by the circumnuclear (100 pc – kpc scale) regions. To ensure that only small-scale (\lesssim kpc) flux is considered, VLA data at 6 cm with the A and B configurations are considered exclusively (e.g. Unger et al., 1987; Ulvestad & Wilson, 1984a, 1984b, 1989). Such radio measurements are available for 25% of the distance-limited sample. Radio fluxes at 1.3 cm (the wavelength of the $6_{16} - 5_{23}$ H₂O transition) are available for even fewer sources, and are not directly addressed here. Although about 10% of Seyferts have a flat radio spectrum nuclear source at centimeter wavelengths (probably due to synchrotron self-absorption), the majority are steep spectrum sources with spectral index $\alpha \simeq 0.7$ between 6 cm and 20 cm, where $S \propto \nu^{-\alpha}$ (e.g. Ulvestad & Wilson, 1984b). We shall use the 6 cm flux and luminosity as indicators of nuclear radio continuum output.

Figures 28 and 29 show histograms of the total nuclear radio flux and power at 6 cm. The radio fluxes of the H₂O-detected galaxies are stronger than the undetected ones at the $\sim 95 - 98\%$ confidence level (Table 3). The radio power of the detected sources may be stronger as well, but with weaker (<92%) statistical significance (Table 3). The statistics are limited by the small number of detected masers with nuclear radio continuum fluxes.

The observed H₂O maser emission might result from amplification of a 1.3 cm nuclear radio source. Such amplification can only occur if the “seed” source of radio continuum radiation is behind and smaller than the masering clouds. If the masers arise in a parsec-scale region or smaller (e.g. Miyoshi et al. 1995) then any radio flux spatially resolved by the VLA cannot contribute to the seed emission; only an unknown fraction of the unresolved radio flux is relevant. For example, the best VLA resolution at 6 cm is $\sim 0.4''$, which corresponds to a linear scale of ~ 20 pc (much larger than the expected scale of the maser emission) for a galaxy at a distance of 10 Mpc.

The source of the compact radio luminosity in Seyfert galaxies is not fully understood, but an interesting clue is that when the compact structure is resolved, it is seen as a linear or jet structure in most cases (Ulvestad & Wilson, 1984b). Such a jet is believed to be collimated by the accretion disk, so the possible trend for masers to be associated with more powerful radio continuum sources may indicate that the masers are related to currently active accretion and jet formation.

4.4. [OIII] Flux and Luminosity

Nuclear [OIII] fluxes for the observed galaxies were compiled primarily from Dahari & De Robertis (1988), Ho, Filippenko & Sargent (1993), Oliva et al. (1994), Stauffer (1982), and Whittle (1992). No corrections have been made for extinction, as this is often unknown.

The distributions of [OIII] $\lambda 5007$ fluxes and luminosities are shown in Figures 30 and 31. Because [OIII] is excited primarily by the nuclear ultraviolet continuum, it can be used as a measure of the power of the AGN at those wavelengths. Large-aperture [OIII] measurements are used when available; otherwise smaller aperture measurements are listed. Unfortunately, [OIII] $\lambda 5007$ fluxes are available for only eight maser-detected galaxies. Nevertheless, the available data show that the H₂O-detected galaxies are well distributed among the range of [OIII] luminosity (and flux), suggesting the UV output of the AGN is not an important parameter for H₂O maser production (cf. Table 3).

A plot of the [OIII]/H β ratio against the [OIII] luminosity for each class of AGN in the distance-limited sample is shown in Figure 32. The three classes occupy distinct regions of this plot, with the LINERs being systematically weakest in [OIII] luminosity, and Seyfert 2s having larger [OIII]/H β ratios than Seyfert 1s (the H β flux of which includes both narrow and broad components). The detected galaxies occupy typical locations on this diagram. The two H₂O-detected LINERs plotted in Figure 32 seem to have higher [OIII] luminosities than the undetected LINER galaxies, but two other LINERs have low values (the log of the [OIII] $\lambda 5007$ luminosity is 40.5 for NGC 4258, and 40.0 for NGC 3079) but are not plotted because they lack a reliable nuclear H β measurement.

4.5. X-ray Properties

Details of the pumping mechanism for H₂O megamasers are not yet understood, but the association of megamasers with AGN suggests that the nonstellar nuclear emission is the ultimate energy source. Neufeld, Maloney & Conger (1994) present a model in which the X-ray source in the AGN heats the nuclear gas, giving rise to a molecular layer in which powerful, collisionally-pumped H₂O masers can exist. In their model, the true luminosity of the maser increases in proportion to the area of gas illuminated by the X-ray source. Neufeld & Maloney (1995) show that this X-ray heating model fits the observations of the masing disk in NGC 4258 (Miyoshi et al. 1995), and they suggest the possibility of even more powerful masers based on reasonable X-ray parameters.

Observations of hard (2 – 10 keV) X-rays have so far been reported in nine of the maser-detected galaxies. In NGC 1068 the observed 2 – 10 keV X-ray luminosity is only $1.4 \pm 0.5 \times 10^{41}$ erg s $^{-1}$ (Koyama et al. 1989, corrected to $H_0 = 75$ km s $^{-1}$ Mpc $^{-1}$), which may be understood as the reflected component of a nuclear X-ray source with an intrinsic luminosity of $10^{43} - 10^{44}$ erg s $^{-1}$ (Koyama et al. 1989) and which is completely obscured by a column of $\gtrsim 10^{25}$ cm $^{-2}$ (e.g. Mulchaey, Mushotzky & Weaver 1992). The Circinus galaxy also exhibits a reflection-dominated X-ray spectrum (Matt et al. 1996). Matt et al. (1996) estimate the X-ray luminosity of the hidden nucleus to be $\sim 4 \times 10^{41}/(\Omega/2\pi)$ erg s $^{-1}$ (Ω being the solid angle subtended at the nucleus by the reflecting matter), and the absorbing column at $> 10^{24}$ cm $^{-2}$. The estimated 2 – 10 keV

luminosities (corrected for absorption) and the equivalent hydrogen column densities inferred from the X-ray spectra are listed in Table 4, and plotted against the observed maser luminosities in Figures 33 and 34, respectively. No trends are apparent in either of these diagrams.

Awaki (1996) has summarized ASCA results from a sample of 17 Seyfert 2 galaxies selected according to [OIII] brightness, polarized broad line detection and previous X-ray observations. Figure 2 in Awaki (1996) shows the distribution of absorbing column for this sample plus 5 additional ASCA-observed Seyfert 2 galaxies, and we have reproduced this diagram as Figure 35 here. Twenty one out of the 22 ASCA-observed Seyfert 2 galaxies were included in our H₂O maser survey (the unobserved galaxy is NGC 6552). Five out of these 21 are H₂O-detected galaxies, and they are shaded in Figure 35. It is interesting to note that, among galaxies in this sample, 3 of the 5 which have been searched for H₂O maser emission and have $\log N_H > 10^{24} \text{ cm}^{-2}$ are maser-detected sources, while only 2 of the 16 with $\log N_H < 10^{24}$ have been detected as H₂O sources. A 2×2 contingency table with these results gives a χ^2 of 4.7, indicating that, among this sample, the masers are found in sources with larger column densities at a significance level of 97%. This result suggests that H₂O megamaser emission in Seyfert 2s is preferentially associated with galaxies having high X-ray absorbing columns. The non-detection of Seyfert 1 galaxies in H₂O maser emission may then be understood in terms of their lack of a large column of cool gas along the line of sight to the nucleus. We caution, however, that this possible association between H₂O megamaser emission and high X-ray column may be subject to selection effects. For example, the three galaxies with $N_H > 10^{24} \text{ cm}^{-2}$ and detected in H₂O emission (NGC 1068, NGC 4945 and the Circinus galaxy) are amongst the nearest of the sample of galaxies searched for H₂O emission; it may be that detection of the reflected component of hard X-rays is only possible in the nearest Seyfert 2s. It is hoped that ASCA observations will be available for the remaining seven H₂O-detected sources in the near future, and will allow further investigation of the relationships between H₂O maser and hard X-ray emission.

5. Results and Conclusions

The strongest effect that we have identified is that H₂O emission is only found in Seyfert 2s and LINERs. No H₂O emission is detected from Seyfert 1s. The detection rates of Seyfert 2s and LINERs are similar; this finding constitutes a strong argument that at least some nuclear LINERs are AGNs rather than starbursts. The lack of detections of Seyfert 1s indicates that either they do not have molecular gas in their nuclei with physical conditions appropriate to produce H₂O masers, or the masers are beamed away from Earth. Our result is completely consistent with the notion that the masers are beamed in the plane of the thick nuclear torus postulated to hide the Seyfert 1 nucleus in Seyfert 2 galaxies.

With good confidence ($> 95\%$), we also preferentially detect H₂O emission from the nearer galaxies and from those which are apparently brighter at mid-infrared (12 and 25 μm), far-infrared

($60 \mu m$), and short centimeter radio (6 cm) wavelengths, and have warm far-infrared IRAS colors. At somewhat lower confidence level ($\sim 90\%$), we find H₂O emission preferentially from galaxies more luminous in 6 cm radio emission.

The general tendency to detect nearer and apparently brighter galaxies is in accordance with general astronomical expectations (cf. Section 2). The strong tendency to detect the apparently brightest galaxies at mid-infrared ($12 \mu m$ and $25 \mu m$) wavelengths, where most of the nuclear bolometric luminosity of Seyfert 2s may be emitted, suggests a correlation between H₂O megamaser and nuclear bolometric luminosities. Further, the tendency to detect galaxies with warm far-infrared IRAS colors suggests that galaxies with nuclear far-infrared emission dominant over disk emission tend to be more easily detectable.

The most significant correlation of H₂O maser detectability with an intrinsic luminosity is that with nuclear centimeter wavelength radio power. As the radio continuum emission is generally extended on the hundreds pc scale, it is unlikely that this correlation simply reflects one between maser luminosity and “seed” photon availability. Radio jets and lobes are one of the best indicators of current nuclear activity in Seyfert 2s and the relationship with maser emission may just reflect a mutual dependence on the level of current activity. Alternatively, a distinct physical process may be involved. For example, radio ejecta are undoubtedly associated with shocks and it is possible that the shock-heated gas may favor H₂O maser emission.

There is a trend for H₂O megamaser emission in Seyfert 2s to be preferentially associated with galaxies exhibiting a very high X-ray absorbing column ($N_H > 10^{24} \text{ cm}^{-2}$). Our data are consistent with the notion that the probability of detecting H₂O maser emission from Seyfert galaxies increases with increasing column of cool gas to the nucleus, from Seyfert 1s through NLXGs to Seyfert 2s.

We have made extensive use of the NASA/IPAC Extragalactic Database (NED) which is operated by the Jet Propulsion Laboratory, California Institute of Technology, under contract with the National Aeronautics and Space Administration. We thank Eric Feigelson for assistance with statistical analysis and for providing the ASURV Rev. 1.2 software (LaValley, Isobe & Feigelson 1992) which implements the methods presented in Feigelson & Nelson (1985). We also thank Kim A. Weaver for valuable discussions on X-ray properties. This research was supported by NASA through grants NAGW-3268, HST GO grant 3724 and by NSF through grant AST-9527289. C.H. acknowledges support from NATO grant SA.5-2-05 (CRG. 960086) 318/96.

REFERENCES

- Antonucci, R.R.J. 1993, ARA&A, 31, 473
- Awaki, H. 1996, to be published in “Emission Lines in Active Galaxies: New Methods and Techniques,” IAU Colloquium No. 159, Eds. B.M. Peterson, F-Z. Cheng & A.S. Wilson (San Francisco: Astronomical Society of the Pacific)
- Braatz, J.A., Wilson, A.S., & Henkel, C., 1995, in Proceedings of the Oxford Torus Workshop, Ed. M.J. Ward, 77
- Braatz, J.A., Wilson, A.S., & Henkel, C., 1996, ApJS, 106, 51 (Paper I)
- Claussen, M.J., & Lo, K.-Y. 1986, ApJ, 308, 592
- Dahari, O. & De Robertis, M.M. 1988, ApJS, 67, 249
- de Vaucouleurs, G., de Vaucouleurs, A., Corwin Jr., H.G., Buta, R., Paturel, G., & Fouqué, P. 1991, Third Reference Catalog of Bright Galaxies (Springer-Verlag: New York)
- Feigelson, E.D. & Nelson, P.I. 1985, ApJ, 293, 192
- Gallimore, J.F., Baum, S.A., O’Dea, C.P., Brinks, E. & Pedlar, A. 1996, ApJ, 462, 740
- Greenhill, L.J., Gwinn, C.R., Antonucci, R.R.J. & Barvainis, R. 1996, ApJ Letters (in press)
- Haschick, A.D. & Baan, W.A. 1990, ApJ, 355, L23
- Haschick, A.D., Baan, W.A., Schnepps, M.H., Reid, M., Moran, J.M. & Güsten, R. 1990, ApJ, 356, 149
- Helou, G. 1986, ApJ, 311, L33
- Henkel, C., Wouterloot, J.G.A. & Bally, J. 1986, A&A, 155, 193
- Ho, L., Filippenko, A. & Sargent, W.L.W. 1993, ApJ, 417, 63
- Huchra, J.P. 1993, private communication
- Huchtmeier, W.K., Eckart, A. & Zensus, A.J. 1988, A&A, 200, 26
- Iwasawa, K., Koyama, K., Awaki, H., Kunieda, H., Makishima, K., Tsuru, T., Ohashi, T. & Nakai, N. 1993, ApJ, 409, 155
- Keel, W. 1980, AJ, 85, 198
- Koekemoer, A.M., Henkel, C., Greenhill, L.J., Dey, A., van Breugel, W., Codella, C., & Antonucci, R. 1995, Nature, 378, 697
- Koyama, K., Inoue, H., Tanaka, Y., Awaki, H. & Takano, S. 1989, PASJ, 41, 731
- LaValley, M.P., Isobe, T. & Feigelson, E.D. 1992, BAAS, 24, 839
- Maiolino, R. & Rieke, G.H. 1995, ApJ, 454, 95
- Makishima, K., Fujimoto, R., Ishisaki, Y., Kii, T., Loewenstein, M., Mushotzky, R., Serlemitsos, P., Sonobe, T., Tashiro, M. & Yaqoob, T. 1994, PASJ, 46, L77

- Matt, G., Fiore, F., Perola, G.C., Piro, L., Fink, H.H., Grandi, P., Matsuoka, M., Oliva, E. & Salvati, M. 1996, MNRAS, 281, L69
- Miley, G.K., Neugebauer, G. & Soifer, B.T. 1985, ApJ, 293, L11
- Miller, J.S. 1995, Proc. N.A.S., 92, 11422
- Miyoshi, M., Moran, J., Herrnstein, J., Greenhill, L., Nakai, N., Diamond, P., & Inoue, M. 1995, Nature, 373, 127
- Moshir, M. et al. 1989, Explanatory Supplement to the IRAS Faint Source Survey (Pasadena: JPL)
- Mulchaey, J.S., Mushotzky, R.F. & Weaver, K.A. 1992, ApJ, 390, L69
- Neufeld, D.A., Lepp, S. & Maloney, P.R. 1995, ApJS, 100, 132
- Neufeld, D.A. & Maloney, P.R. 1995, ApJ, 447, L17
- Neufeld, D.A., Maloney, P.R., & Conger, S. 1994, ApJ, 436, L127
- Oliva, E., Salvati, M., Moorwood, A.F.M., Marconi, A. 1994, A&A, 288, 457
- Rowan-Robinson, M. & Crawford, J. 1989, MNRAS, 238, 523
- Schmidt, M. 1968, ApJ, 151, 393
- Serlemitsos, P., Ptak, A. & Yaqoob, T. 1996, in “The Physics of Liners in View of Recent Observations,” ASP Conference Series, 103, 70
- Stauffer, J.R. 1982, ApJ, 262, 66
- Tully, R.B. 1988, Nearby Galaxies Catalog (Cambridge University Press: New York)
- Turner, T.J. & Pounds, K.A. 1989, MNRAS, 240, 833
- Ulvestad J.S. & Wilson, A.S. 1984a, ApJ, 278, 544
- Ulvestad J.S. & Wilson, A.S. 1984b, ApJ, 285, 439
- Ulvestad J.S. & Wilson, A.S. 1989, ApJ, 343, 659
- Unger, S.W., Lawrence, A., Wilson, A.S., Elvis, M. & Wright, A.E. 1987, MNRAS, 228, 521
- Véron-Cetty, M.P., & Véron, P. 1991, E.S.O. Sci. Rep. 10
- Whittle, M. 1992, ApJS, 79, 49
- Wilson, A.S. & Tsvetanov, Z.I. 1994, AJ, 107, 1227

Table 2

Sample (1)	Properties of the Statistical Samples							
	Total (2)	Seyfert 1 (3)	Seyfert 2 (4)	LINER (5)	Unspecified (6)	Huchra (7)	Véron (8)	Both (9)
Detected Masers	15	0	10	5	0	13	12	11
Magnitude-limited	241	54	112	63	12	186	206	152
Distance-limited	278	57	141	67	13	207	238	168
Sensitivity-limited	165	30	73	52	10	127	147	110
All in above samples	299	70	149	67	13	226	255	183

Note. — All 15 maser-detected galaxies are included in the distance- and sensitivity-limited samples, but only 13 are included in the magnitude-limited sample, Mrk 1 and ESO 103-G35 being too faint. The columns show (1) the sample, (2) the total number of galaxies for that sample (note that one maser-detected galaxy – TXFS 2226-184 – is not in any of our samples), (3) the number of Seyfert 1 galaxies, (4) the number of Seyfert 2 galaxies, (5) the number of LINERs, (6) the number of AGNs included which have no detailed classification available, (7) the number from the Huchra catalog, (8) the number from the Véron & Véron-Cetty catalog, and (9) the number common to both the Huchra and Véron & Véron-Cetty catalogs.

Table 4

Hard X-ray Observations of H ₂ O Megamaser Galaxies			
Source	N _H (cm ⁻²)	L _X ^a (erg s ⁻¹)	Ref ^b
NGC 1068	> 10 ²⁵	10 ⁴³ - 10 ⁴⁴	1
NGC 1386	5 ± 3 × 10 ²³	-	2
Mrk 1210	1.1 ± 0.8 × 10 ²³	-	2
NGC 3079	1.6 ^{+2.4} _{-1.6} × 10 ²²	5.8 × 10 ⁴⁰	3
NGC 4258	1.5 ± 0.2 × 10 ²³	4 ± 1 × 10 ⁴⁰	4
NGC 4945	5.4 ± 0.5 × 10 ²⁴	1 × 10 ⁴²	5
Circinus	> 10 ²⁴	4 × 10 ⁴¹ - 4 × 10 ⁴³	6
NGC 5506	2.8 ± 0.5 × 10 ²²	1.7 × 10 ⁴³	7
ESO 103-G35	1.35 ^{+.33} _{-.23} × 10 ²³	3.3 × 10 ⁴³	7

^a2 – 10 keV luminosity, corrected for photoelectric absorption.

^b(1) Koyama et al. (1989); (2) Awaki (1996); (3) Serlemitsos et al. (1996); (4) Makishima et al. (1994); (5) Iwasawa et al. (1993); (6) Matt et al. (1996); (7) Turner & Pounds (1989)

Figure 1. The positions of all observed galaxies are plotted in Galactic coordinates using the Aitoff projection. Equal areas on this plot correspond to equal areas on the sky. Galaxies detected in H₂O are shown as filled circles, undetected galaxies which are a member of either the distance- or magnitude-limited sample are represented by diamonds, and other undetected galaxies are shown as squares. The Galactic center is at the origin in the middle of the plot.

Figure 2. The distribution of recession velocity for the detected and undetected galaxies are compared. The undetected galaxies in the sensitivity-limited sample are represented by the dark shaded region. They make up a subset of the undetected galaxies in the distance-limited sample, which are represented by the lighter shaded region. The undetected galaxies in the magnitude-limited sample are plotted as filled triangles. These data are scaled according to the left axis. The detected galaxies are represented by vertical bars, and they are plotted using the magnified scale shown on the right axis. The entire set of observed galaxies (detected and undetected) is represented by the open squares, and are plotted according to the scale on the left axis. All histograms in this chapter follow a scheme similar to this one.

Figure 3. The values of $\langle V/V_{max} \rangle$ are plotted as a function of recession velocity for galaxies in the distance-limited sample. The open markers show $\langle V/V_{max} \rangle$ for the individual AGN classes, according to the legend, and the filled squares show the complete distance-limited sample.

Figure 4. The values of $\langle V/V_{max} \rangle$ are plotted as a function of B magnitude for galaxies in the magnitude-limited sample. The open markers show $\langle V/V_{max} \rangle$ for the individual AGN classes, according to the legend, and the filled squares show the complete magnitude-limited sample.

Figure 5. The distribution of galactic inclinations for the distance-limited sample is compared to the inclinations of randomly oriented thin disks.

Figure 6. The distributions of the integrated apparent magnitude, m_B , of the detected and undetected galaxies are compared. Magnitudes are not corrected for Galactic or internal extinction.

Figure 7. The distributions of the integrated absolute magnitude, M_B , of the detected and undetected galaxies are compared. Magnitudes are calculated from the apparent face-on magnitude, corrected for Galactic and internal extinction.

Figure 8. The distributions of Hubble stage index for the detected and undetected galaxies are compared. The definition and values of T are taken from RC3.

Figure 9. The distributions of inclination (in degrees) of the detected and undetected galaxies are compared. Elliptical galaxies ($T \leq -3$) are omitted from this histogram.

Figure 10. The distribution of inclination (in degrees) is shown for the three AGN classes individually. The vertical bars represent the detected galaxies and the lines show the distributions for undetected galaxies in the distance-limited sample. Elliptical galaxies ($T \leq -3$) are omitted from this histogram.

Figure 11. Isotropic maser luminosity (in L_{\odot}) is plotted against galactic inclination (in degrees). The luminosities plotted here are representative values taken from Table 2 of Paper I and are assigned a nominal uncertainty of 25%. The elliptical galaxy NGC 1052 is not included in this figure.

Figure 12. A representative peak maser luminosity (in $L_{\odot}(kms^{-1})^{-1}$) is plotted against inclination (in degrees) for each of the detected galaxies. The luminosities are calculated from the peak maser fluxes listed in Table 2 of Paper I. Peak maser luminosities, being extremely variable, are plotted with arbitrary 50% error bars. The elliptical galaxy NGC 1052 is not included in this figure.

Figure 13. The distributions of the $12 \mu m$ flux, $S(12)$ (in Jy), from IRAS for the detected and undetected galaxies are compared.

Figure 14. The distributions of the $12 \mu m$ power, $P(12)$ (in $W Hz^{-1}$), from IRAS for the detected and undetected galaxies are compared.

Figure 15. The distributions of the $25 \mu m$ flux, $S(25)$ (in Jy), from IRAS for the detected and undetected galaxies are compared.

Figure 16. The distributions of the $25 \mu m$ power, $P(25)$ (in $W Hz^{-1}$), from IRAS for the detected and undetected galaxies are compared.

Figure 17. The distributions of the $60 \mu m$ flux, $S(60)$ (in Jy), from IRAS for the detected and undetected galaxies are compared.

Figure 18. The distributions of the $60 \mu m$ power, $P(60)$ (in $W Hz^{-1}$), from IRAS for the detected and undetected galaxies are compared.

Figure 19. The distributions of the $100 \mu m$ flux, $S(100)$ (in Jy), from IRAS for the detected and undetected galaxies are compared.

Figure 20. The distributions of the $100 \mu m$ power, $P(100)$ (in $W Hz^{-1}$), from IRAS for the detected and undetected galaxies are compared.

Figure 21. The log of the $60 \mu m$ flux is plotted against the log of the $25 \mu m$ flux for all galaxies detected at both 25 and $60 \mu m$ in the distance-limited and H_2O maser detected samples. AGN classes are differentiated according to the symbols defined in the legend.

Figure 22. The far-IR color $S(60 \mu m)/S(100 \mu m)$ is plotted against the mid-IR color $S(12 \mu m)/S(25 \mu m)$ for each galaxy in the distance-limited sample and for each galaxy with detected H_2O megamaser emission.

Figure 23. The distributions of the $S(60 \mu m)/S(100 \mu m)$ IRAS flux ratio for the detected and undetected galaxies are compared.

Figure 24. The IR color $S(25 \mu m)/S(60 \mu m)$ is plotted against the power in the $25 \mu m$ IRAS band (in $W \text{ Hz}^{-1}$) for each galaxy in the distance-limited sample and for the H_2O detected galaxies.

Figure 25. The distributions of the $S(25 \mu m)/S(60 \mu m)$ IRAS flux ratio for the detected and undetected galaxies are compared.

Figure 26. The distributions of small aperture ($\lesssim 15''$) measurements of apparent V magnitude for the detected and undetected galaxies are compared.

Figure 27. The distributions of absolute nuclear V magnitude for the detected and undetected galaxies are compared. The magnitudes have been calculated from small aperture ($\lesssim 15''$) measurements.

Figure 28. The distributions of the log of the nuclear 6 cm radio flux (in mJy) for the detected and undetected galaxies are compared.

Figure 29. The distributions of the log of the nuclear 6 cm radio power (in $W \text{ Hz}^{-1}$) for the detected and undetected galaxies are compared.

Figure 30. The distributions of the log of the [OIII] $\lambda 5007$ flux (in $\text{erg cm}^{-2} \text{ s}^{-1}$) for the detected and undetected galaxies are compared.

Figure 31. The distributions of the log of the [OIII] $\lambda 5007$ luminosity (in erg s^{-1}) for the detected and undetected galaxies are compared.

Figure 32. The ratio [OIII] $\lambda 5007/H\beta$ is plotted against the [OIII] $\lambda 5007$ luminosity (in erg s^{-1}) for the maser-detected galaxies and galaxies in the distance-limited sample.

Figure 33. The X-ray luminosity in the $2 - 10 \text{ keV}$ band (in erg s^{-1}) is plotted against the isotropic maser luminosity (in L_\odot) for the six maser-detected galaxies with available hard X-ray luminosities.

Figure 34. The equivalent hydrogen column density N_H (in cm^{-2}), determined by model fits to the X-ray spectrum, is plotted against the isotropic maser luminosity (in L_\odot) for the nine maser-detected galaxies with available column densities.

Figure 35. The data for this histogram of column densities N_H (in cm^{-2}) of ASCA-observed Seyfert 2 galaxies is taken from Awaki (1996). We have shaded the H_2O maser-detected sources. The arrow (and bin separation at $\log N_H = 24$) indicates that all sources with $N_H > 10^{24} \text{ cm}^{-2}$ are plotted in the rightmost bin.

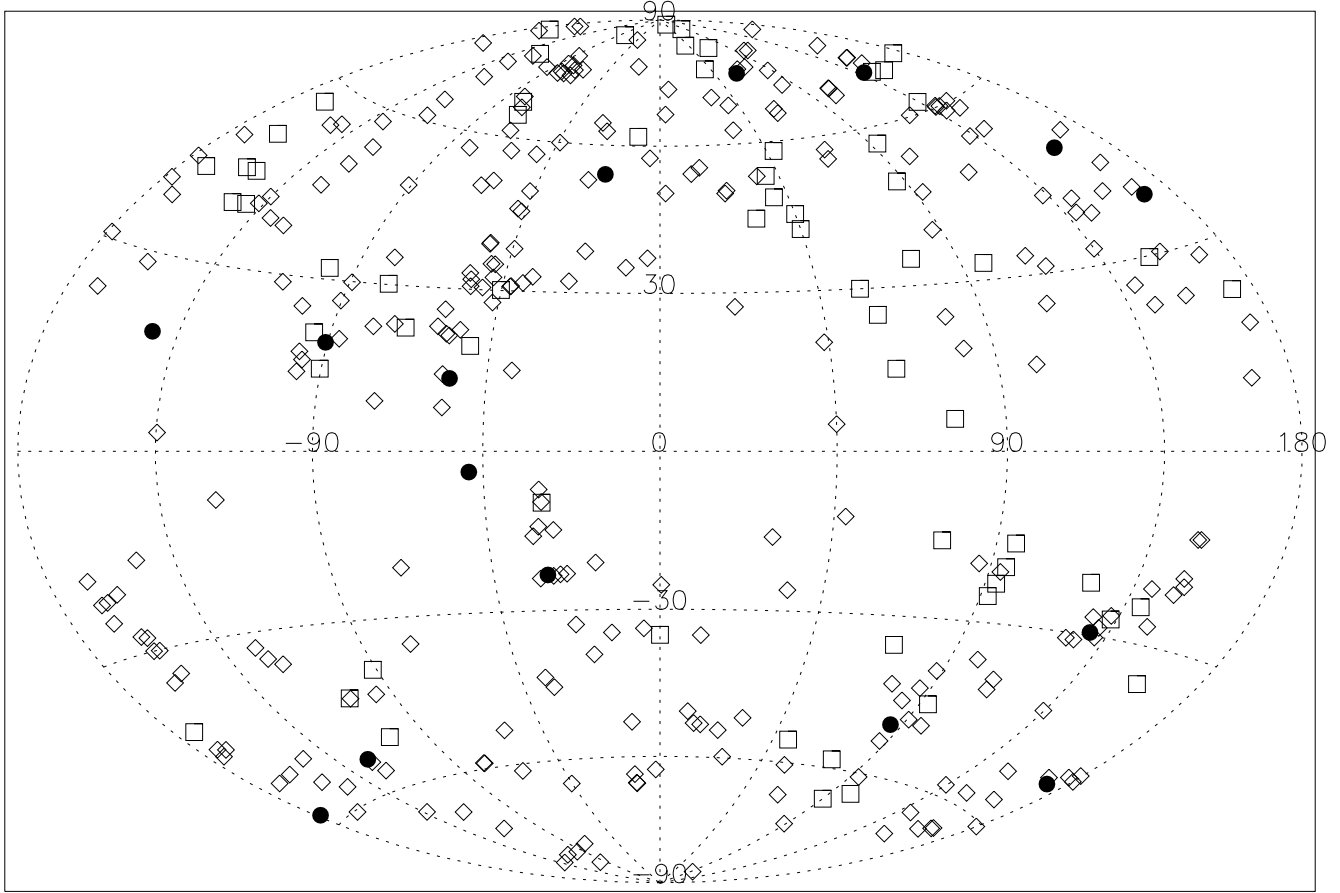


TABLE 1-A
PROPERTIES OF OBSERVED GALAXIES

Source (1)	M (2)	D (3)	S (4)	V (km s ⁻¹) (5)	Dist (Mpc) (6)	Class (7)	T (8)	Inc (degrees) (9)	m_B (10)	M_B (11)	m_V (12)	M_V (13)	S_{5007} (cgs) (14)	$S_{H\beta}$ (cgs) (15)	$\log P_{5007}$ (cgs) (16)
Mrk 334	1	1	1	6600	84.4	2	99	45	14.38	14.62	-19.99	4.9	3.3	42.61	
Mrk 335	1	0	0	7688	99.2	1	0	27	13.75	13.85	-21.11	23	95	43.42	
Mrk 937	0	0	0	8851	115	2		0	16	13.8	-21.47				
Mrk 938	1	1	0	5931	75.0	2	99	72	14	13.52	-20.84	1.1	0.15	41.86	
0017-5133	1	1	0	6586	86.2	L	-1	74	14.48	-20.32					
Mrk 945	0	0	0	4431	54.9	O		0	15	14.54	-19.14				
NGC 224	0	0	0	-300	0.7	O	3	76	4.36	-20.89	10.57	-13.66			
NGC 235A	1	1	0	6664	87.7	2	-5	59	14.08	-20.91	14.2	-20.49			
Mrk 348	1	1	1	4467	56.5	2	0	16	13.9	-19.81	14.59	-19.16	42	4	43.20
Mrk 352	0	1	1	4456	55.9	1	-2	50	14.8	-19.23	14.81	-18.91	4.9	22	42.26
ESO 079-G16	1	1	0	6036	78.8	2	0	72	14.31	-20.84	14.38	-20.08			
NGC 404	1	1	1	-48	2.4	L	-3	0	11.21	-15.98	11.72	-15.18	2.5	1.79	39.24
Tol 0109-383	1	1	0	3496	43.2	2	0	75	13.73	-19.77	14.12	-19.05	42	9.1	42.97
IC 1657	1	1	0	3552	44.4	2	4	85	13.15	-21.03					
NGC 454	1	1	0	3645	46.9	2	99		13.12	13.58	-19.76				
Mrk 1	0	1	1	4839	61.0	2	0	45	15.01	-19.46	14.96	-18.95	60	5.4	43.42
Mrk 565	1	1	0	5446	69.0	U	-2	38	13.35	-20.97	13.5	-20.67			
0120-0214	0	1	0	4730	59.4	2	0	71	14.88	-19.87	14.95	-18.90			
NGC 513	1	1	0	5859	76.4	2	0	67	13.9	-21.22	13.4	-20.99			
NGC 526A	0	1	0	5762	74.5	2	-2	60	14.76	-19.74	14.6	-19.74	27	2.1	43.25
Mrk 993	1	1	1	4658	58.9	2	1	75	14.39	-20.29	13.96	-19.87	3	0.52	42.09
Mrk 359	1	1	1	5007	63.8	2	-2	43	14.16		14.22	-19.79	11	3.5	42.72
0129-3323	1	1	0	4958	63.6	2	4	31	13.67	-20.46					
NGC 600	1	1	1	1842	22.9	L	6	33	12.92	-19.09	12.57	-19.23			
NGC 591	1	1	1	4547	57.6	2	0	34	13.89	-20.16	13.9	-19.89	23	2.3	42.95
NGC 613	1	1	0	1475	16.6	U	4		10.74	-20.56	12.71	-18.38			
Mrk 1158	0	0	0	4585	58.0	O		32	15.03	-19.01	14.96	-18.84	8.8	3.7	42.54
Mrk 573	1	1	0	5096	64.7	2	-1	20	13.68	-20.47	14.07	-19.97	160	13	43.90
0147-0740	0	1	0	5306	67.7	2	-4		15.5	15.62	-18.51				
0152+0622	1	1	1	5164	65.7	2	3	41	14.18	-20.21	14.5	-19.57			
IC 184	0	1	0	5382	68.8	2	1	62	14.66		14.1	-20.07			
NGC 788	1	1	1	4078	51.6	2	0	35	13	-20.75	12.76	-20.79	15	1.5	42.67
ESO 153-IG16	0	1	0	5798	77.9	2	6	65	15.04	-19.88	15.64	-18.80			
ESO 153-G020	1	1	0	5917	78.2	2	3		14.03	-20.95	14.31	-20.14			
NGC 824	1	1	0	5836	76.0	U	4		14.11	-20.45	14.1	-20.28			
4C 35.03	0	0	0	11173	149	R	-5		14.1	-22.06					
NGC 863	1	0	0	7910	103	1	1	25	13.85	-21.38	13.81	-21.24	5.3	6	42.82
Ark 79	1	1	1	5157	66.4	1	1	82	14.1	-21.07	13.84	-20.25	3.2	0.4	42.22
NGC 931	1	1	1	4927	64.1	1	4	81	14.46	-21.79	14.74	-19.28	13	14	42.80
Mrk 1044	1	1	0	4932	63.2	1		32	14.5	14.29	-19.70	5.4	33	42.40	
IC 1816	1	1	0	5037	67.3	2	2	32	13.83	-20.46	13.6	-20.52			
NGC 1019	1	0	0	7251	94.7	1	4	25	14.34	-20.69	14.95	-19.91			
NGC 1052	1	1	1	1470	17.8	L	-5	47	11.41	-19.90	12.31	-18.94	11.74	5.93	41.65
NGC 1068	1	1	1	1136	14.4	2	3	29	9.61	-21.32	10.83	-19.96	1995	169	43.69
NGC 1097	1	1	1	1275	14.5	1	3	49	10.23	-20.89	12.78	-18.03			
Mrk 372	0	0	0	9300	123	2	0	38	14.9	-21.07	14.81	-20.61	13	10	43.36
Mrk 1058	0	1	1	5138	66.4	2	1	65	15.38	-19.52	14.54	-19.55	5.6	0.4	42.46
NGC 1125	1	1	0	3297	41.6	2	0	62	13.43		13.13	-19.96			

TABLE 1-A—*Continued*

Source	M	D	S	V (km s ⁻¹)	Dist (Mpc)	Class	T	Inc (degrees)	m_B	M_B	m_V	M_V	S_{5007} (cgs)	$S_{H\beta}$ (cgs)	$\log P_{5007}$
(1)	(2)	(3)	(4)	(5)	(6)	(7)	(8)	(9)	(10)	(11)	(12)	(13)	(14)	(15)	(16)
NGC 1144	1	0	0	8647	114	2		52	13.78	-22.05	14.41	-20.85	4.3	0.33	42.81
Mrk 1066	1	1	1	3605	45.9	2	-1	42	13.64	-20.26	13.96	-19.34	24	5.5	42.78
NGC 1167	1	1	1	4945	64.1	L	-3	36	13.38	-21.26	12.77	-21.25	6.95	2.51	42.53
H0258-015	1	1	1	4017	51.2	1			14.36		14.36	-19.17			
NGC 1194	1	1	0	3957	50.5	1	-1	58	13.83		14.18	-19.32			
NGC 1241	1	1	0	4030	51.6	2	3	54	12.84	-21.47	12.7	-20.85	1	<.03	41.50
Mrk 1073	1	1	0	6991	92.1	2	3	32	13.7	-21.90	14.18	-20.62	22	2.8	43.34
0314-2303	1	1	0	3880	50.7	L	2	35	13.17	-20.46					
NGC 1275	1	1	0	5260	68.6	1	99	40	12.64		12.55	-21.61	283	74.7	44.20
NGC 1301	1	1	0	3944	51.7	L	3	80	14.1	-20.59					
NGC 1326	1	1	1	1362	16.9	L	-1	43	11.41	-19.75					
Mrk 607	1	1	1	2716	37.7	2	1	76	13.32		14	-18.88	14	1.4	42.38

TABLE 1-A—Continued

Source	M	D	S	V (km s ⁻¹)	Dist (Mpc)	Class	T	Inc (degrees)	m_B	M_B	m_V	M_V	S_{5007} (cgs)	$S_{H\beta}$ (cgs)	$\log P_{5007}$
(1)	(2)	(3)	(4)	(5)	(6)	(7)	(8)	(9)	(10)	(11)	(12)	(13)	(14)	(15)	(16)
MCG -2-9-40	0	1	0	4495	58.3	2		74	15		14.15	-19.66			
Mrk 612	0	1	0	6041	79.2	2	0	59	15.5		14.25	-20.22	18	1.8	43.12
NGC 1358	1	1	1	4013	51.9	2	0	42	13.04	-20.86	13.05	-20.51	13	1.7	42.62
NGC 1365	1	1	1	1662	16.9	2	3	58	10.32	-21.21	12.95	-18.19			
NGC 1386	1	1	1	924	16.9	2	-1	67	12.09	-19.02	12.84	-18.30	80	5.3	42.44
III Zw 55	0	0	0	7527	99.6	2	-5	0	15.4		15.22	-19.75	5.9	1	42.83
0339-2124	1	1	0	4341	56.6	1	1	46	12.83	-21.15	13.68	-20.07			
NGC 1433	0	0	0	1075	11.6	O	2		10.75	-19.68					
NGC 1566	1	1	1	1496	13.4	1	4	38	10.13	-20.48	13.17	-17.47	30	18	41.81
0425-0440	0	1	0	4647	61.5	2			14.6						
ESO 202-G23	1	1	0	4947	66.2	2	99	32	13.48		14.9	-19.19			
NGC 1598	0	0	0	5106	68.4	O	5		13.88	-20.72					
0438-0828	1	1	0	4527	60.1	2	0		14				0.77		41.52
NGC 1672	0	0	0	1350	14.5	O	3	34	10.28	-20.56	12.23	-18.58			
NGC 1667	1	1	1	4547	60.6	2	5	38	12.77	-21.49	12.86	-21.04	6.04	0.49	42.42
H0448-041	1	1	1	3897	51.8	1			14.18		14.18	-19.38			
NGC 1685	1	1	1	4527	60.3	2	0	47	14.5		15.18	-18.71			
0450-0317	1	1	0	4737	63.2	2			13.6		15	-18.99	4	0.26	42.27
0456+04	1	1	1	4723	63.0	1	1	57	13.83	-20.90	14.41	-19.57	4.8	8.5	42.35
ESO 033-G02	0	1	0	5426	73.5	2					14.6	-19.71			
0459+0328	0	1	1	4497	60.1	1			14.75		15	-18.88			
NGC 1808	1	1	1	989	10.8	2	1	55	10.76	-19.72	12.55	-17.62			
UGC 3255	0	1	1	5689	76.3	2	3	81	15.35	-20.48	15.6	-18.79			
ESO 362-G8	1	1	0	4785	64.5	2	0	62	13.6	-20.52	12.65	-21.38			
H0510+031	0	1	1	4917	66.0	1			14.8		14.8	-19.28			
Ark 120	1	0	0	9354	135	1	0	48	14.1	-22.13	13.92	-21.69	9.3	170	43.29
0517-3242	1	1	0	3777	50.9	1	0		13.78	-19.94	13.37	-20.15			
NGC 2110	1	1	1	2284	31.3	2	-3	43	14		13.51	-18.96	17	3.4	42.30
MCG 8-11-11	0	1	0	6141	82.9	1	1	28	15	-21.54	14.62	-19.95	71	29	43.76
Mrk 3	1	1	1	4050	53.6	2	-2	28	14.03	-20.24	13.34	-20.29	347	29	44.07
NGC 2273	1	1	1	1840	28.4	2	1	45	12.55	-20.25	13.54	-18.73	33	3.3	42.50
Mrk 6	0	1	0	5516	78.4	1	0	54	15	-19.97	14.19	-20.26	75	32	43.73
0648+458	0	1	0	6506	88.7	2		67	15.3		15.3	-19.41			
Mrk 376	0	0	0	16770	231	1			14.91	-22.50	14.62	-22.14	4.9	16	43.47
0714-2914	1	1	1	1630	24.1	2	-2	56	13.26	-19.93	13.52	-18.38			
NGC 2377	1	1	1	2457	31.8	L	4	41	13.54	-21.96	14.77	-17.74	0.45	0.69	40.74
Mrk 78	0	0	0	11202	153	2	1	55	15		14.58	-21.30	66	5	44.25
Mrk 79	1	1	0	6652	91.1	1	3	47	13.9	-21.44	14.27	-20.50	37	55	43.56
UGC 3995A	1	1	1	4740	66.1	2		53	13.6	-21.48					
Mrk 10	1	0	0	8753	119	1	3	69	13.34	-22.47	14.71	-20.64	14	19	43.37
Mrk 1210	1	1	1	4046	57.5	2		0	14.34	-19.57	15	-18.78			
Mrk 622	0	1	0	6964	96.2	2	-2	26	14.6	-20.63	14.08	-20.81	4	0.3	42.64
0816+2116	0	1	1	5488	76.9	2		59	14.82	-20.23	15.5	-18.91			
ESO 018-G009	0	1	0	5341	72.8	2									
NGC 2639	1	1	1	3336	46.0	L	1	54	12.56	-21.11	11.88	-21.42	1.82	0.48	41.66
TON 951	1	0	0	19200	267	1			14						
NGC 2655	1	1	1	1404	24.4	L	0	34	10.96	-21.12	11.08	-20.86			
NGC 2681	1	1	1	692	13.3	U	0	24	11.09	-19.74	11.33	-19.29			

TABLE 1-A—*Continued*

Source (1)	M (2)	D (3)	S (4)	V (km s ⁻¹) (5)	Dist (Mpc) (6)	Class (7)	T (8)	Inc (degrees) (9)	m_B (10)	M_B (11)	m_V (12)	M_V (13)	S_{5007} (cgs) (14)	$S_{H\beta}$ (cgs) (15)	$\log P_{5007}$ (cgs) (16)
NGC 2691	1	1	1	3981	56.1	1	1	50	13.93	-20.13	14.1	-19.63			
NGC 2768	1	1	1	1335	23.7	L	-5	60	10.84	-21.17	11.9	-19.97			
NGC 2782	1	1	1	2562	37.3	2	1	43	12.3	-20.85	13.45	-19.41			
NGC 2787	1	1	1	696	13.0	U	-1	53	11.82	-18.96	11.79	-18.78			
Mrk 704	0	0	0	8968	125	1	1	70	15.38	-20.57	14.2	-21.26	13	26	43.37
0915+32	0	0	0	18587	259	R									
NGC 2841	1	1	1	638	12.0	L	3	67	10.09	-20.82	12.41	-17.99	0.95	0.63	40.21
Mrk 705	0	0	0	8658	121	1	-2	35	14.88	-20.89	14.6	-20.79	9	28	43.19
NGC 2911	1	1	1	3183	46.8	L	-2	40	12.5	-21.09	13.83	-19.51			
ESO 373-G013	0	1	0	2700	40.0	L									
0936+368	0	1	0	6021	84.4	1		38	15.35	-19.42					
Mrk 403	0	0	0	7225	101	2		28	15.4		14.53	-20.47	9.4	0.62	43.05

TABLE 1-A—Continued

Source	M	D	S	V (km s ⁻¹)	Dist (Mpc)	Class	T	Inc (degrees)	<i>m_B</i>	<i>M_B</i>	<i>m_V</i>	<i>M_V</i>	<i>S₅₀₀₇</i> (cgs)	<i>S_{H_β}</i> (cgs)	log P ₅₀₀₇
(1)	(2)	(3)	(4)	(5)	(6)	(7)	(8)	(9)	(10)	(11)	(12)	(13)	(14)	(15)	(16)
Mrk 1419	1	1	1	4932	70.6	L	1	50	13.29	-21.22	15	-19.22	4.4		42.41
0939+2355	0	1	0	6407	90.2	1			15.3						
0942+09	0	1	1	3897	56.6	2			15.5		15.5	-18.25			
NGC 2992	1	1	1	2314	30.5	2	1	62	13.14	-20.26	13.78	-18.64	91	8.1	43.01
0945-30	1	1	0	2482	37.3	2	0	65	14.07	-19.31	13.69	-19.16	0.15	0.37	40.39
ESO 373-G29	1	1	0	2802	41.4	2	2	59	14						
NGC 2985	1	1	1	1322	22.4	U	2	39	11.18	-20.77	10.6	-21.15			
NGC 3010B	0	1	1	4760	66.7	L		57	15.1						
NGC 3032	0	0	0	1533	24.5	O	-2	26	13.18	-19.11					
Mrk 1239	1	1	0	5816	82.8	2		38	14.5		14.39	-20.18	23	17	43.27
NGC 3031	1	1	1	-34	1.4	L	2	60	7.89	-18.33	11.63	-14.10	29.8	6.38	39.84
NGC 3081	1	1	1	2394	32.5	2	0	33	12.85	-19.97	13.55	-19.01	125	8.1	43.20
NGC 3079	1	1	1	1125	20.4	L	7	85	11.54	-21.14	12.05	-19.50	0.18		39.95
ESO 374-G025	0	0	0	7006	98.5	1			15.02	-20.73	15.29	-19.65			
NGC 3125	0	0	0	865	18.6	O	-5		13.26	-18.24	13.55	-17.80			
NGC 3169	1	1	1	1200	19.7	U	1		11.42	-20.51	12.41	-19.06			
IC 2560	1	1	0	2873	42.7	2	3	53	12.53	-21.22	13.31	-19.83			
NGC 3185	1	1	1	1218	21.3	L	1	50	12	-18.99			3.1	0.6	41.23
H1016+336	0	0	0	7345	103	1			15.93		15.93	-19.10			
NGC 3227	1	1	1	1157	20.6	2	1	57	11.1	-20.39	11.79	-19.78	64	25	42.51
ESO 568-G11	0	0	0	8970	126	L	4	48	14.56						
NGC 3281	1	1	0	3460	50.3	2	2	59	12.7	-21.57	14.02	-19.47	5.5	0.5	42.22
1034+0609	0	1	1	3487	51.4	2		50	14.7		14.7	-18.84			
NGC 3312	1	1	1	2869	48.6	L	3	70	12.68	-21.62	12.6	-20.83	2	0.7	41.75
NGC 3362	1	0	0	8318	117	2	5	39	13.48	-22.09	15	-20.31	6.8	0.7	43.04
NGC 3367	1	1	1	3038	45.3	U	5	29	12.05	-21.35	14.14	-19.13			
NGC 3393	1	1	1	4107	54.6	2	1	25	13.09	-21.03	13.1	-20.57			
ESO 215-G014	0	1	0	5581	78.2	1					15.8	-18.65			
NGC 3516	1	1	1	2602	38.9	1	-2	44	12.5	-20.81	12.4	-20.55	48	73	42.94
Fair 1150	1	1	0	2930	43.2	1	5	32	13.52	-20.13	13.11	-20.07			
Mrk 732	1	0	0	8768	123	1	-4	0	14.04	-21.53	14	-21.42			
NGC 3627	1	1	1	727	6.6	U	3	65	9.65	-19.97	11.94	-17.16			
NGC 3642	1	1	1	1588	27.5	L	4	34	11.65	-20.74	14.04	-18.16	0.88	0.51	40.90
NGC 3660	0	1	1	3678	54.2	2	4	36	15.5		14.45	-19.20			
1121-2806	1	1	0	4047	58.7	2			13						
NGC 3665	0	0	0	2080	32.4	R	-2	38	11.77	-20.86					
Mrk 40	0	1	1	6323	87.2	1	-2	90	16.8		15.39	-19.29	7.2	6.2	42.81
ESO 439-G009	0	0	0	7162	105	2	1		14.71	-21.37	14.8	-20.28			
NGC 3718	1	1	1	1247	17.0	1	1	63	11.59	-19.96					
NGC 3783	1	1	0	3208	43.3	1	1	37	12.64	-21.13	13.43	-19.74	130	130	43.46
NGC 3786	1	1	1	2723	41.6	1	1	58	13.24	-20.13	13.74	-19.36	8.4	1	42.24
Mrk 745	0	1	1	3209	47.4	2		50	14.6		14.62	-18.75			
NGC 3884	1	1	0	6948	98.0	1	0	53	13.5	-21.67	12.88	-22.05			
NGC 3898	1	1	1	1176	21.9	L	2	55	11.6	-20.38	11.83	-19.87			
NGC 3921	1	1	1	5838	81.2	L	0	53	13.06	-21.63	13.35	-21.17	0.84		41.81
Fair 1151	0	0	0	3232	47.3	O	1		13.28	-20.83					
Mrk 42	0	0	0	7200	100	1	3	42	15.28	-19.95	15.45	-19.53	1.22	3.7	42.15
NGC 3982	1	1	1	1109	17.0	2	3	30	11.78	-19.47	11.7	-19.45	15	0.5	41.71

TABLE 1-A—*Continued*

Source	M	D	S	V (km s ⁻¹)	Dist (Mpc)	Class	T	Inc (degrees)	m_B	M_B	m_V	M_V	S_{5007} (cgs)	$S_{H\beta}$ (cgs)	$\log P_{5007}$ (cgs)
(1)	(2)	(3)	(4)	(5)	(6)	(7)	(8)	(9)	(10)	(11)	(12)	(13)	(14)	(15)	(16)
NGC 3998	1	1	1	1040	21.6	L	-2	36	11.61	-20.18	12.1	-19.57	5.07	2.39	41.45
Mrk 1310	1	1	0	5830	83.3	1	-5	53	14.49	-20.25	15.46	-19.12	8.6	11	42.84
NGC 4036	1	1	1	1397	24.6	L	-3	70	11.57	-20.46	11.2	-20.75			
Was 41	0	0	0	7050	99.4	2		30	15	-20.20	14.9	-20.06			
NGC 4051	1	1	1	725	17.0	1	4	40	10.83	-20.41	12.92	-18.23	39	25	42.13
NGC 4074	0	1	0	6793	95.9	2	-2	54	15.4		14.44	-20.44	16	1	43.24
Was 45	1	0	0	7494	105	2		0	14	-20.97	14.01	-21.07			
NGC 4111	1	1	1	807	17.0	L	-1	85	11.63	-19.55	11.22	-19.93			
NGC 4117	1	1	1	871	17.0	2	-2	62	14.04	-17.12	14.3	-16.85			
Mrk 198	0	0	0	7183	99.8	2	-2	31	14.97	-20.11	14.73	-20.24	12.6	1.5	43.17
NGC 4151	1	1	1	995	20.3	1	2	26	11.5	-20.83	11.85	-19.69	1160	442	43.76
NGC 4192	1	1	1	-142	16.8	L	2	78	10.95	-21.11	13.26	-17.87			

TABLE 1-A—Continued

Source (1)	M (2)	D (3)	S (4)	V (km s ⁻¹) (5)	Dist (Mpc) (6)	Class (7)	T (8)	Inc (degrees) (9)	<i>m_B</i> (10)	<i>M_B</i> (11)	<i>m_V</i> (12)	<i>M_V</i> (13)	<i>S₅₀₀₇</i> (cgs) (14)	<i>S_{H_β}</i> (cgs) (15)	log P ₅₀₀₇ (cgs) (16)
Mrk 201	0	0	0	2506	39.1	O	10	54	13.01	-20.10	13.3	-19.66			
Was 49B	0	0	0	18900	264	1					15.4	-21.64			
NGC 4235	1	1	1	2410	35.1	1	1	90	12.62	-20.84	13.6	-19.13	2.4	6.6	41.55
NGC 4253	1	1	1	3876	55.1	1	1	38	14	-19.90	13.57	-20.12	59	19	43.32
NGC 4258	1	1	1	448	6.8	L	4	70	9.1	-20.63	11.65	-17.51	5.5		40.48
NGC 4261	0	0	0	2210	35.1	R	-5	29	11.41	-21.37					
NGC 4278	1	1	1	649	9.7	L	-5	23	11.09	-18.96	10.87	-19.06			
NGC 4303	1	1	1	1569	15.2	L	4	27	10.18	-20.79	12.6	-18.31	3.1	2.6	40.93
Mrk 50	0	0	0	7025	99.4	1		39	15	-20.07	15.17	-19.79			
NGC 4388	1	1	1	2524	16.8	2	3	78	11.76	-20.34	13.9	-17.23	48	3.8	42.21
NGC 4395	1	1	1	318	3.6	1	9	34	10.64	-17.21	10.7	-17.08	12.59	1.87	40.29
NGC 4418	1	1	1	2198	33.7	U	1		13.99	-19.03					
NGC 4419	1	1	1	-261	16.8	L	1	74	12.08	-19.53	11.71	-19.42	0.29		39.99
NGC 4438	1	1	1	69	16.8	L	0	71	11.02	-20.64	12.81	-18.32	0.97	0.79	40.52
NGC 4450	1	1	1	1956	16.8	L	2	42	10.9	-20.38	13.19	-17.94	0.53		40.25
NGC 4486	1	1	1	1282	16.8	L	-4	38	9.59	-21.64	12.86	-18.27			
NGC 4501	1	1	1	2280	16.8	L	3	59	10.36	-21.27	13.18	-17.95	2.9	0.5	40.99
NGC 4507	1	1	0	3523	50.7	2	2	35	12.92	-21.23	13.54	-19.97	110	11.5	43.52
NGC 4569	1	1	1	-235	16.8	L	2	65	10.26	-21.34	12.31	-18.82	5.4	2.4	41.26
NGC 4579	1	1	1	1519	16.8	L	3	38	10.48	-20.84	11.72	-19.41	1.1	0.44	40.57
NGC 4593	1	1	1	2338	39.5	1	3	40	11.67	-21.55	13.15	-19.83	17.2	64	42.51
NGC 4594	1	1	1	1091	20.0	1	1	69	8.98	-23.13	9.25	-22.26			
Tol 74	1	1	0	3285	48.3	2	4	0	13	-20.70	13.5	-19.91			
NGC 4639	1	1	1	1010	16.8	1	4	49	12.24	-19.28					
1243+26	0	0	0	26711	372	R				15.1					
ESO 172-G010	0	1	0	1829	24.7	2									
NGC 4696	1	1	0	2958	46.4	L	-4	46	11.39	-22.48					
1249-1308	0	1	0	4385	63.3	1			15		14.03	-19.96	23	26	43.04
ESO 323-G32	1	1	0	4857	67.8	2	-1	46	13.86	-20.84	13.9	-20.24			
NGC 4785	1	1	0	3735	53.4	2	3	60	13.21	-21.83	13.2	-20.42			
Mrk 231	1	0	0	12660	169	1	5	41	14.41	-22.12	13.85	-22.25	23	61	43.88
NGC 4826	1	1	1	408	4.1	L	2	59	9.36	-19.24	12.14	-15.92	0.42		38.93
1254+27	0	0	0	7387	103	R	-4	64	13.02	-22.22					
1255-2930	1	1	0	3055	45.0	L	0	51	13.81	-20.03					
NGC 4903	1	1	0	4955	70.6	L	5	31	13.72	-21.09	12.5	-21.73			
NGC 4922B	0	0	0	7153	99.2	2	90	56	14.9		15	-19.96	3.1	0.85	42.55
1300-3158	1	1	0	4858	69.2	L	3	72	13.95	-21.19					
NGC 4941	1	1	1	1111	6.4	2	2	60	11.9	-17.39	12.23	-16.80	22	1.3	41.03
NGC 4945	1	1	1	560	5.2	2	6	85	9.3	-21.15	14.4	-14.18			
1303-4008	1	1	0	4477	63.7	1	-2	50	13.56	-20.91	13.42	-20.58			
ESO 508-G05	1	1	1	2947	43.5	2	-1	41	13.58	-19.95	13.6	-19.58			
NGC 4968	1	1	0	2957	44.2	2	-2	66	13.75	-19.81	13.8	-19.41	10	0.4	42.36
1305-2407	0	1	0	4227	60.8	2			16						
NGC 5005	1	1	1	946	21.3	L	4	63	10.61	-21.45	13.67	-17.97	0.75	0.13	40.61
NGC 5033	1	1	1	878	18.7	1	5	64	10.75	-21.15	12.03	-19.33	5.3	0.56	41.35
IC 4218	0	1	0	5815	82.5	1		83	14.6	-20.93	14.73	-19.83			
1314-1532	0	1	1	3900	56.5	U			20		20	-13.74			
IC 4214	1	1	1	2281	34.3	L	1	55	12.16	-21.10					

TABLE 1-A—*Continued*

Source (1)	M (2)	D (3)	S (4)	V (km s ⁻¹) (5)	Dist (Mpc) (6)	Class (7)	T (8)	Inc (degrees) (9)	m_B (10)	M_B (11)	m_V (12)	M_V (13)	S_{5007} (cgs) (14)	$S_{H\beta}$ (cgs) (15)	$\log P_{5007}$ (cgs) (16)
NGC 5077	1	1	1	2832	40.6	L	-5	39	12.38	-20.83	12.85	-20.19			
NGC 5101	1	1	1	1861	27.4	L	0	32	11.6	-21.18					
1319-1627	1	1	0	5152	71.9	2		76	14.5		13.9	-20.36	150	13	43.96
1321+31	0	0	0	4782	67.5	R		39	12.9	-21.32					
1322+2918	0	0	0	7050	98.5	2	-5		16.2						
NGC 5128	0	0	0	547	4.9	O			7.7	-21.15	13.47	-14.98			
NGC 5135	1	1	0	4112	58.8	2	2	24	12.88	-21.46	13.35	-20.48	22	4.3	42.95
NGC 5194	1	1	1	463	7.7	L	4	54	8.96	-20.75	13.47	-15.96	6.5		40.66
NGC 5195	1	1	1	465	9.3	L	90	38	10.45	-19.44	12.3	-17.54			
IC 894	0	1	0	6507	91.4	2		69	14.9						
1331-2325	0	1	1	2577	39.3	2		65	14.63	-19.17	14.7	-18.26	3.4	1.1	41.79
MCG -6-30-15	1	1	1	2248	35.1	1		55	13.7	-19.38	13.61	-19.10	0.31	0.02	40.66

TABLE 1-A—Continued

Source	M	D	S	V (km s ⁻¹)	Dist (Mpc)	Class	T	Inc (degrees)	m_B	M_B	m_V	M_V	S_{5007} (cgs)	$S_{H\beta}$ (cgs)	$\log P_{5007}$
(1)	(2)	(3)	(4)	(5)	(6)	(7)	(8)	(9)	(10)	(11)	(12)	(13)	(14)	(15)	(16)
1335+39	1	1	0	6023	83.9	2		0	14.27	-20.42	14.2	-20.40			
NGC 5252	1	1	0	6890	96.9	2	-2	61	14.04	-20.98	14.21	-20.70			
NGC 5256	1	0	0	8353	115	2	99		14.1		13.42	-21.86	3.2	0.67	42.69
NGC 5253	0	0	0	404	3.2	O	10	71	10.87	-17.06	13.16	-14.37			
NGC 5283	1	1	1	2700	41.4	2	-2	33	14.2	-18.97	14.05	-19.04	27	2.2	42.74
NGC 5273	1	1	1	1054	21.3	1	-2	33	12.44	-19.26	13.12	-18.52	2.2	0.2	41.08
1344+038	0	1	0	6870	96.5	2			15.2	-19.83	16	-18.90			
Mrk 461	0	1	1	4856	68.2	2		46	14.61	-19.80	14.5	-19.65			
NGC 5298	1	1	0	4412	62.8	L	3	62	14	-20.71					
IC 4329A	1	1	0	4813	68.0	1	-1	90	14	-20.47	13.66	-20.48	34	65	43.27
NGC 5347	1	1	1	2278	36.7	2	2	41	13.4	-19.72	12.7	-20.12			
NGC 5371	1	1	1	2553	37.8	L	4	38	11.32	-21.72	12.63	-20.26			
Mrk 463	1	0	0	14904	211	2	1	55	14.4	-22.53	14.22	-22.35	73	11	44.57
NGC 5393	1	1	1	5980	84.0	L	1	40	13.97	-21.02					
1357+28	0	0	0	18850	259	R									
NGC 5427	1	1	1	2730	38.1	2	5	32	11.93	-21.17	13.96	-18.94	7.3	0.9	42.10
IC 4374	1	1	0	6517	91.3	L	-3	42	13.59	-21.48					
Mrk 1370	0	0	0	7370	103	2			16		16	-19.04			
1408+1347	0	1	1	4836	68.3	2			15.2						
Circinus	1	1	1	436	4.2	2	3	67	12.1	-19.62			8.5	0.6	40.25
NGC 5506	1	1	1	1815	28.7	2	1	90	12.79	-20.03	14.38	-17.91	45	5.5	42.65
NGC 5548	1	1	1	5149	72.0	1	0	33	13.3	-21.46	13.73	-20.54	58	83	43.55
NGC 5635	1	1	1	4316	60.6	L		64	13.46	-20.97					
NGC 5643	1	1	1	1199	16.9	2	5	23	10.74	-20.91	13.6	-17.54	80	4.8	42.44
NGC 5675	1	1	1	4169	58.3	L		72	13.7	-20.87	14	-19.81			
NGC 5674	1	0	0	7472	104	2	5	25	13.7	-21.49	13.7	-21.36			
Mrk 817	1	0	0	9430	128	1	0	27	14.5	-21.15	13.79	-21.72	13	40	43.40
NGC 5695	1	1	1	4225	58.9	2		44	13.58	-20.47	13.6	-20.24	7.2	0.61	42.47
Mrk 477	0	0	0	11340	156	2		44	15.4	-20.70	15.03	-20.90	150	17	44.62
NGC 5728	1	1	1	2788	42.2	2	1	56	12.37	-21.41	13.4	-19.73	68	5.8	43.16
ESO 512-G20	1	1	0	3420	48.7	1	-1	47	14.43		14.5	-18.93			
Mrk 1388	0	1	0	6296	87.3	2			15.7		16	-18.68	26	2.4	43.37
Mrk 841	1	0	0	10850	150	1			14		14.27	-21.57	25	65	43.81
1502+035	0	1	0	5996	83.4	1									
NGC 5851	0	1	0	6486	89.9	L		77	15.04	-20.77					
NGC 5899	1	1	1	2562	39.8	L	5	71	12.5	-21.22	12.08	-20.92	6.9	0.6	42.12
NGC 5929	1	1	1	2561	38.5	2	2	18	14.1		13.4	-19.53	9.3	2.3	42.22
1525+29	0	0	0	19600	270	R									
1530-085	1	1	0	6888	96.4	2		70	14.5		15.7	-19.19			
NGC 5953	1	1	1	1965	33.0	2	1	37	13.3		13.1	-19.49	8.2	2.7	42.03
IC 4553	1	1	0	5434	74.9	2		38	13.94	-20.74	14.4	-19.95			
1533+14	0	1	0	5910	81.5	2		38	15.3	-19.42	14.7	-19.83			
Mrk 486	0	0	0	11679	159	1		57	15.2		14.78	-21.19	8.2	36	43.38
Mrk 860	0	0	0	6869	94.2	O		62	15.5		14.8	-20.05			
NGC 5985	1	1	1	2520	39.2	U	3	59	11.87	-21.59					
1545-1336	0	1	0	2622	37.0	2									
1553+24	0	0	0	12775	175	R			15.42	-21.14					
Mrk 298	0	0	0	10098	140	2	-1	46	15.17	-20.75	15.19	-20.51	4.9	2.2	43.05

TABLE 1-A—*Continued*

Source	M	D	S	V (km s ⁻¹)	Dist (Mpc)	Class	T	Inc (degrees)	m_B	M_B	m_V	M_V	S_{5007} (cgs)	$S_{H\beta}$ (cgs)	$\log P_{5007}$ (cgs)	
(1)	(2)	(3)	(4)	(5)	(6)	(7)	(8)	(9)	(10)	(11)	(12)	(13)	(14)	(15)	(16)	
+27	0	0	0	19400	267	R										
ESO 0137-G34	1	1	1	2620	36.0	2	0	39	12.21	-23.42	12.2	-20.57				
NGC 6217	1	1	1	1362	23.9	U	4	34	11.79	-20.23	13.88	-18.01				
1637+27	0	0	0	26400	367	R										
NGC 6251	1	1	0	6900	92.7	L	-5	34	13.64	-21.59						
NGC 6211	1	1	0	5966	80.2	2	-1	41	13.63		14.3	-20.20				
ESO 0138-G01	1	1	1	2740	37.4	2			62	14.31	-19.52	13.63	-19.23			
NGC 6221	0	0	0	1482	19.4	O	5	43	10.66	-21.67	13.45	-17.99	6.2	8.4	41.45	
NGC 6240	1	0	0	7339	98.9	2	90	60	13.8		13.37	-21.58				
NGC 6300	1	1	1	1110	14.3	2	3	52	10.98	-20.58	13.08	-17.70				
Arp 102B	0	0	0	7245	97.4	1	-5	40	15.12	-19.98	14.81	-20.11				
NGC 6328	1	1	0	4260	57.6	L	2	56	13.16	-21.28	15.5	-18.29				

TABLE 1-A—Continued

Source	M	D	S	V (km s ⁻¹)	Dist (Mpc)	Class	T	Inc (degrees)	m_B	M_B	m_V	M_V	S_{5007} (cgs)	$S_{H\beta}$ (cgs)	$\log P_{5007}$
(1)	(2)	(3)	(4)	(5)	(6)	(7)	(8)	(9)	(10)	(11)	(12)	(13)	(14)	(15)	(16)
ESO 139-G012	1	1	0	5200	70.2	2	4		13.59	-21.15	13.6	-20.61			
1736+32	0	0	0	22200	307	R									
Ark 524	0	0	0	7345	98.5	1		38	15.6			15.6	-19.34		
1752+32	0	0	0	13460	183	R									
NGC 6500	1	1	1	3003	39.3	L	2	44	13.05	-20.50	13.7	-19.26			
1827+32	0	0	0	19770	271	R			15.1						
Ark 539	0	1	1	5065	66.8	2		50	15.4	-19.03	15	-19.11	1.3	0.14	41.83
1832-5926	1	1	0	6065	81.3	2			13.2						
ESO 103-G35	0	1	0	3983	53.2	2	0	72	14.7	-19.30	14.53	-19.09			
IC 4729	1	1	0	4419	59.2	2			13.57	-20.91	11.8	-22.04			
Fair 182	0	1	0	3300	43.9	2	0	53	14.99	-18.65	14.5	-18.70			
Fair 51	0	1	0	4210	56.1	1	3	61	14.7	-20.07	14.1	-19.63	28	32	43.02
IC 4777	0	1	0	5555	74.0	2	0	40	14.59	-20.01	14.63	-19.70			
3C 390.3	1	0	0	16680	228	1			14.37		15.38	-21.35			
Padova I	0	1	1	2650	33.5	1					15	-17.62			
NGC 6764	1	1	1	2416	37.0	2	4	57	12.56	-20.70	14.03	-18.81	3.7	6.2	41.78
Fair 1163	0	1	0	5640	74.0	2	2	0	14.93	-20.06	14.97	-19.36			
NGC 6814	1	1	1	1563	22.8	1	4	20	12.06	-20.47	14.21	-17.58	13.6	4.4	41.93
1953+0916	0	1	0	7000	91.3	1			15.1						
Cyg A	0	0	0	16815	228	2			17.04	-22.15	15.1	-21.63			
NGC 6860	1	1	0	4462	58.8	1	3	54	13.68	-20.62	13.53	-20.30			
20100-4156	0	0	0	38850	549	L									
NGC 6890	1	1	1	2419	31.8	2	3	39	13.01	-19.69	14.02	-18.49	19	0.9	42.36
IC 4995	1	1	0	4887	61.5	2	-2	50	14.28	-19.85	14.06	-19.87			
2031-307	0	1	0	5700	73.9	1									
NGC 6951	1	1	1	1426	24.1	L	4	36	11.64	-21.20	14.04	-17.87	0.92	0.05	40.81
Mrk 509	1	0	0	10200	135	1	-3	43	13		13.12	-22.49	81	165	44.23
IC 5063	1	1	1	3402	43.7	2	-1	55	12.89	-20.61	13.6	-19.59	93	9	43.32
NGC 7052	0	0	0	4920	62.1	R	-5	58	13.4	-21.26					
IC 5135	1	1	0	4842	61.4	2	1	29	12.98	-21.05	13.87	-20.06			
2157-3357	1	1	0	4463	56.4	L		83	14.5	-20.19					
2159-2244	0	1	0	5313	67.4	L	0	62	14.73	-19.80					
NGC 7172	1	1	1	2575	33.9	2	1	58	12.85	-20.11	13.61	-19.04			
ESO 108-G10	1	1	1	3118	40.8	2		55	14.29		15.8	-17.24			
NGC 7212	0	0	0	7795	101	2	1	60	14.78	-20.98			70	6.5	43.92
NGC 7217	1	1	1	946	16.0	L	2	36	11.02	-20.49	11.92	-19.10	3.62	2.02	41.04
NGC 7213	1	1	0	1792	22.0	1	1	26	11.01	-20.58	12.08	-19.63			
NGC 7214	1	1	0	6832	88.0	1	4	52	13.33	-21.87	14.1	-20.60	6.3	11	42.76
ESO 108-IG017	0	1	0	1919	24.7	2					14	-17.96			
3C 449	0	0	0	5122	64.9	O	-3		14.49	-20.19					
NGC 7314	1	1	1	1422	18.3	2	4	65	11.62	-20.22	13.11	-18.20	6.1	0.65	41.39
NGC 7319	1	1	0	6764	85.0	2	4	41	14.11	-21.02	13.53	-21.09	6.4	0.76	42.73
Mrk 915	0	0	0	7255	93.2	1	1	69	15		14.5	-20.32	46	11	43.67
2236+35	0	0	0	8255	107	O	0		14.37	-21.23					
2237+0747	1	0	0	7375	96.2	1	1	30	14.24	-21.10	14.3	-20.59			
Mrk 917	0	0	0	7317	94.3	2	1	0	14.6	-20.85	14.1	-20.75	11	1.3	43.06
Ark 564	0	0	0	7195	95.4	1	3	43	14.55	-21.00	14.16	-20.71	19	19	43.31
NGC 7410	1	1	1	1751	20.1	2	1	76	11.24	-20.72	11.8	-19.72			

TABLE 1-A—*Continued*

Source	M	D	S	V (km s ⁻¹)	Dist (Mpc)	Class	T (degrees)	Inc (degrees)	m_B	M_B	m_V	M_V	S_{5007} (cgs)	$S_{H\beta}$ (cgs)	$\log P_{5007}$ (cgs)
(1)	(2)	(3)	(4)	(5)	(6)	(7)	(8)	(9)	(10)	(11)	(12)	(13)	(14)	(15)	(16)
NGC 7450	1	1	1	3191	38.1	2	1	24	14.5	14.33	-18.57	12	3.7	42.32	
Mrk 313	1	1	1	1950	21.5	2	-1		13.31	-18.58	14	-17.65			
NGC 7469	1	1	1	4916	60.9	1	1	53	13	-21.27	13.04	-20.87	58	98	43.40
NGC 7479	1	1	1	2382	32.4	L	5	42	11.6	-21.33	13.88	-18.67	1.09	0.33	41.14
NGC 7496	1	1	1	1649	20.1	2	3	25	11.91	-19.68	13.9	-17.62			
NGC 7582	1	1	1	1575	17.6	2	2	62	11.37	-20.40	13.57	-17.66	35	14	42.11
NGC 7592	0	0	0	7345	93.9	O	-1		15		13.56	-21.28			
NGC 7590	1	1	1	1596	17.3	2	4	71	12.11	-19.73	13.76	-17.43			
IC 1481	1	1	1	6118	77.5	L		30	14.39	-20.42					
NGC 7672	0	0	0	4117	50.4	O	3	42	14.7	-19.19	14.21	-19.29			
NGC 7674	1	0	0	8698	114	2	4	23	13.92	-21.64	14.36	-20.89	49	3.8	43.87
NGC 7678	1	1	1	3500	42.1	2	5		12.66	-20.94	15.3	-17.81			

TABLE 1-A—*Continued*

Source (1)	M (2)	D (3)	S (4)	V (km s ⁻¹) (5)	Dist (Mpc) (6)	Class (7)	T (8)	Inc (degrees) (9)	m_B (10)	M_B (11)	m_V (12)	M_V (13)	S_{5007} (cgs) (14)	$S_{H\beta}$ (cgs) (15)	log P ₅₀₀₇ (cgs) (16)
NGC 7682	1	1	0	5120	64.0	2	3	36	14.1	-20.34	14.3	-19.71	23		43.05
IC 1495	1	1	0	6375	81.3	2	3	41	13.5						
NGC 7743	1	1	1	1710	24.4	L	-1	31	12.38	-19.78	13.28	-18.66	5.39	0.67	41.58
IC 1515	1	1	0	6726	85.9	2	2	33	14.45	-20.48					

NOTE.—This appendix lists some important parameters of the 364 galaxies observed for H₂O maser emission. The columns list (1) the source name, with galaxies detected as H₂O megamasers in boldface; (2 – 4) indicators showing whether the galaxy is a member of the magnitude-limited, distance-limited, or sensitivity-limited sample (a “1” is entered in the column if the galaxy is a member of the sample); (5) the recession velocity in km s⁻¹ primarily from the NED database; (6) the assumed luminosity distance in Mpc, derived from the recession velocity referred to the rest frame of the 3° K background radiation (according to the precepts in RC3) and based on $H_0 = 75$ km s⁻¹ Mpc⁻¹ and $q_0 = 0$, except for the nearest galaxies, the distances of which were taken from Tully (1988); (7) the AGN classification taken primarily from Huchra (1993) or Véron-Cetty & Véron (1991), where 1 = Seyfert 1, 2 = Seyfert 2, U = Unspecified Seyfert, L = LINER, R = Radio galaxy, and O = Other type; (8) the Hubble type index, primarily from RC3; (9) galactic inclination in degrees, from Whittle (1992) or derived from major and minor axis measurements (from NED) as described in the text; (10) apparent B magnitude from RC3 (B_T when available, otherwise m_B), Huchra (1993) or NED; (11) absolute B magnitude derived from apparent “face-on” magnitude (from RC3); (12) apparent nuclear V magnitude from Huchra (1993) or Véron-Cetty & Véron (1991); (13) absolute nuclear V magnitude; (14) [OIII] $\lambda 5007$ line flux in 10^{-14} erg s⁻¹ cm⁻² from Dahari & De Robertis (1988), Ho, Filippenko & Sargent (1993), Stauffer (1982) or Whittle (1992); (15) H β line flux in 10^{-14} erg s⁻¹ cm⁻² from Dahari & De Robertis (1988), Ho, Filippenko & Sargent (1993), Stauffer (1982) or Whittle (1992); (16) log of [OIII] $\lambda 5007$ line luminosity in erg s⁻¹ derived from column (14)

TABLE 1-B
PROPERTIES OF OBSERVED GALAXIES

Source (1)	S(12) (Jy) (2)	S(25) (Jy) (3)	S(60) (Jy) (4)	S(100) (Jy) (5)	P(12) (W Hz ⁻¹) (6)	P(25) (W Hz ⁻¹) (7)	P(60) (W Hz ⁻¹) (8)	P(100) (W Hz ⁻¹) (9)	S _{6cm} (mJy) (10)	log P _{6cm} (W Hz ⁻¹) (11)
Mrk 334	0.23	1.05	4.35	4.32	23.28	23.94	24.56	24.56	8.5	21.85
Mrk 335	0.30	0.38	0.34	<0.57	23.54	23.64	23.60	<23.		
Mrk 937	<0.14	<0.24	0.52	1.25	<23.34	<23.57	23.91	24.29		
Mrk 938	0.40	2.37	16.62	17.16	23.42	24.20	25.04	25.05		
0017-5133										
Mrk 945										
NGC 224	1.70	1.02	10.79	<140.9	20.00	19.78	20.80	<21.		
NGC 235A										
Mrk 348	0.31	0.84	1.29	1.55	23.06	23.50	23.69	23.77	480	23.26
Mrk 352										
ESO 079-G16	0.18	0.74	2.98	2.85	23.11	23.73	24.34	24.32		
NGC 404	<0.11	0.20	2.14	3.98	<19.10	20.15	21.17	21.44		
Tol 0109-383	1.10	1.74	1.80	1.82	23.39	23.59	23.60	23.61	14.9	21.52
IC 1657	<0.21	0.27	2.77	7.48	<22.68	22.80	23.81	24.24		
NGC 454	<0.21	<0.42	<1.48	2.82	<22.74	<23.04	<23.5	23.87		
Mrk 1	<0.19	0.87	2.53	2.92	<22.92	23.58	24.05	24.11	28	22.09
Mrk 565	<0.21	<0.14	1.50	3.42	<23.07	<22.89	23.92	24.28		
0120-0214	<0.14	0.30	1.69	2.30	<22.76	23.10	23.85	23.98		
NGC 513	0.17	0.28	1.94	4.05	23.06	23.28	24.12	24.44		
NGC 526A	0.28	0.45	0.22	<0.87	23.27	23.47	23.16		4	21.42
Mrk 993	<0.13	<0.13	0.30	1.32	<22.73	<22.72	23.08	23.73		
Mrk 359	0.12	0.44	1.13	1.74	22.76	23.32	23.73	23.92		
0129-3323	0.18	0.30	2.16	5.76	22.94	23.15	24.01	24.44		
NGC 600	<0.12	<0.17	0.56	2.57	<21.88	<22.02	22.55	23.21		
NGC 591	0.16	0.45	1.99	3.48	22.78	23.24	23.89	24.13	7.9	21.49
NGC 613	1.00	2.45	22.01	49.95	22.51	22.90	23.86	24.21		
Mrk 1158	<0.19	0.22	0.97	1.02	<22.89	22.94	23.58	23.61		
Mrk 573	<0.25	<0.93	1.09	1.26	<23.09	<23.66	23.73	23.79	5.5	21.43
0147-0740	0.31	<0.96	1.05	0.65	23.22	<23.71	23.75	23.54		
0152+0622	<0.08	<0.17	0.47	1.20	<22.59	<22.92	23.38	23.79		
IC 184	<0.10	<0.24	0.39	0.91	<22.75	<23.12	23.34	23.71		
NGC 788	0.19	<0.51	0.51	0.59	22.77	<23.21	23.21	23.27	1.2	20.58
ESO 153-IG16	<0.06	<0.05	0.26	<0.98	<22.60	<22.56	23.26	<23.		
ESO 153-G020	0.10	0.20	0.89	<3.02	22.84	23.15	23.81	<24.		
NGC 824										
4C 35.03										
NGC 863	0.19	0.22	0.49	1.46	23.38	23.44	23.79	24.26	3.5	21.64
Ark 79										
NGC 931	0.61	1.32	2.56	4.55	23.47	23.80	24.09	24.34		
Mrk 1044	0.10	0.22	0.43	0.88	22.68	23.00	23.31	23.62		
IC 1816	0.16	0.39	1.39	2.34	22.93	23.32	23.87	24.10		
NGC 1019	<0.14	<0.15	0.36	<1.37	<23.16	<23.18	23.57	<24.		
NGC 1052	0.20	0.49	0.90	1.52	21.89	22.27	22.53	22.76	1000	22.58
NGC 1068	39.70	85.04	176.20	224.00	23.99	24.32	24.64	24.75	1090	22.43
NGC 1097	1.99	5.51	44.54	85.34	22.70	23.14	24.05	24.33		
Mrk 372	<0.13	0.17	0.30	<0.19	<23.35	23.47	23.73	<23.		
Mrk 1058	<0.14	0.17	0.59	1.39	<22.86	22.95	23.48	23.86		
NGC 1125	0.17	0.83	3.31	3.94	22.55	23.23	23.83	23.91		

TABLE 1-B—*Continued*

Source (1)	S(12) (Jy) (2)	S(25) (Jy) (3)	S(60) (Jy) (4)	S(100) (Jy) (5)	P(12) (W Hz ⁻¹) (6)	P(25) (W Hz ⁻¹) (7)	P(60) (W Hz ⁻¹) (8)	P(100) (W Hz ⁻¹) (9)	S _{6cm} (mJy) (10)	log P _{6cm} (W Hz ⁻¹) (11)
NGC 1144	0.28	0.63	5.30	11.34	23.62	23.98	24.90	25.24		
Mrk 1066	0.45	2.26	10.98	12.15	23.05	23.75	24.44	24.48	35.5	21.95
NGC 1167										
H0258-015										
NGC 1194	0.27	0.51	0.77	<0.93	22.90	23.19	23.37	<23.		
NGC 1241	0.24	0.45	3.59	10.32	22.88	23.15	24.05	24.51		
Mrk 1073	0.44	1.41	8.17	11.11	23.64	24.15	24.91	25.04		
0314-2303	0.09	0.15	0.71	1.96	22.46	22.66	23.33	23.77		
NGC 1275	1.07	3.54	7.15	6.98	23.77	24.29	24.60	24.59		
NGC 1301	<0.09	0.11	0.52	2.01	<22.47	22.52	23.21	23.80		
NGC 1326	0.32	0.78	8.06	13.31	22.03	22.43	23.44	23.66		
Mrk 607	0.33	1.07	2.15	2.75	22.75	23.26	23.56	23.67		

TABLE 1-B—Continued

Source (1)	S(12) (Jy) (2)	S(25) (Jy) (3)	S(60) (Jy) (4)	S(100) (Jy) (5)	P(12) (W Hz ⁻¹) (6)	P(25) (W Hz ⁻¹) (7)	P(60) (W Hz ⁻¹) (8)	P(100) (W Hz ⁻¹) (9)	S _{6cm} (mJy) (10)	log P _{6cm} (W Hz ⁻¹) (11)
MCG -2-9-40	<0.12	0.33	1.38	3.53	<22.67	23.11	23.74	24.15		
Mrk 612	0.13	0.27	1.16	1.81	22.97	23.30	23.93	24.12		
NGC 1358	<0.08	<0.12	0.38	0.93	<22.42	<22.59	23.08	23.47	1.2	20.58
NGC 1365	3.37	10.82	76.13	142.50	23.06	23.57	24.42	24.69	191	21.81
NGC 1386	0.49	1.43	5.40	9.64	22.23	22.69	23.27	23.52	13	20.65
III Zw 55	<0.12	0.19	0.87	2.18	<23.14	23.33	24.00	24.40		
0339-2124	0.25	0.10	0.60	1.49	22.97	22.57	23.36	23.75		
NGC 1433	0.24	0.23	3.49	14.23	21.58	21.57	22.75	23.36		
NGC 1566	0.83	1.22	14.71	46.36	22.25	22.42	23.50	24.00		
0425-0440	0.16	1.41	4.13	3.30	22.84	23.80	24.26	24.17		
ESO 202-G23	0.08	0.20	1.87	3.58	22.63	23.01	23.98	24.27		
NGC 1598	0.11	0.19	1.40	4.22	22.80	23.01	23.89	24.37		
0438-0828	0.43	1.62	2.77	2.53	23.26	23.84	24.07	24.03		
NGC 1672	1.67	4.03	32.96	69.89	22.62	23.01	23.92	24.25		
NGC 1667	0.43	0.68	5.95	14.73	23.27	23.47	24.41	24.80	1	20.64
H0448-041										
NGC 1685	<0.10	0.22	0.98	1.53	<22.62	22.97	23.62	23.82		
0450-0317	0.12	0.38	0.83	1.23	22.76	23.25	23.59	23.76		
0456+04	0.09	0.27	1.61	3.20	22.64	23.10	23.88	24.18		
ESO 033-G02	0.21	0.45	0.68	<2.08	23.12	23.45	23.63	<24.		
0459+0328										
NGC 1808	4.44	16.14	87.81	137.20	22.79	23.35	24.09	24.28		
UGC 3255	<0.25	<0.25	1.14	2.58	<23.23	<23.23	23.89	24.25		
ESO 362-G8	0.07	0.18	0.64	<1.50	22.51	22.95	23.50	<23.		
H0510+031										
Ark 120	0.32	0.41	0.64	1.08	23.83	23.93	24.13	24.36		
0517-3242	0.22	0.57	1.40	1.99	22.84	23.24	23.63	23.79		
NGC 2110	0.35	0.84	4.13	5.68	22.61	22.99	23.68	23.82	170	22.30
MCG 8-11-11	0.64	1.95	3.01	4.24	23.71	24.20	24.38	24.53	71	22.76
Mrk 3	0.71	2.90	3.77	3.36	23.38	23.99	24.11	24.06	361	23.09
NGC 2273	0.40	1.36	6.02	10.00	22.59	23.12	23.76	23.98	19	21.26
Mrk 6	0.22	0.69	1.18	<1.66	23.21	23.69	23.93	<24.	100	22.86
0648+458	<0.17	0.44	2.24	3.41	<23.21	23.61	24.31	24.50		
Mrk 376	0.25	0.51	0.81	1.39	24.18	24.49	24.69	24.92		
0714-2914	0.44	1.77	4.40	6.04	22.48	23.09	23.48	23.62	28.2	21.29
NGC 2377	0.42	0.95	8.93	17.94	22.71	23.06	24.03	24.34		
Mrk 78	0.13	0.56	1.11	1.13	23.54	24.17	24.48	24.48	12	22.51
Mrk 79	0.31	0.76	1.50	2.36	23.47	23.87	24.16	24.36	4.2	21.61
UGC 3995A	0.22	0.31	0.56	1.99	23.06	23.20	23.46	24.01		
Mrk 10	0.14	0.22	0.81	1.95	23.37	23.56	24.13	24.51		
Mrk 1210	0.50	2.08	1.89	1.30	23.29	23.91	23.87	23.71		
Mrk 622	<0.19	0.41	1.28	1.43	<23.31	23.64	24.14	24.19		
0816+2116	<0.20	0.23	0.81	2.09	<23.14	23.21	23.75	24.16		
ESO 018-G009	0.17	0.42	<2.17	<8.10	23.03	23.42	<24.1	<24.		
NGC 2639	0.16	0.21	1.99	7.06	22.61	22.72	23.70	24.25	54.5	22.14
TON 951										
NGC 2655	0.18	0.21	1.67	4.98	22.10	22.18	23.08	23.55		
NGC 2681	0.27	0.56	6.19	11.77	21.75	22.08	23.12	23.40		

TABLE 1-B—*Continued*

TABLE 1-B—Continued

Source (1)	S(12) (Jy) (2)	S(25) (Jy) (3)	S(60) (Jy) (4)	S(100) (Jy) (5)	P(12) (W Hz ⁻¹) (6)	P(25) (W Hz ⁻¹) (7)	P(60) (W Hz ⁻¹) (8)	P(100) (W Hz ⁻¹) (9)	S _{6cm} (mJy) (10)	log P _{6cm} (W Hz ⁻¹) (11)
Mrk 1419	<0.13	<0.26	0.71	1.66	<22.89	<23.18	23.62	23.99		
0939+2355	<0.15	0.33	0.62	0.72	<23.17	23.50	23.77	23.84		
0942+09									<0.4	<20.17
NGC 2992	0.49	1.26	<8.50	<29.36	22.74	23.15	<23.9	<24.	77	21.93
0945-30									6	21.00
ESO 373-G29										
NGC 2985	0.42	0.46	5.00	19.94	22.40	22.44	23.48	24.08		
NGC 3010B										
NGC 3032	<0.25	0.19	1.78	4.26	<22.26	22.13	23.11	23.49		
Mrk 1239	0.65	1.14	1.23	<0.24	23.72	23.96	23.99	<23.		
NGC 3031	0.75	0.78	6.81	32.03	20.24	20.26	21.20	21.88	58	19.13
NGC 3081									0.9	20.06
NGC 3079	1.52	2.27	44.50	89.22	22.88	23.05	24.35	24.65	78	21.59
ESO 374-G025										
NGC 3125	0.20	0.79	5.04	5.13	21.92	22.51	23.32	23.33		
NGC 3169	0.59	0.56	6.51	20.55	22.44	22.41	23.48	23.98		
IC 2560	0.30	0.94	3.24	6.11	22.80	23.31	23.84	24.12		
NGC 3185	0.16	0.14	1.43	3.67	21.93	21.88	22.89	23.30		
H1016+336										
NGC 3227	0.67	1.76	7.83	17.59	22.53	22.95	23.60	23.95	34	21.24
ESO 568-G11	<0.07	<0.19	0.56	1.32	<23.12	<23.53	24.02	24.39		
NGC 3281	0.89	2.63	6.86	7.51	23.42	23.90	24.31	24.35	26.7	21.90
1034+0609	<0.16	<0.25	0.39	<0.11	<22.71	<22.89	23.08	<22.	<0.4	<20.09
NGC 3312	<0.18	<0.17	0.82	3.36	<22.71	<22.68	23.36	23.98		
NGC 3362										
NGC 3367	0.48	1.09	6.01	12.56	23.06	23.42	24.16	24.48		
NGC 3393	0.13	0.75	2.25	3.87	22.66	23.42	23.90	24.13		
ESO 215-G014	<0.32	<0.25	0.34	<8.61	<23.36	<23.25	23.39	<24.		
NGC 3516	0.43	0.89	1.76	2.26	22.89	23.21	23.50	23.61	4.3	20.89
Fair 1150	0.13	0.24	1.00	2.93	22.46	22.74	23.35	23.82		
Mrk 732	0.16	<0.25	1.75	3.39	23.45	<23.65	24.49	24.78		
NGC 3627	4.96	7.83	67.80	137.44	22.41	22.61	23.55	23.86		
NGC 3642	0.13	0.10	1.44	4.58	22.06	21.95	23.11	23.62		
NGC 3660	0.19	0.22	1.87	4.54	22.83	22.89	23.81	24.20		
1121-2806	0.16	0.34	0.57	<0.84	22.82	23.14	23.36	<23.		
NGC 3665	<0.25	<0.26	2.00	6.37	<22.50	<22.51	23.40	23.90		
Mrk 40										
ESO 439-G009	<0.16	0.31	0.65	1.04	<23.30	23.60	23.92	24.13		
NGC 3718	0.17	0.10	0.70	2.29	21.77	21.53	22.38	22.90		
NGC 3783	0.84	2.49	3.26	4.90	23.27	23.74	23.86	24.04	13	21.46
NGC 3786									3.4	20.85
Mrk 745									<0.5	<20.12
NGC 3884										
NGC 3898	0.11	<0.07	0.42	2.02	21.80	<21.63	22.38	23.06		
NGC 3921	<0.12	0.11	0.83		<22.96	22.92	23.81			
Fair 1151	0.53	2.32	32.68	41.62	23.15	23.79	24.94	25.04		
Mrk 42	<0.10	<0.14	0.32	<0.91	<23.06	<23.21	23.57	<24.		
NGC 3982	0.51	0.83	6.57	15.23	22.24	22.46	23.36	23.72	2.2	19.88

TABLE 1-B—*Continued*

Source (1)	S(12) (Jy) (2)	S(25) (Jy) (3)	S(60) (Jy) (4)	S(100) (Jy) (5)	P(12) (W Hz ⁻¹) (6)	P(25) (W Hz ⁻¹) (7)	P(60) (W Hz ⁻¹) (8)	P(100) (W Hz ⁻¹) (9)	S _{6cm} (mJy) (10)	log P _{6cm} (W Hz ⁻¹) (11)
NGC 3998	0.14	0.16	0.44	0.93	21.89	21.95	22.39	22.72		
Mrk 1310										
NGC 4036	0.09	<0.10	0.50	1.45	21.79	<21.85	22.56	23.02		
Was 41										
NGC 4051	0.86	1.59	7.13	23.92	22.47	22.74	23.39	23.92	6	20.32
NGC 4074										
Was 45	0.17	0.38	2.75	5.57	23.34	23.69	24.55	24.85		
NGC 4111										
NGC 4117									<0.6	<19.31
Mrk 198	<0.12	0.14	0.62	0.86	<23.15	23.20	23.86	24.00		
NGC 4151									125	21.79
NGC 4192	0.36	0.44	5.92	19.68	22.08	22.17	23.30	23.82		

TABLE 1-B—Continued

Source (1)	S(12) (Jy) (2)	S(25) (Jy) (3)	S(60) (Jy) (4)	S(100) (Jy) (5)	P(12) (W Hz ⁻¹) (6)	P(25) (W Hz ⁻¹) (7)	P(60) (W Hz ⁻¹) (8)	P(100) (W Hz ⁻¹) (9)	S _{6cm} (mJy) (10)	log P _{6cm} (W Hz ⁻¹) (11)
Mrk 201	0.83	46.77	21.38	25.88	23.18	24.93	24.59	24.68	38	21.84
Was 49B										
NGC 4235	0.00	0.00	0.32	0.65			22.67	22.98	5.3	20.89
NGC 4253	0.39	1.30	4.03	4.66	23.14	23.67	24.16	24.22	15.1	21.73
NGC 4258	2.25	2.81	21.60	78.39	22.10	22.19	23.08	23.64	1.8	19.00
NGC 4261										
NGC 4278	<0.19	<0.08	0.56	1.57	<21.33	<20.98	21.80	22.25	290	21.51
NGC 4303	1.06	1.40	23.64	64.65	22.47	22.59	23.82	24.25		
Mrk 50										
NGC 4388	1.00	3.46	10.24	18.10	22.53	23.07	23.54	23.79	76	21.41
NGC 4395	<0.13	0.21	2.38	6.34	<20.30	20.50	21.57	21.99		
NGC 4418	0.93	9.32	40.68	32.80	23.10	24.10	24.74	24.65		
NGC 4419	0.54	1.44	7.99	16.85	22.26	22.69	23.43	23.76		
NGC 4438	0.21	0.17	3.76	11.27	21.85	21.77	23.10	23.58		
NGC 4450	0.11	<0.13	1.34	6.95	21.57	<21.64	22.66	23.37		
NGC 4486	0.23	<0.24	0.39	<1.02	21.89	<21.91	22.12	<22.		
NGC 4501	1.02	1.28	13.71	54.65	22.54	22.64	23.67	24.27		
NGC 4507	0.46	1.39	4.31	5.40	23.14	23.63	24.12	24.22		
NGC 4569	0.48	1.05	7.56	23.66	22.21	22.55	23.41	23.90		
NGC 4579	0.35	0.38	4.74	18.09	22.07	22.11	23.20	23.79		
NGC 4593	0.34	0.81	3.05	5.95	22.81	23.18	23.76	24.05	1.6	20.48
NGC 4594	0.39	0.50	3.11	14.13	22.27	22.38	23.17	23.83		
Tol 74	0.64	2.26	7.52	10.73	23.25	23.80	24.32	24.47	>13.6	>21.57
NGC 4639	<0.18	<0.22	1.41	4.63	<21.78	<21.88	22.68	23.19		
1243+26										
ESO 172-G010	<0.26	0.26	2.37	3.99	<22.28	22.28	23.24	23.46		
NGC 4696										
1249-1308	0.17	0.37	1.16	2.22	22.91	23.24	23.74	24.02		
ESO 323-G32	0.11	0.31	0.99	1.91	22.77	23.22	23.73	24.01		
NGC 4785	0.31	0.48	3.64	10.47	23.02	23.21	24.09	24.55		
Mrk 231	1.87	8.66	31.99	30.29	24.79	25.46	26.02	26.00	170	23.75
NGC 4826	1.91	2.54	34.38	74.50	21.59	21.71	22.84	23.18		
1254+27										
1255-2930	0.24	0.93	5.96	7.92	22.76	23.35	24.15	24.28		
NGC 4903	<0.11	0.29	0.77	2.40	<22.81	23.23	23.65	24.15		
NGC 4922B	0.23	1.29	5.73	7.54	23.43	24.17	24.82	24.94		
1300-3158	<0.12	<0.15	0.58	2.16	<22.84	<22.91	23.51	24.09		
NGC 4941	0.19	0.53	1.38	4.19	20.96	21.41	21.83	22.31	4.3	19.32
NGC 4945	3.95	14.45	359.30	620.50	22.11	22.67	24.07	24.30		
1303-4008	0.68	1.22	5.66	8.79	23.51	23.77	24.43	24.62		
ESO 508-G05	<0.13	<0.15	0.82	2.31	<22.46	<22.53	23.26	23.71		
NGC 4968	0.39	1.05	2.38	2.94	22.96	23.38	23.74	23.83		
1305-2407	<0.15	0.67	1.44	1.49	<22.80	23.47	23.80	23.81		
NGC 5005	0.95	1.21	19.65	54.26	22.71	22.82	24.03	24.47		
NGC 5033	0.95	1.15	13.80	43.85	22.60	22.68	23.76	24.26	3.3	20.14
IC 4218										
1314-1532										
IC 4214	0.27	0.39	4.28	11.12	22.58	22.73	23.78	24.19		

TABLE 1-B—*Continued*

Source (1)	S(12) (Jy) (2)	S(25) (Jy) (3)	S(60) (Jy) (4)	S(100) (Jy) (5)	P(12) (W Hz ⁻¹) (6)	P(25) (W Hz ⁻¹) (7)	P(60) (W Hz ⁻¹) (8)	P(100) (W Hz ⁻¹) (9)	S _{6cm} (mJy) (10)	log P _{6cm} (W Hz ⁻¹) (11)
NGC 5077										
NGC 5101	0.12	<0.17	0.89	3.57	22.01	<22.18	22.90	23.51		
1319-1627	0.88	2.86	5.90	5.48	23.73	24.24	24.55	24.52		
1321+31										
1322+2918										
NGC 5128	13.26	17.26	162.20	313.80	22.58	22.70	23.67	23.96		
NGC 5135	0.64	2.40	16.91	28.64	23.42	23.99	24.84	25.07	58.8	22.38
NGC 5194	1.80	2.61	32.68	137.70	22.11	22.27	23.37	23.99	1.65	19.07
NGC 5195	0.72	1.45	10.35	<74.38	21.87	22.18	23.03	<23.		
IC 894										
1331-2325	<0.07	<0.26	0.83	<3.86	<22.13	<22.67	23.18	<23.		
MCG -6-30-15	0.38	0.81	1.09	1.10	22.74	23.07	23.20	23.20	1	20.16

TABLE 1-B—*Continued*

TABLE 1-B—*Continued*

TABLE 1-B—Continued

Source (1)	S(12) (Jy) (2)	S(25) (Jy) (3)	S(60) (Jy) (4)	S(100) (Jy) (5)	P(12) (W Hz ⁻¹) (6)	P(25) (W Hz ⁻¹) (7)	P(60) (W Hz ⁻¹) (8)	P(100) (W Hz ⁻¹) (9)	S _{6cm} (mJy) (10)	log P _{6cm} (W Hz ⁻¹) (11)
ESO 139-G012	0.12	0.17	0.66	1.61	22.85	23.00	23.58	23.97		
1736+32										
Ark 524										
1752+32										
NGC 6500	0.10	0.10	0.64	2.55	22.27	22.27	23.07	23.67		
1827+32										
Ark 539										
1832-5926	0.62	1.39	3.23	3.91	23.68	24.03	24.40	24.48		
ESO 103-G35	0.61	2.36	2.31	1.05	23.31	23.90	23.89	23.55		
IC 4729	0.12	0.16	1.43	4.49	22.69	22.81	23.77	24.27		
Fair 182	<0.11	0.19	0.93	1.84	<22.41	22.63	23.33	23.62		
Fair 51	<0.47	1.04	1.84	2.79	<23.24	23.58	23.84	24.02		
IC 4777	<0.09	<0.14	0.61	0.97	<22.78	<22.97	23.60	23.79		
3C 390.3	0.13	0.29	0.20	<0.62	23.88	24.23	24.08	<24.		
Padova I										
NGC 6764	0.36	1.29	6.33	11.56	22.77	23.33	24.02	24.28	35	21.76
Fair 1163										
NGC 6814	<0.49	0.60	5.52	18.88	<22.48	22.57	23.54	24.07	2.2	20.14
1953+0916	<0.66	<0.25	0.52	<7.38	<23.81	<23.39	23.71	<24.		
Cyg A	<0.25	1.06	2.33	<8.28	<24.17	24.80	25.14	<25.		
NGC 6860	0.24	0.33	0.95	2.47	22.99	23.13	23.59	24.00		
20100-4156										
NGC 6890	0.34	0.65	3.86	8.16	22.62	22.90	23.67	23.99	4.2	20.71
IC 4995	0.09	0.33	0.83	1.25	22.58	23.17	23.57	23.75		
2031-307										
NGC 6951	0.62	1.37	13.21	37.47	22.63	22.98	23.96	24.42		
Mrk 509	0.32	0.70	1.36	1.52	23.82	24.17	24.46	24.50	4.5	21.98
IC 5063	1.07	3.91	5.34	4.17	23.38	23.95	24.08	23.97		
NGC 7052	<0.25	<0.25	0.45	1.48	<23.06	<23.06	23.31	23.83		
IC 5135	0.59	2.12	16.48	25.57	23.42	23.97	24.87	25.06		
2157-3357	<0.12	<0.16	0.42	1.05	<22.65	<22.78	23.20	23.60		
2159-2244	<0.12	<0.18	0.25	0.70	<22.80	<22.97	23.12	23.57		
NGC 7172	0.44	0.76	5.71	12.29	22.78	23.02	23.90	24.23	1.8	20.39
ESO 108-G10	<0.10	0.13	1.00	1.64	<22.31	22.42	23.30	23.51		
NGC 7212	0.20	0.77	2.89	4.90	23.36	23.96	24.53	24.76		
NGC 7217	0.38	0.30	4.96	18.45	22.06	21.96	23.18	23.75		
NGC 7213	0.61	0.74	2.67	8.18	22.55	22.63	23.19	23.68		
NGC 7214	0.16	0.37	1.92	5.33	23.16	23.53	24.24	24.68		
ESO 108-IG017	<0.09	0.20	1.37	2.17	<21.80	22.16	23.00	23.20		
3C 449										
NGC 7314	0.27	0.58	3.74	14.15	22.03	22.37	23.18	23.75	1.9	19.88
NGC 7319	<0.16	<0.23	0.88	2.54	<23.12	<23.29	23.87	24.33		
Mrk 915	<0.17	0.35	0.46	1.01	<23.25	23.56	23.67	24.01		
2236+35										
2237+0747	0.20	0.34	0.83	<2.48	23.34	23.57	23.95	<24.		
Mrk 917	0.19	0.61	3.71	5.95	23.29	23.80	24.59	24.79		
Ark 564	<0.30	0.57	0.83	1.14	<23.50	23.78	23.94	24.08	11	22.07
NGC 7410	0.11	<0.08	0.71	2.97	21.71	<21.61	22.54	23.16		

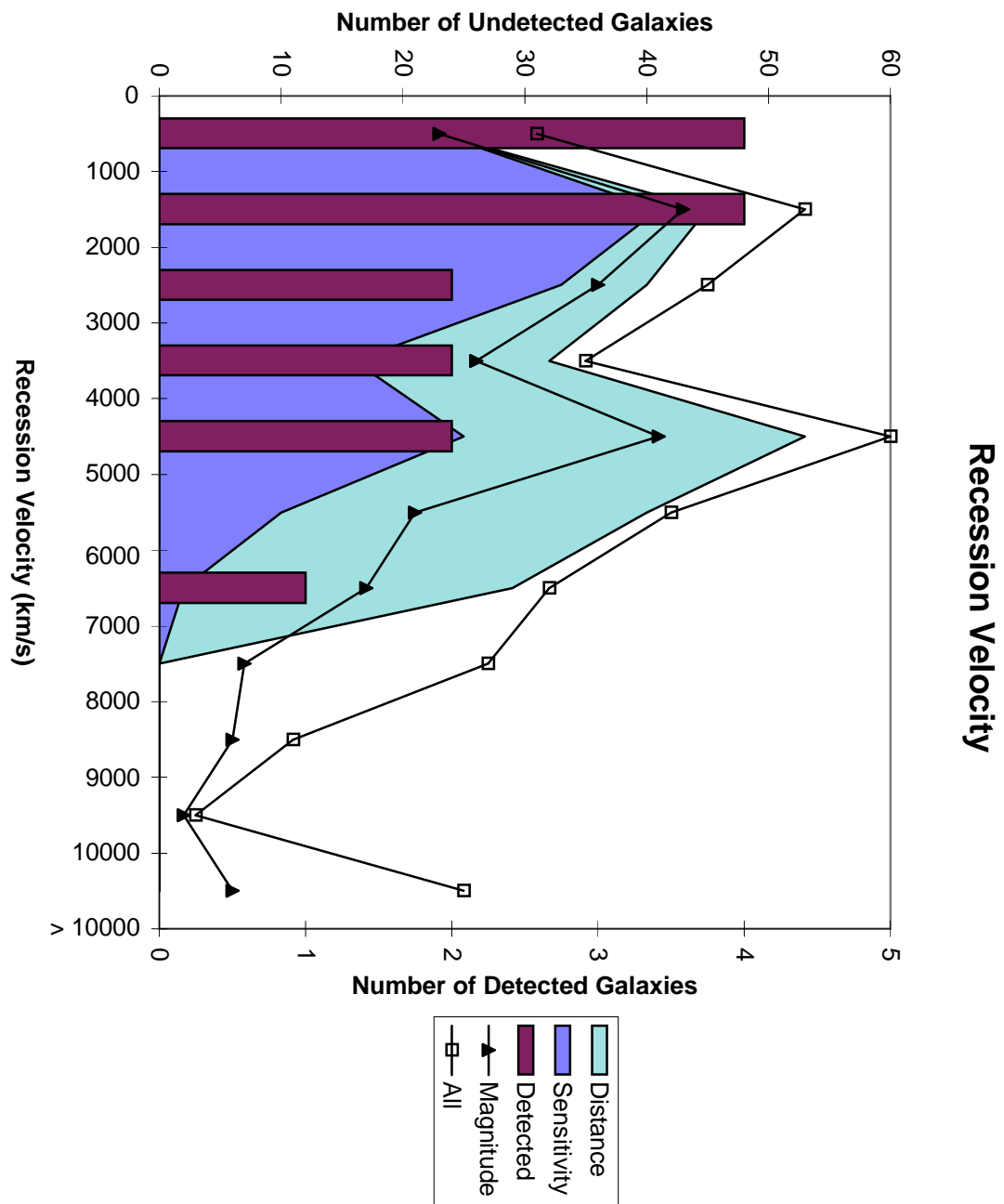
TABLE 1-B—*Continued*

Source (1)	S(12) (Jy) (2)	S(25) (Jy) (3)	S(60) (Jy) (4)	S(100) (Jy) (5)	P(12) (W Hz ⁻¹) (6)	P(25) (W Hz ⁻¹) (7)	P(60) (W Hz ⁻¹) (8)	P(100) (W Hz ⁻¹) (9)	S _{6cm} (mJy) (10)	log P _{6cm} (W Hz ⁻¹) (11)
NGC 7450									1.7	20.47
Mrk 313	0.28	0.39	<4.94	<13.70	22.19	22.33	<23.4	<23.		
NGC 7469	1.35	5.79	25.87	34.90	23.77	24.40	25.05	25.18	65	22.45
NGC 7479	0.88	3.68	12.84	23.56	23.04	23.67	24.21	24.47		
NGC 7496	0.35	1.60	8.46	15.55	22.22	22.89	23.61	23.88		
NGC 7582	1.62	6.44	49.10	72.92	22.78	23.38	24.26	24.43	69	21.41
NGC 7592	0.28	0.90	7.80	10.25	23.46	23.97	24.91	25.02		
NGC 7590	0.56	0.83	6.91	<23.70	22.30	22.47	23.39	<23.		
IC 1481	<0.13	0.28	1.41	1.51	<22.98	23.29	24.00	24.03		
NGC 7672	<0.09	<0.15	0.46	<2.46	<22.44	<22.67	23.14	<23.	1	20.48
NGC 7674	0.67	1.90	5.59	8.15	24.00	24.45	24.92	25.09		
NGC 7678	0.41	0.87	6.59	14.69	22.93	23.26	24.14	24.49		

TABLE 1-B—*Continued*

Source (1)	S(12) (Jy) (2)	S(25) (Jy) (3)	S(60) (Jy) (4)	S(100) (Jy) (5)	P(12) (W Hz ⁻¹) (6)	P(25) (W Hz ⁻¹) (7)	P(60) (W Hz ⁻¹) (8)	P(100) (W Hz ⁻¹) (9)	S _{6cm} log P _{6cm} (mJy W Hz ⁻¹) (10)	log P _{6cm} (11)
NGC 7682										
IC 1495	<0.12	<0.36	0.94	<4.27	<22.97	<23.44	23.86	<24.		
NGC 7743	<0.11	<0.20	0.79	2.53	<21.90	<22.15	22.75	23.26		
IC 1515	<0.15	<0.23	0.57	1.33	<23.12	<23.31	23.69	24.06		

NOTE.—This appendix lists some important parameters of the 364 galaxies observed for H₂O maser emission. The columns list (1) the source name, with galaxies detected as H₂O megamasers in boldface; (2 – 5) the IRAS flux at 12, 25, 60 and 100 μm , in Jy, from the IRAS Faint Source Catalog (e.g. Moshir et al. 1989); (6 – 9) the log of power derived from the IRAS fluxes at 12, 25, 60 and 100 μm , in W Hz⁻¹; (10) the 6 cm nuclear radio continuum flux in mJy from Unger et al. 1987, Ulvestad & Wilson 1984a, 1984b, or 1989; (11) the log of power, in W Hz⁻¹, derived from the 6 cm nuclear radio continuum flux.



$\langle V/V_m \rangle$ for the Distance-Limited Sample

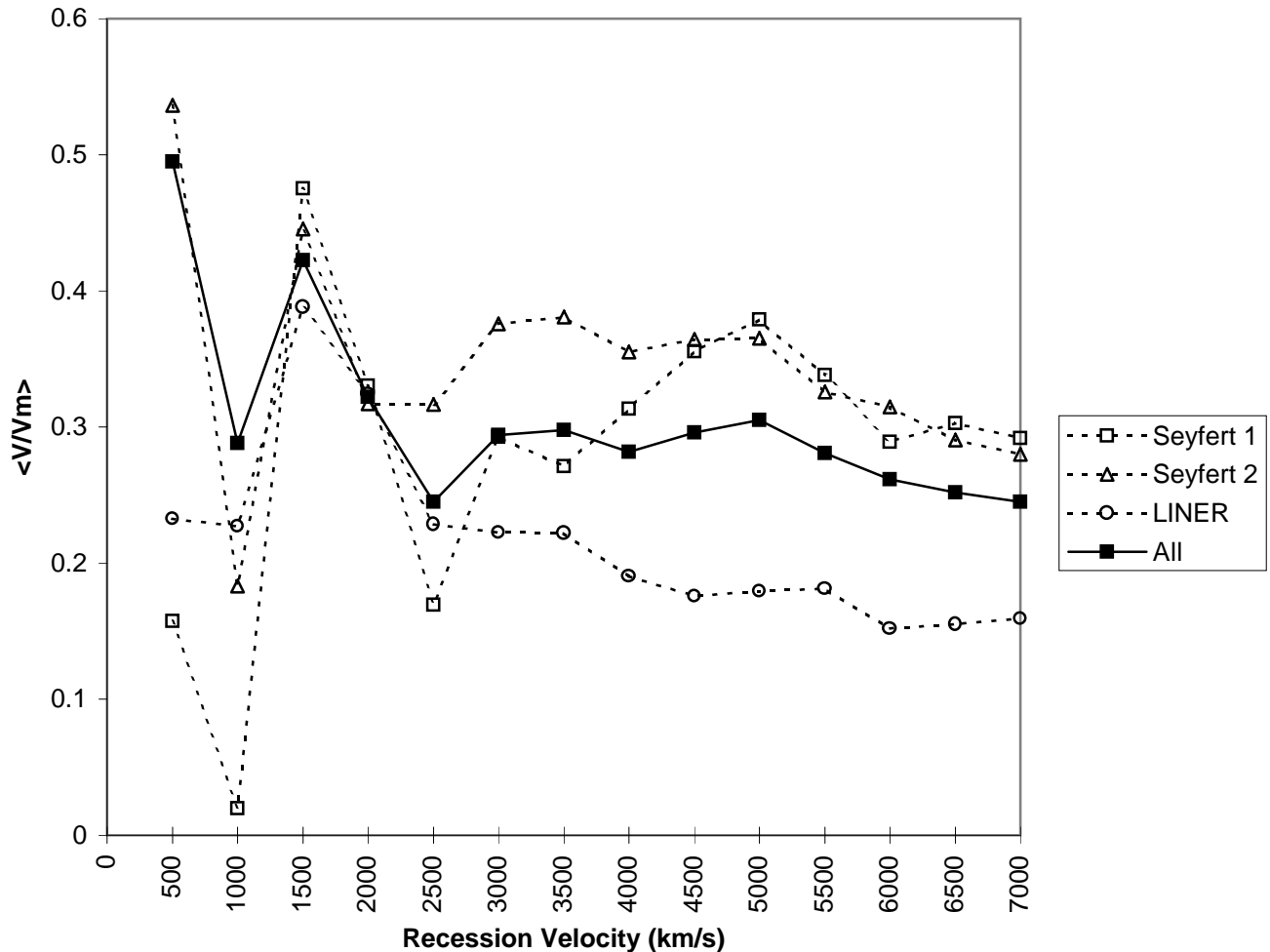


TABLE 3
RESULTS OF STATISTICAL COMPARISONS

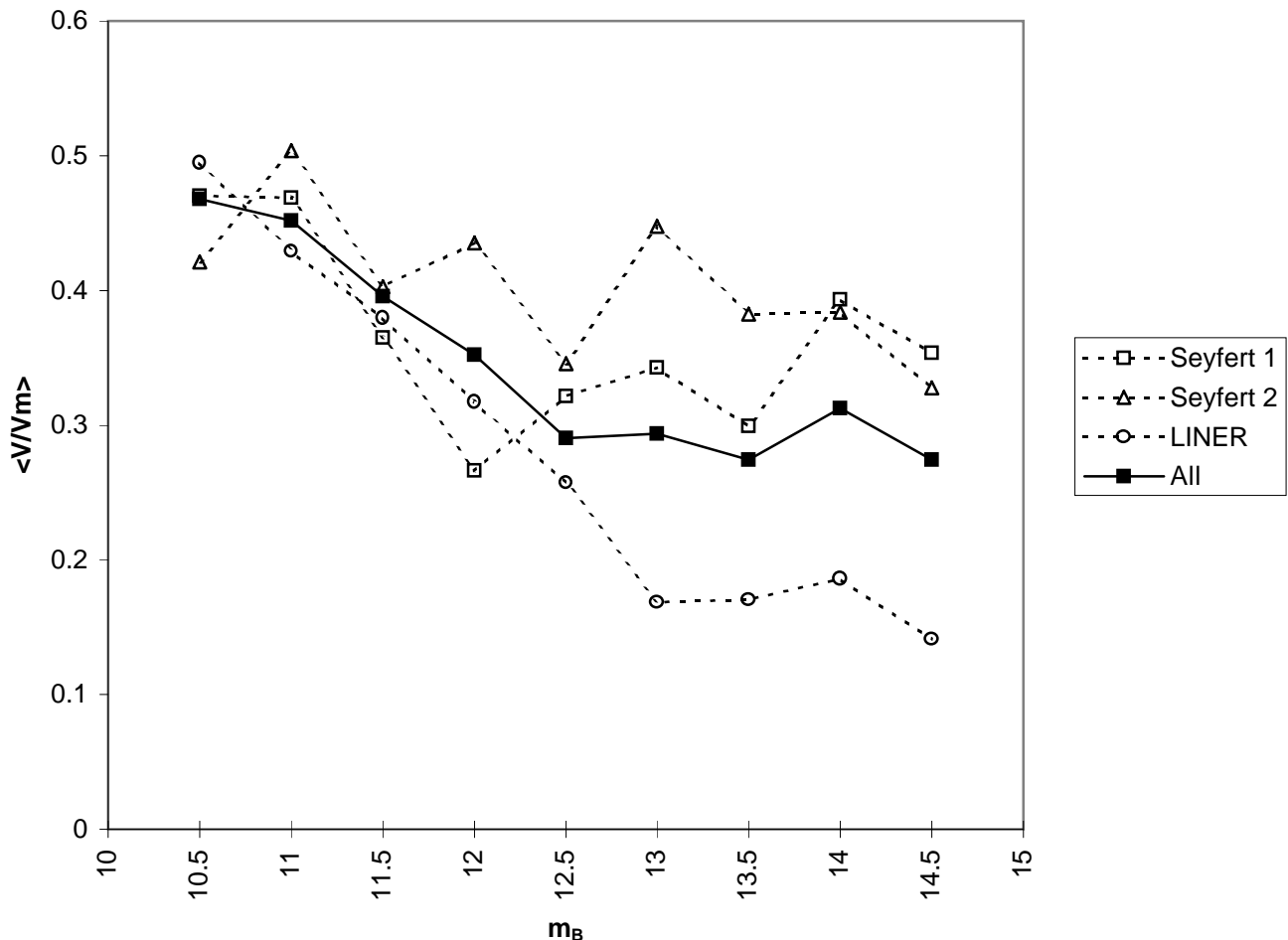
Prop (1)	Fig (2)	Det Gal's (3)	M (4)	D (5)	S (6)	Cens Entries (7)	K-S (8)	Gehan A (9)	Gehan B (10)	Logrank (11)	P-P (12)	P-Pr (13)
Recession Velocity	2	15	228	263	150	-	.09	.01	<.01	.01	-	-
Recession Velocity ^a	2	15	228	263	150	-	.65	.42	.39	.72	-	-
m_B	6	15	228	252	149	-	.10	.10	.07	.14	-	-
m_B^a	6	15	228	252	149	-	.84	.79	.78	.81	-	-
m_B^b	-	15	-	187	-	-	.07	.09	.06	.13	-	-
M_B	7	15	192	201	128	51	-	.12	.11	.11	.12	.13
M_B^b	-	15	-	187	-	38	-	.13	.12	.13	.13	.14
Hubble T	8	13	203	207	128	-	-	.47	.49	.58	-	-
Inclination	9	14	192	210	132	-	.12	.19	.21	.06	-	-
Inclination ^b	-	14	-	165	-	-	.13	.18	.20	.03	-	-
IRAS S(12)	13	13	165	158	101	58	-	<.01	<.01	<.01	<.01	<.01
IRAS P(12)	14	13	165	158	101	58	-	.51	.50	.28	.48	.49
IRAS S(25)	15	15	163	170	100	44	-	<.01	<.01	<.01	<.01	<.01
IRAS P(25)	16	15	163	170	100	44	-	.13	.11	.05	.12	.13
IRAS S(60)	17	15	195	210	124	5	-	.01	<.01	<.01	.01	.01
IRAS P(60)	18	15	195	210	124	5	-	.25	.23	.25	.25	.25
IRAS S(100)	19	15	177	186	113	28	-	.12	.09	.18	.13	.10
IRAS P(100)	20	15	177	186	113	28	-	.98	.98	.70	>.99	>.99
IRAS S(12)/S(25)	22	13	-	146	-	-	.34	.22	.19	.13	-	-
IRAS S(60)/S(100)	23	15	176	185	113	-	.02	.01	.03	.01	-	-
IRAS S(60)/S(100) ^b	24	15	-	140	-	-	.02	.02	.03	.02	-	-
IRAS S(25)/S(60)	25	15	160	166	97	-	.13	.16	.18	.12	-	-
Nuclear m_V	26	13	198	218	137	-	.17	.26	.21	.47	-	-
Nuclear M_V	27	13	198	218	137	-	.44	.25	.28	.29	-	-
S(6 cm)	28	9	56	54	42	6	-	.04	.02	.03	.04	.03
P(6 cm)	29	9	56	54	42	6	-	.12	.08	.51	.13	.10
S([OIII])	30	8	112	113	81	-	.59	.48	.49	.18	-	-
P([OIII])	31	8	112	113	81	-	.52	.39	.35	.65	-	-
Total sample	-	15	228	263	150	-	-	-	-	-	-	-

^aThe significance values in these rows describe a comparison between the galaxies detected in H₂O maser emission and the undetected galaxies in the sensitivity-limited sample. The values in all other rows describe a comparison of the detected galaxies with the undetected galaxies in the distance-limited sample.

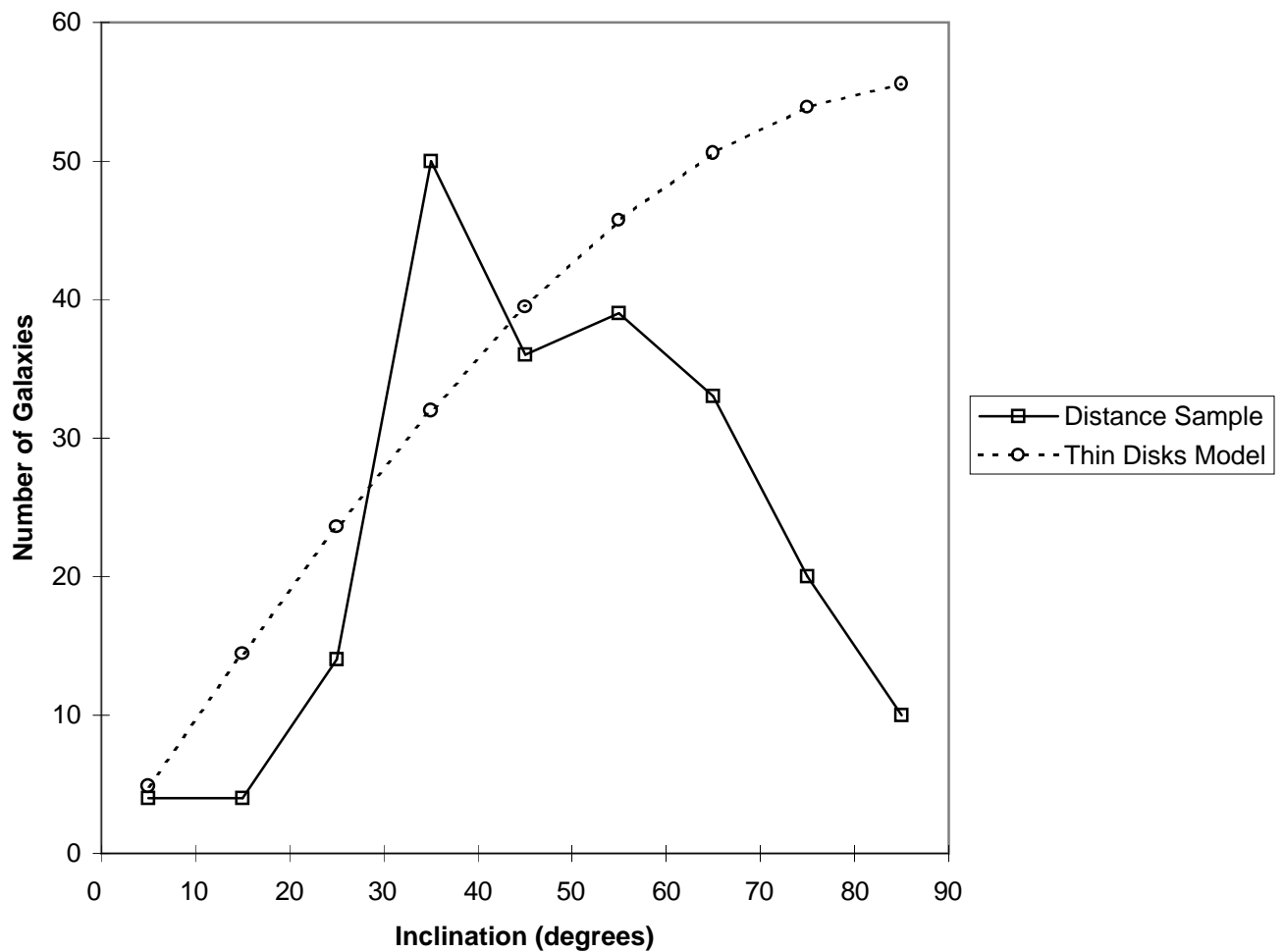
^bIn these rows, the H₂O-detected galaxies are compared to the undetected galaxies from the distance-limited sample which are classified as either a Seyfert 2 or LINER (i.e. Seyfert 1s are omitted).

NOTE.—The columns list (1) the physical property being compared, (2) the corresponding figure showing a histogram of the comparison, (3) the number of detected H₂O maser galaxies included in the comparison, (4) the number of undetected galaxies from the magnitude-limited sample represented in the histogram, (5) the number of undetected galaxies from the distance-limited sample represented in the histogram, (6) the number of undetected galaxies from the sensitivity-limited sample represented in the histogram, (7) the number of censored data values (i.e. only a limit, rather than a detection, is available) used in the statistical calculations (8) the probability that one parent population would produce the detected and undetected galaxy samples, based on the Kolmogorov-Smirnov test, (9) the probability that one parent population would produce the detected and undetected galaxy samples, based on Gehan's generalized Wilcoxon test with permutation variance, (10) the probability that one parent population would produce the detected and undetected galaxy samples, based on Gehan's generalized Wilcoxon test with hypergeometric variance, (11) the probability that one parent population would produce the detected and undetected galaxy samples, based on the logrank test, (12) the probability that one parent population would produce the detected and undetected galaxy samples, based on the Peto-Peto test, (13) the probability that one parent population would produce the detected and undetected galaxy samples, based on the Peto-Prentice test.

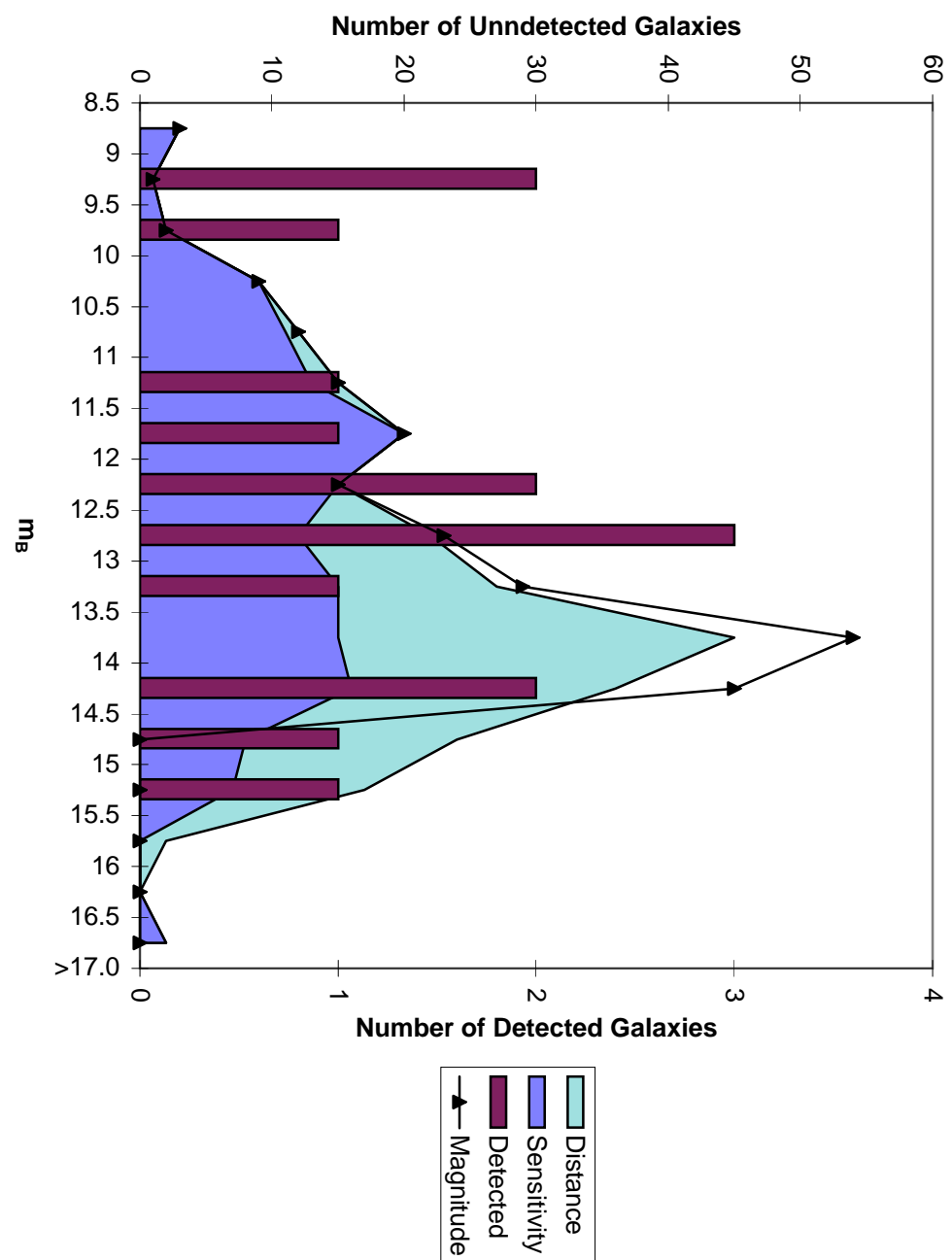
<V/V_m> for Magnitude-Limited Sample



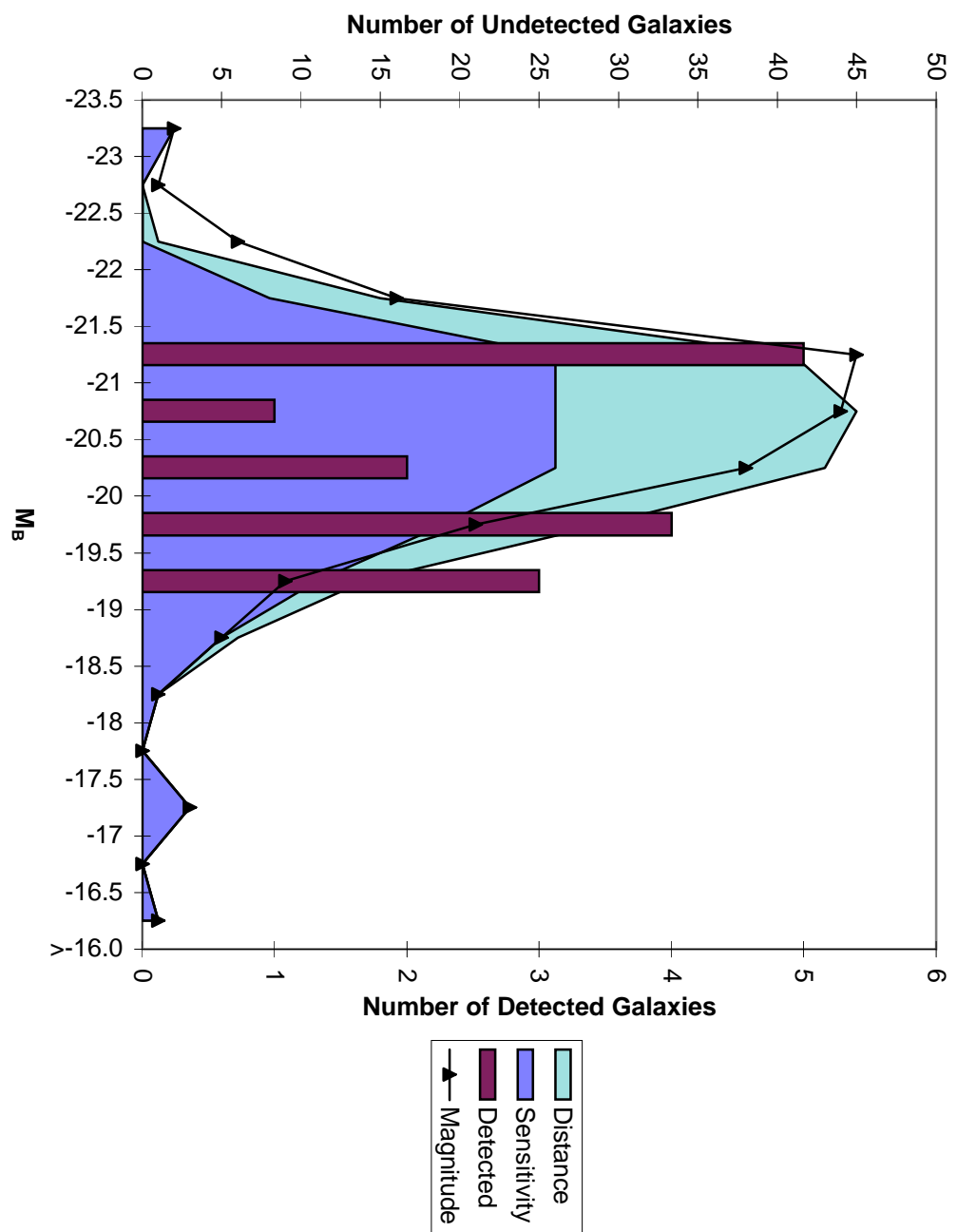
Inclination Angle

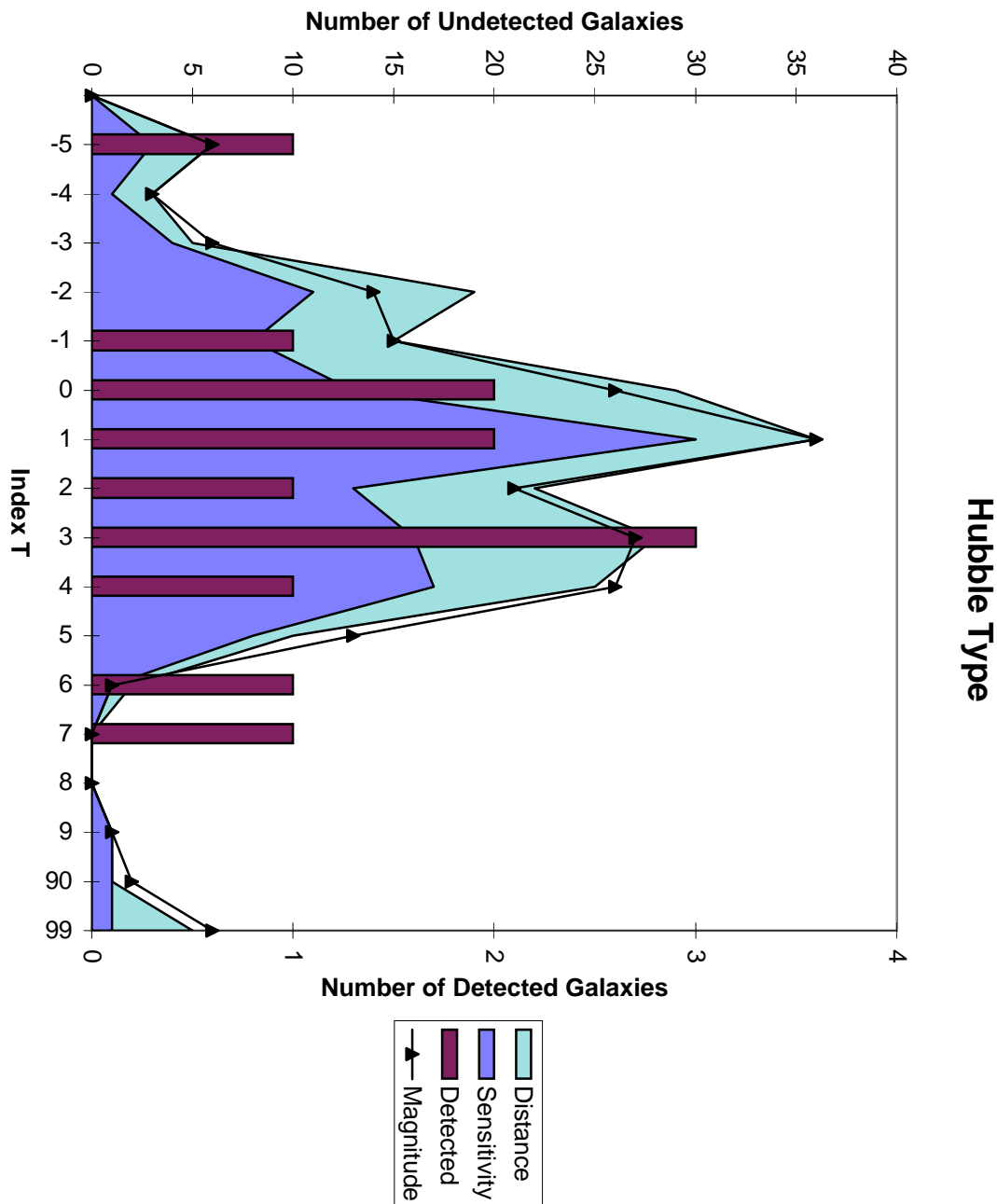


B Magnitude

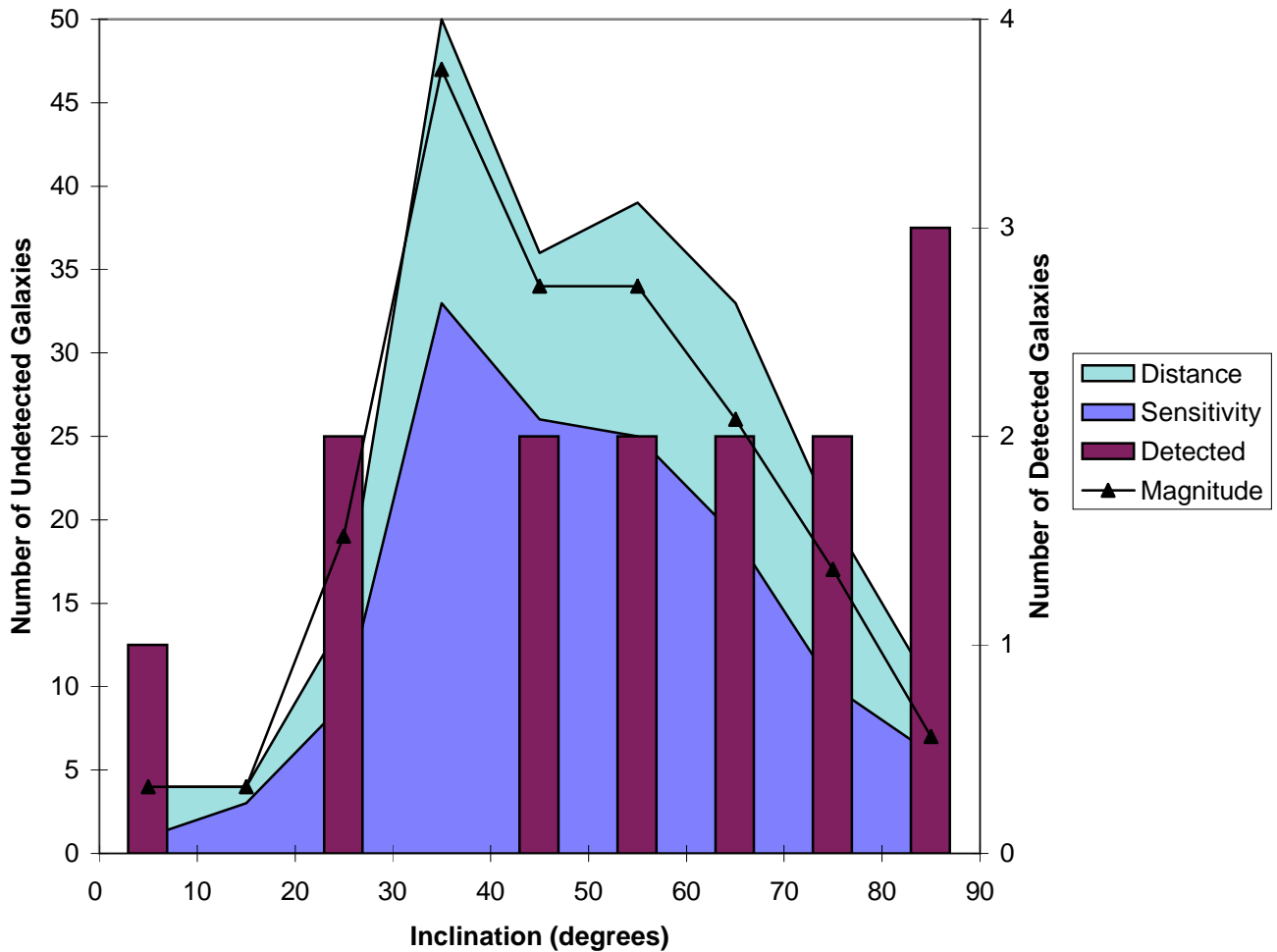


Absolute B Magnitude

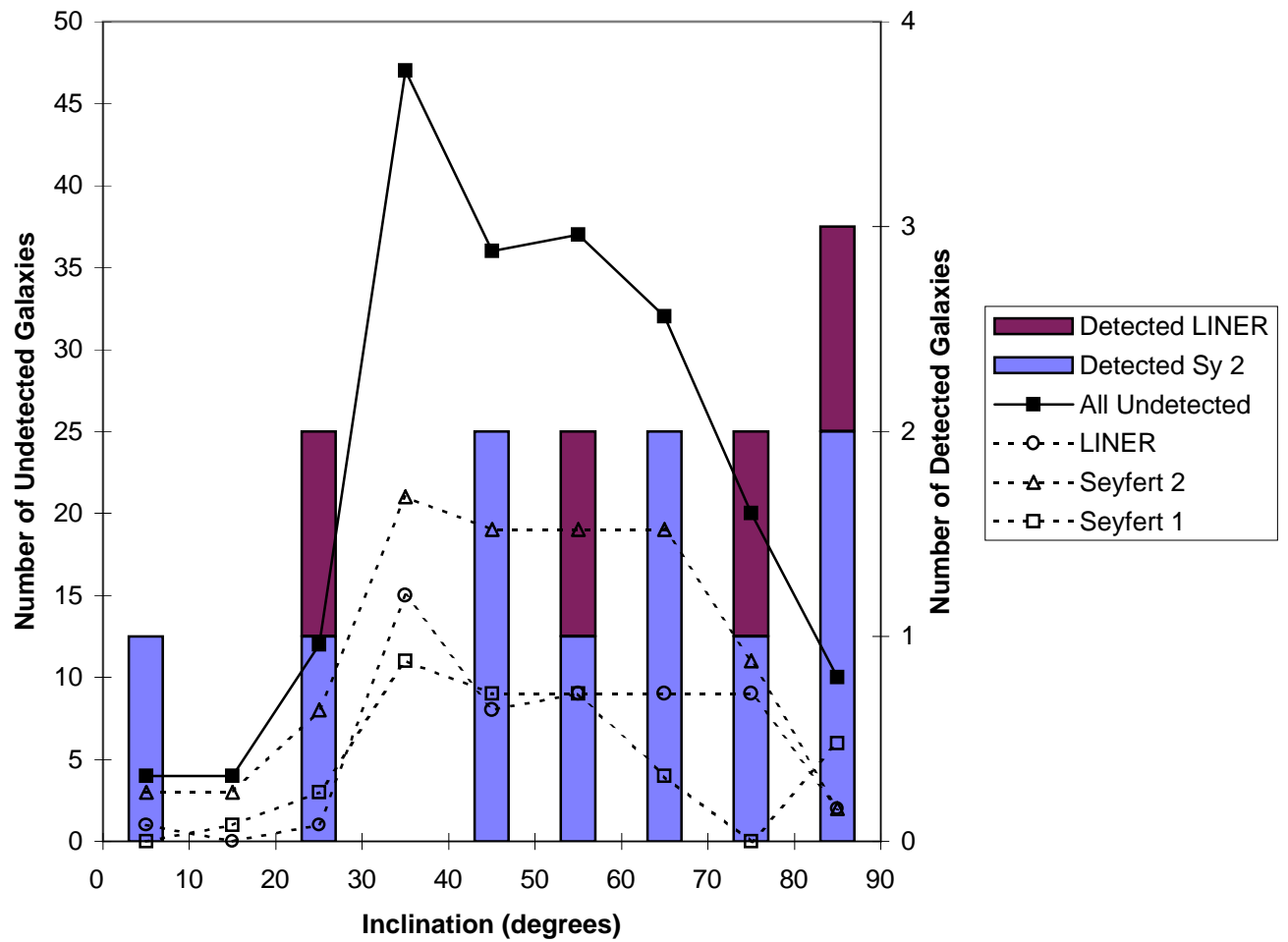




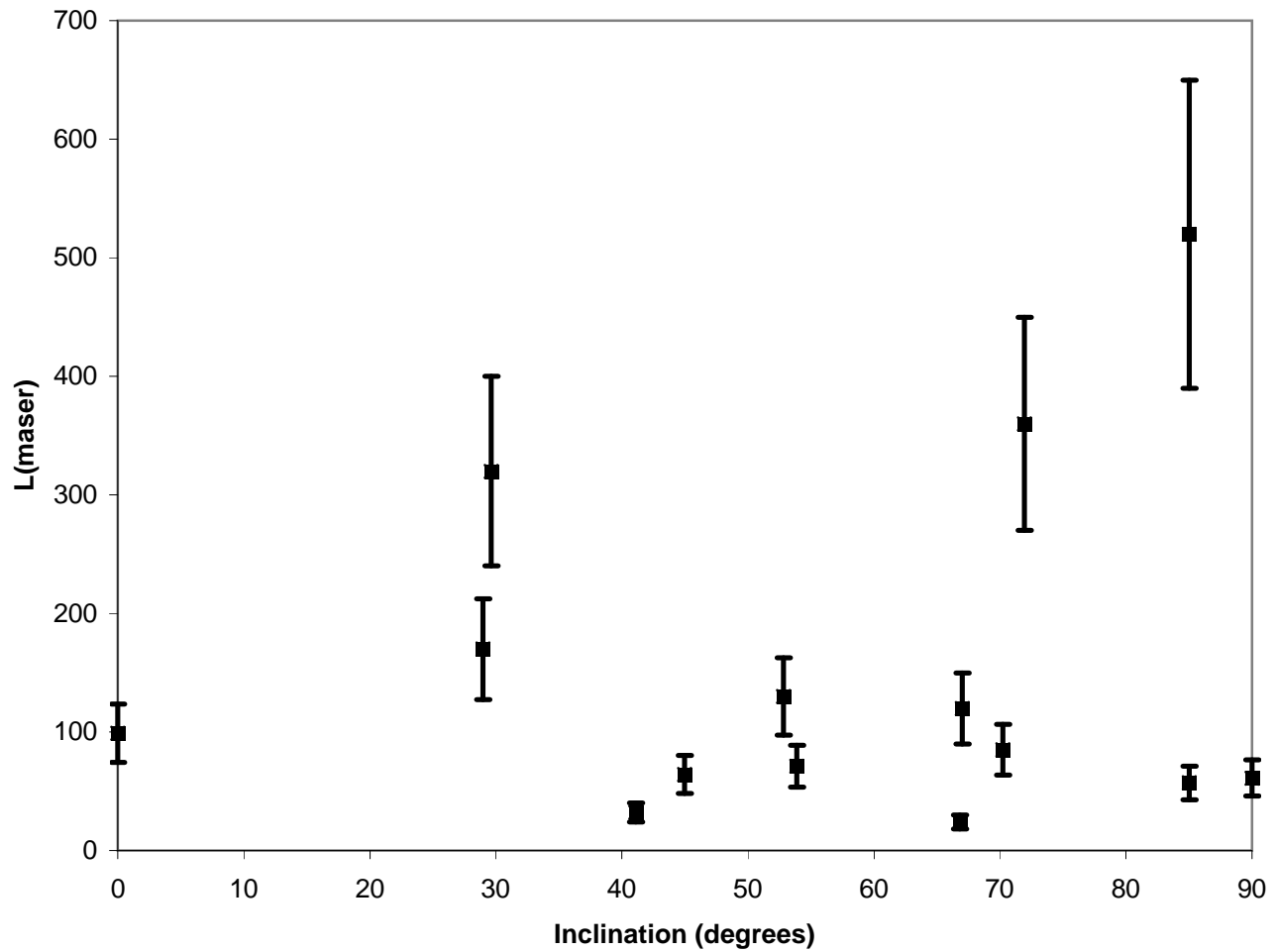
Inclination of Host Galaxies



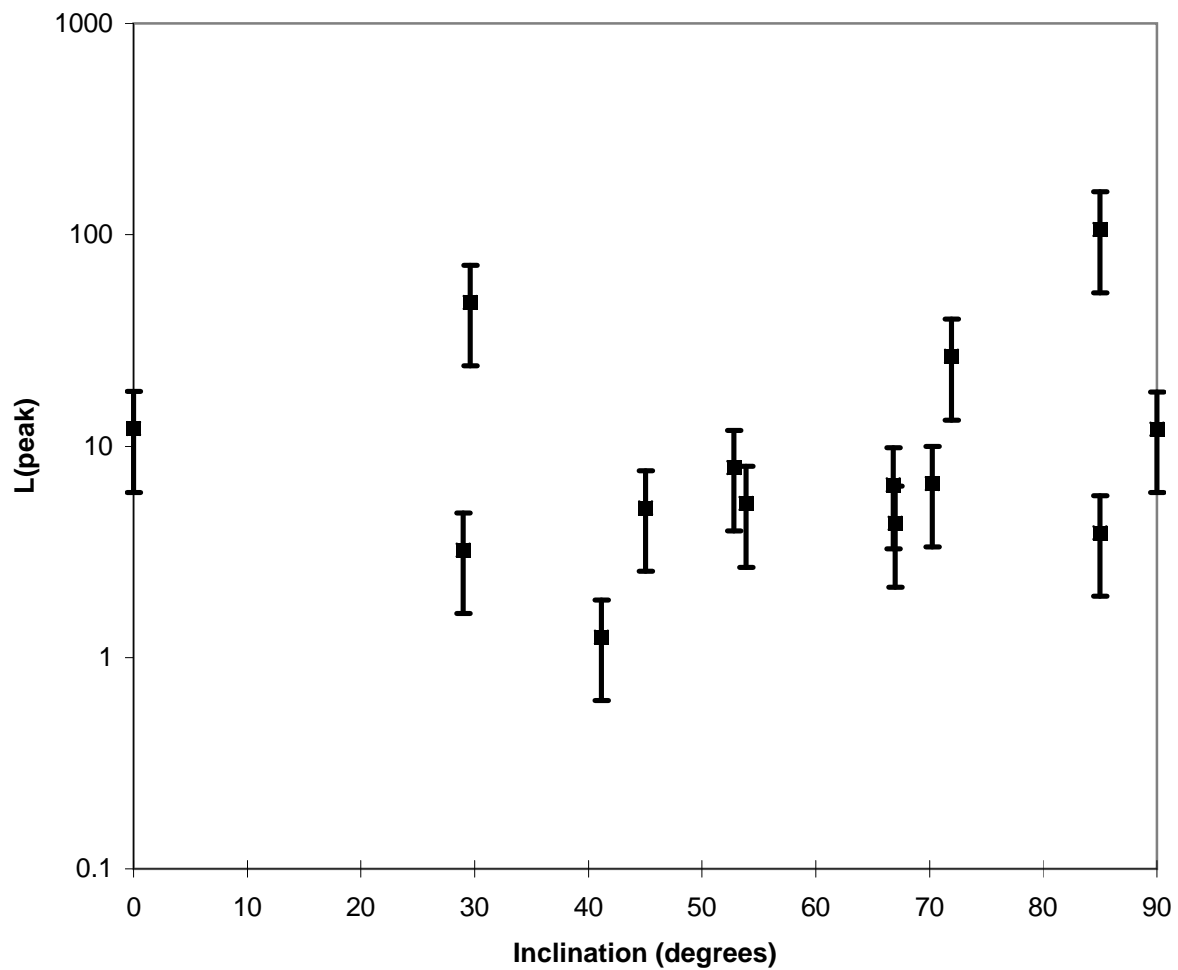
Inclination by AGN Type



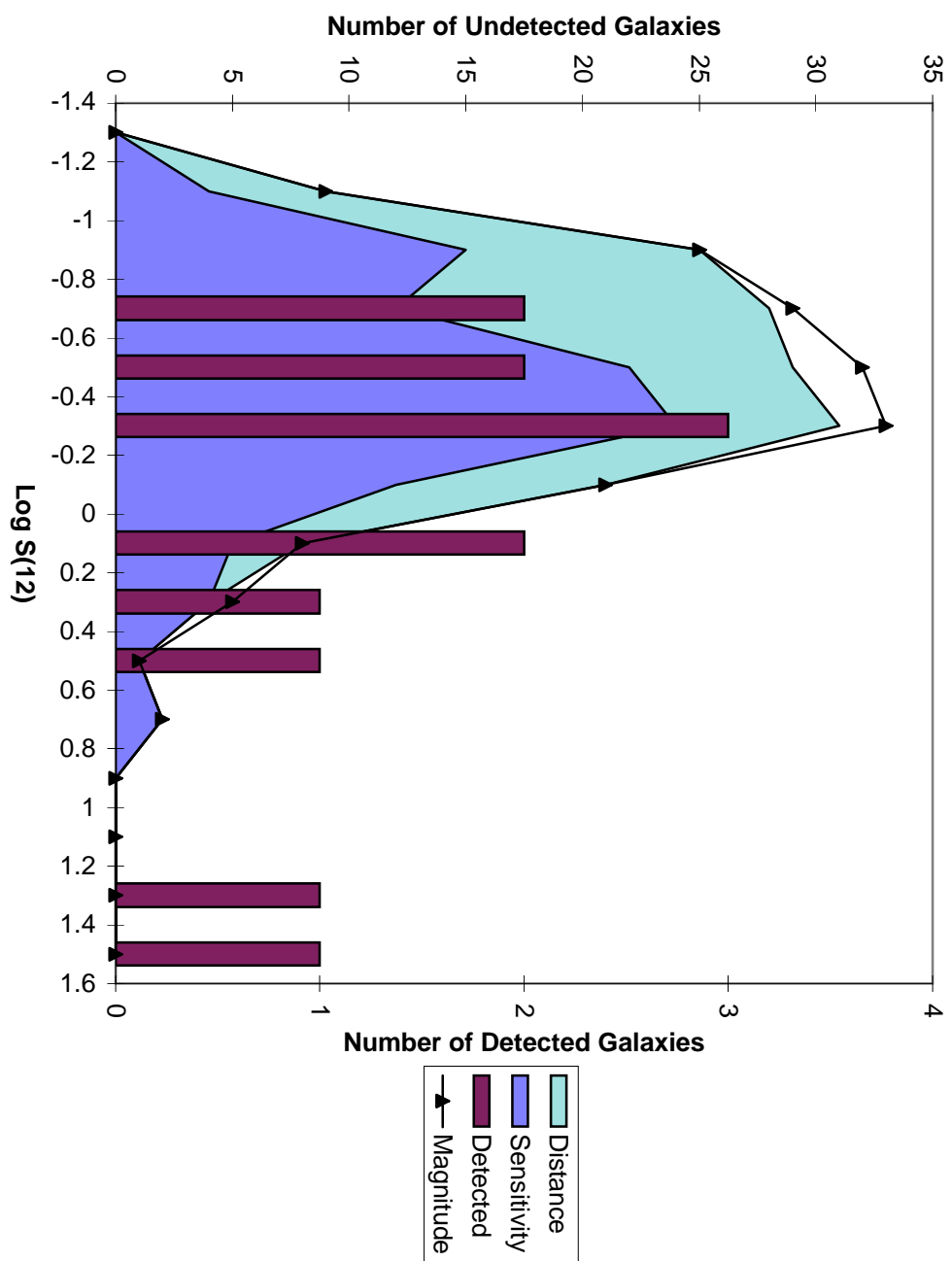
Isotropic Maser Luminosity vs. Inclination Angle of Galactic Disk



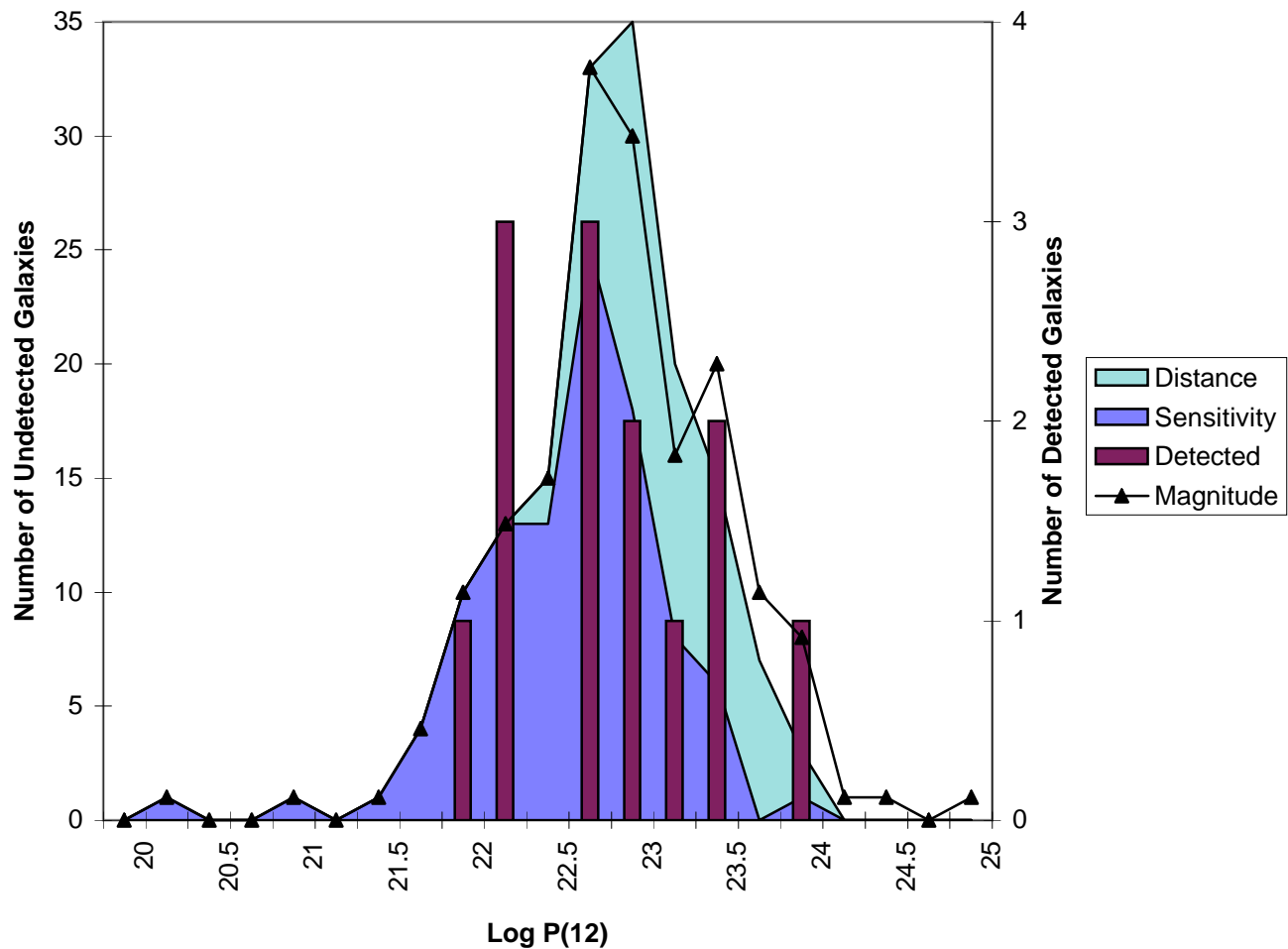
Peak Maser "Luminosity" vs. Inclination Angle of Galactic Disk



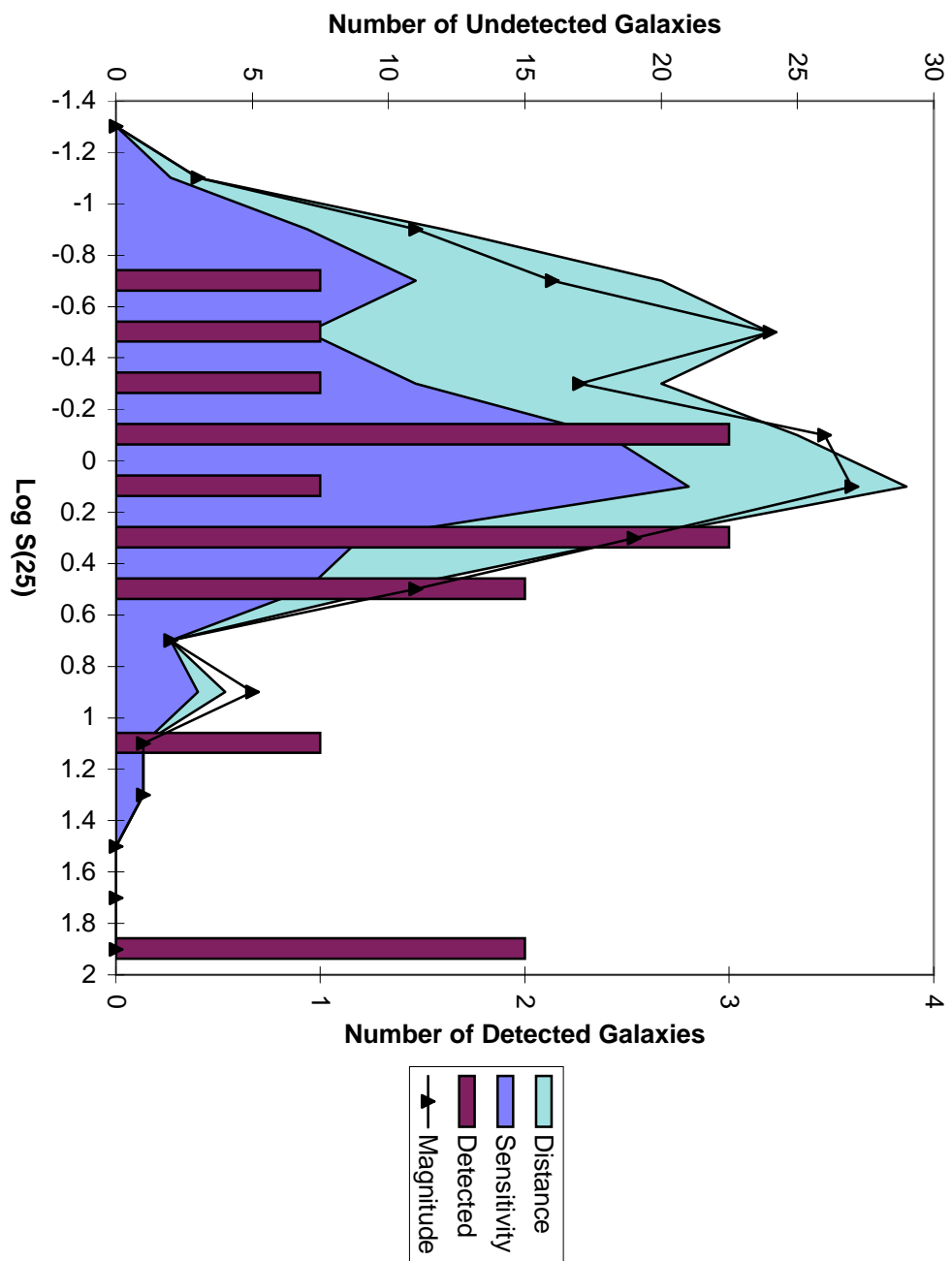
IRAS 12 micron Flux



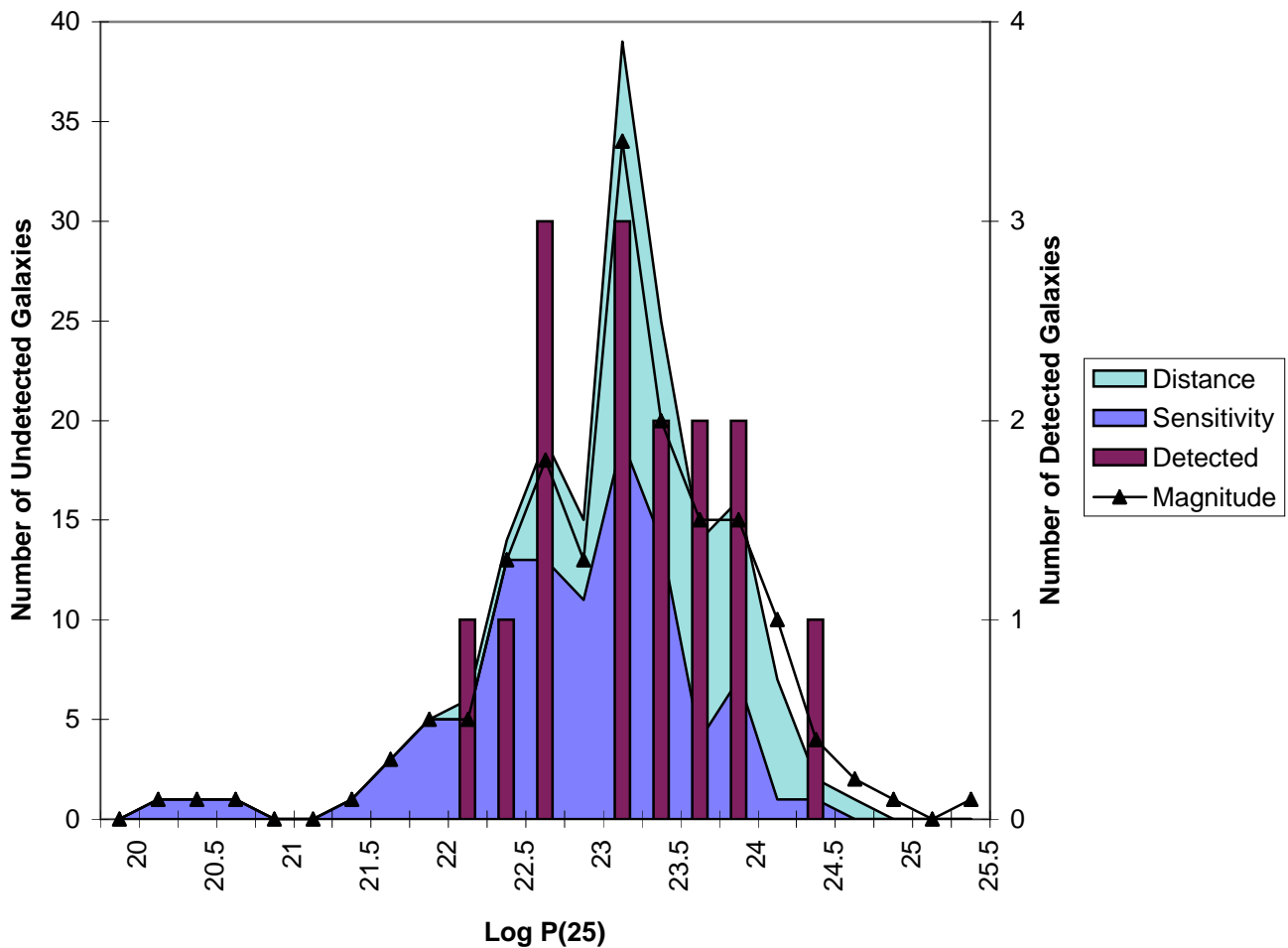
Power in the IRAS 12 Micron Band



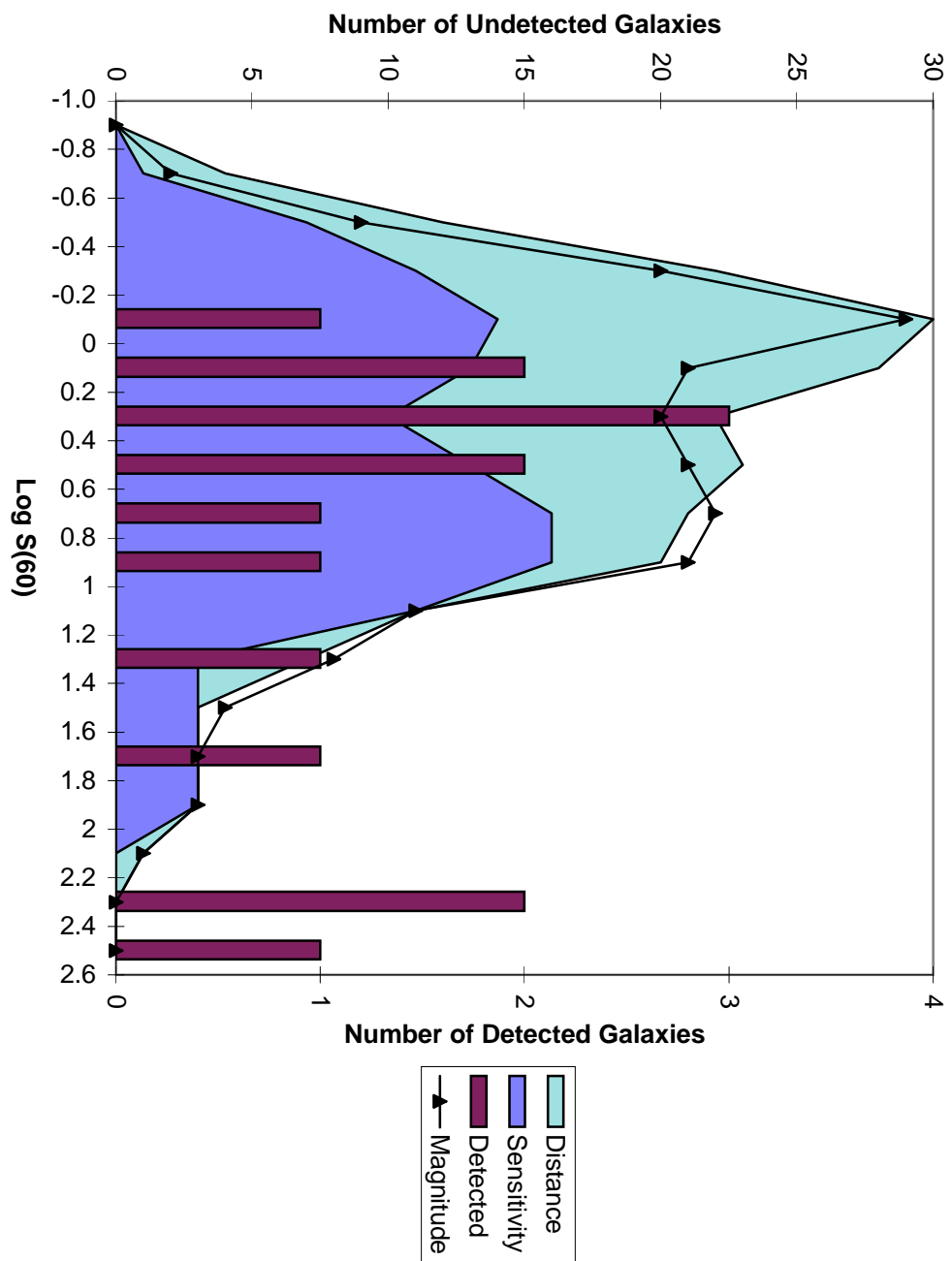
IRAS 25 Micron Flux



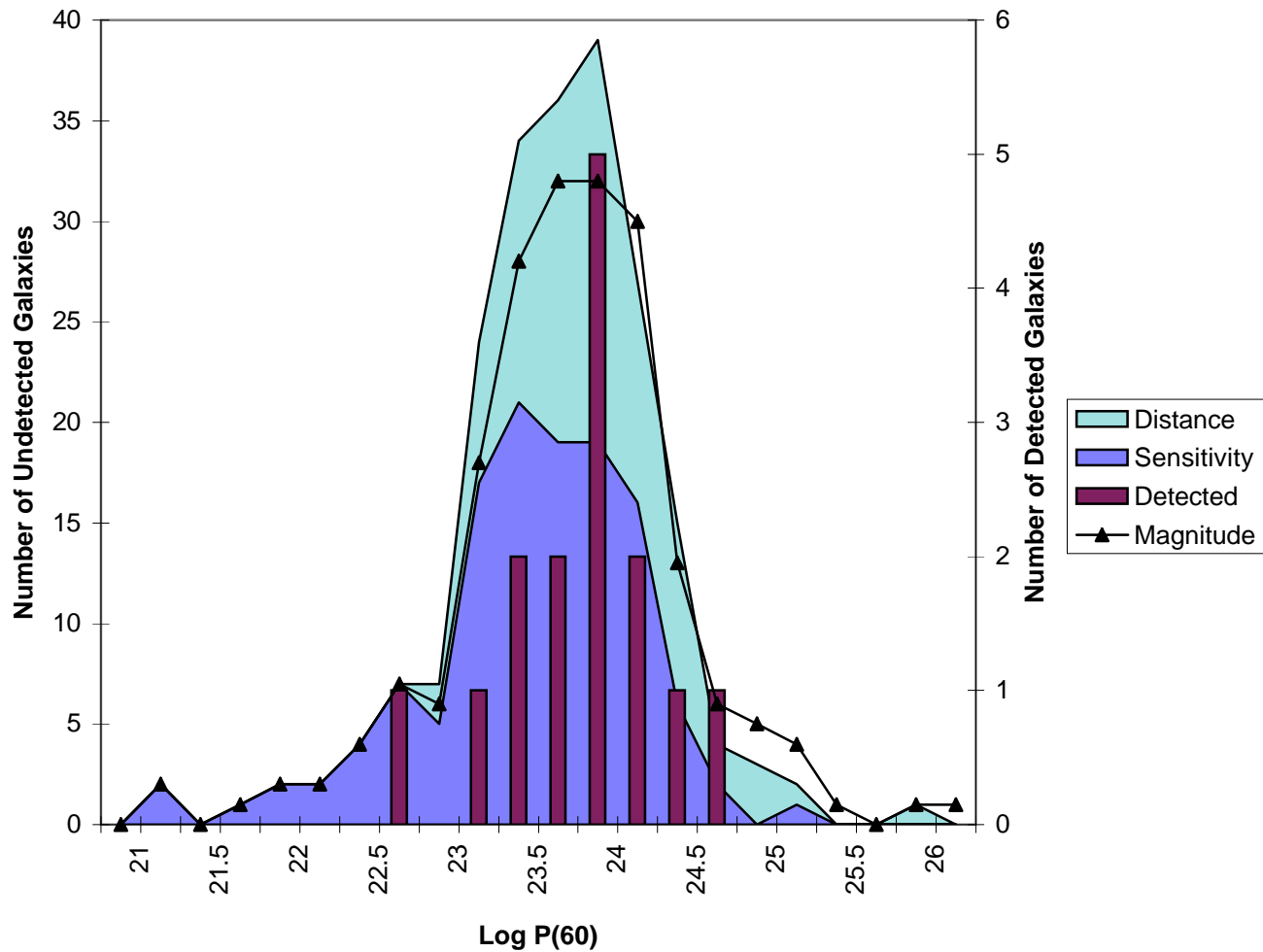
Power in the IRAS 25 Micron Band



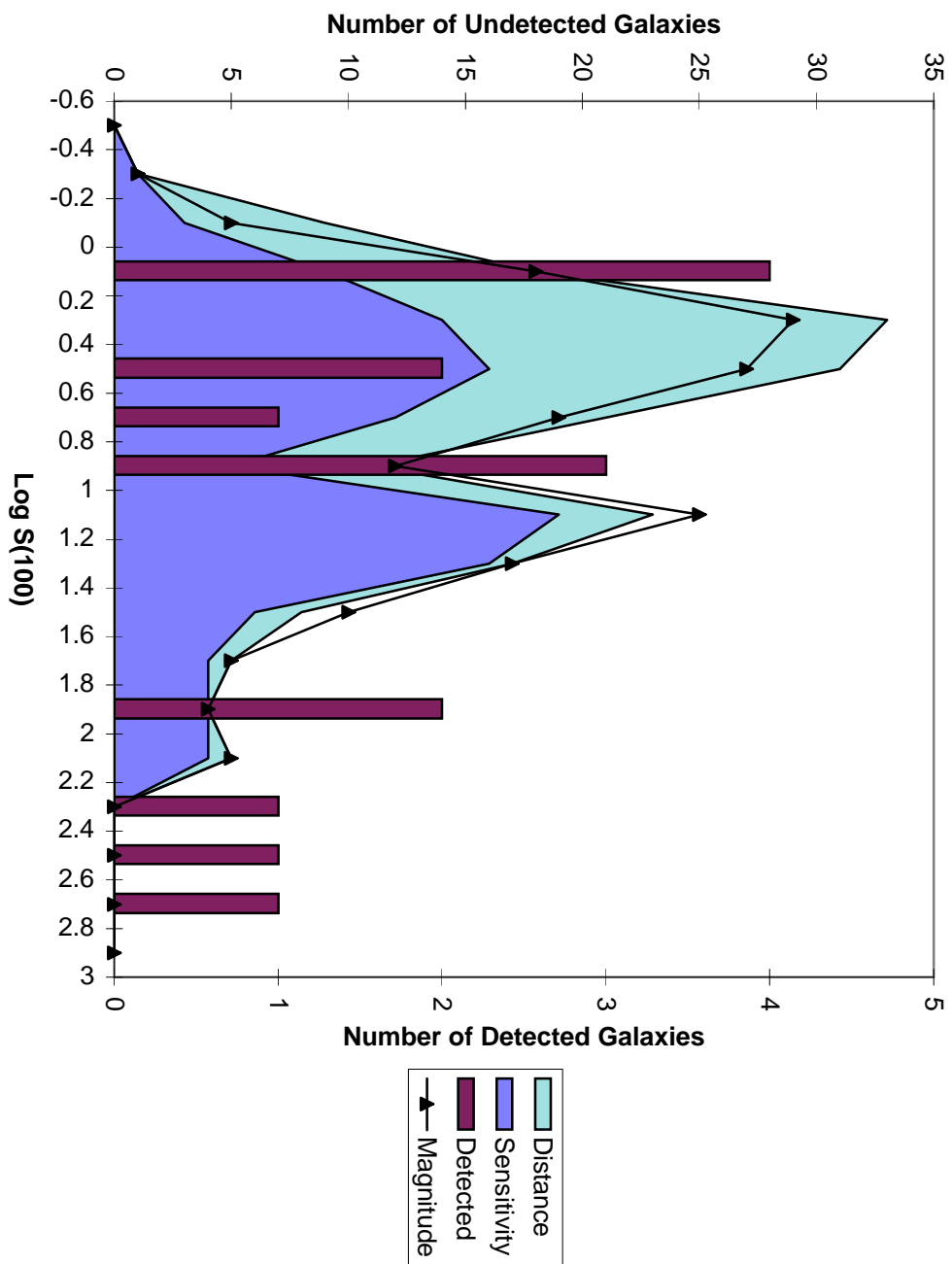
IRAS 60 Micron Flux



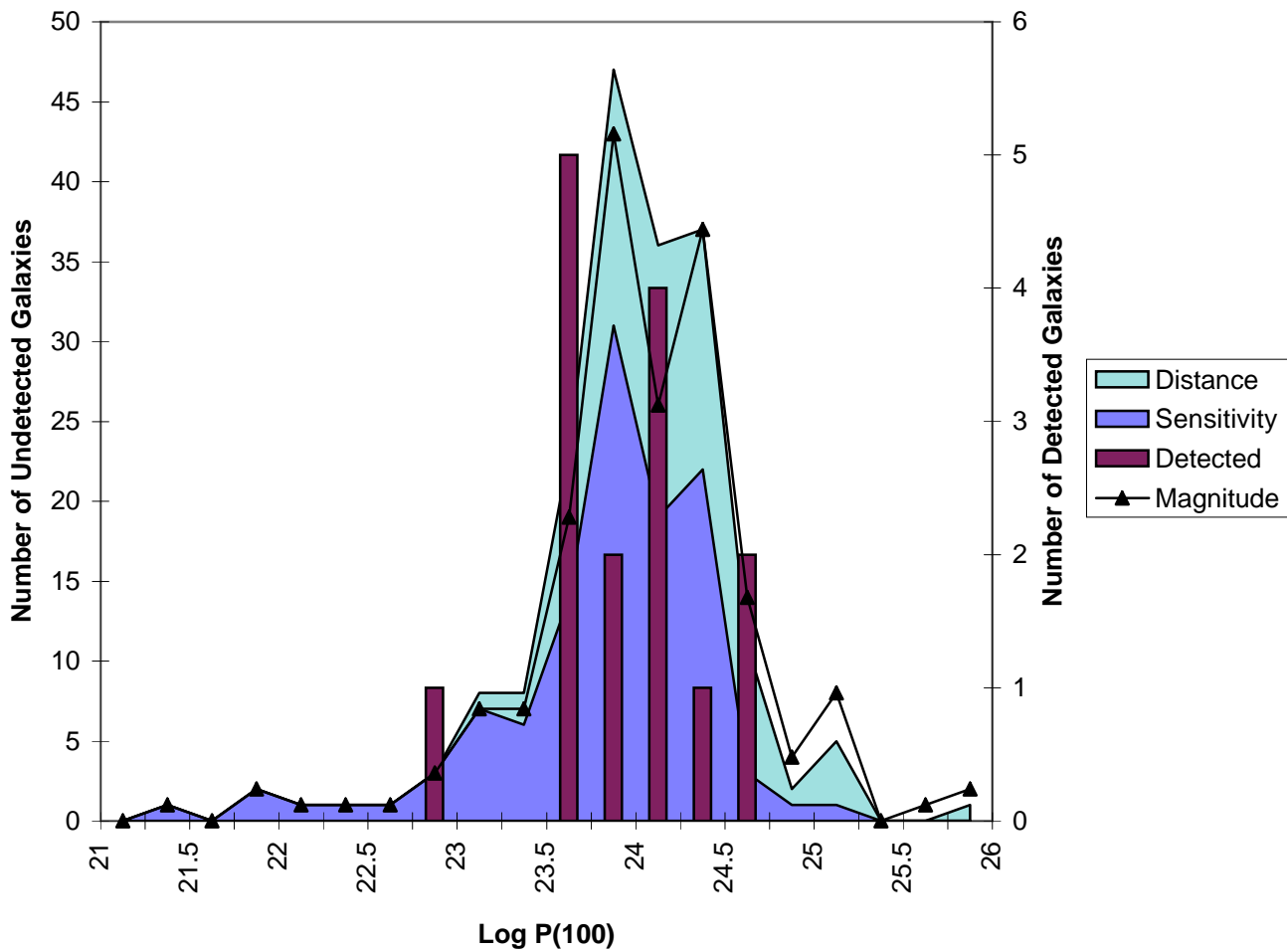
Power in the IRAS 60 Micron Band



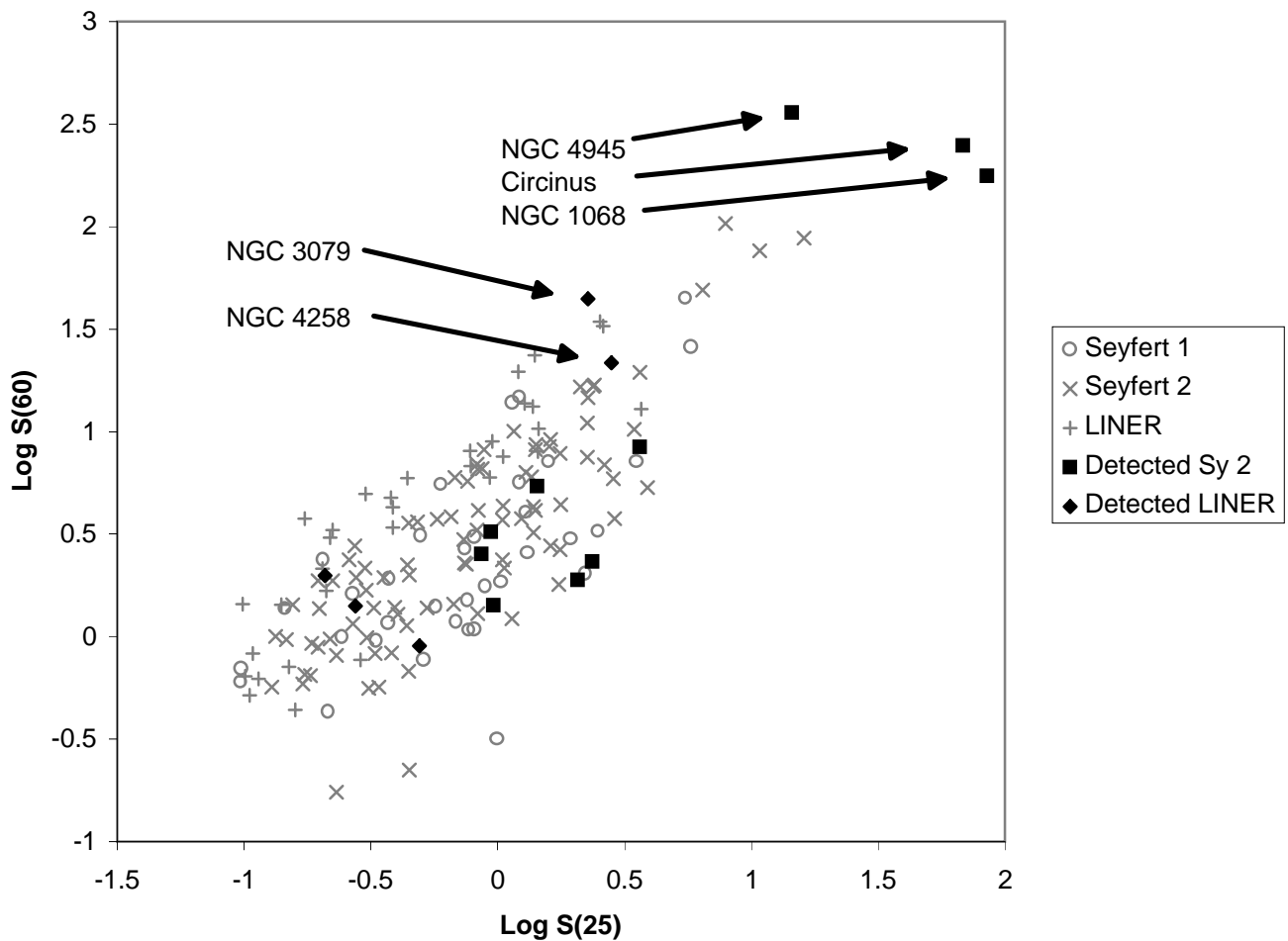
IRAS 100 Micron Flux



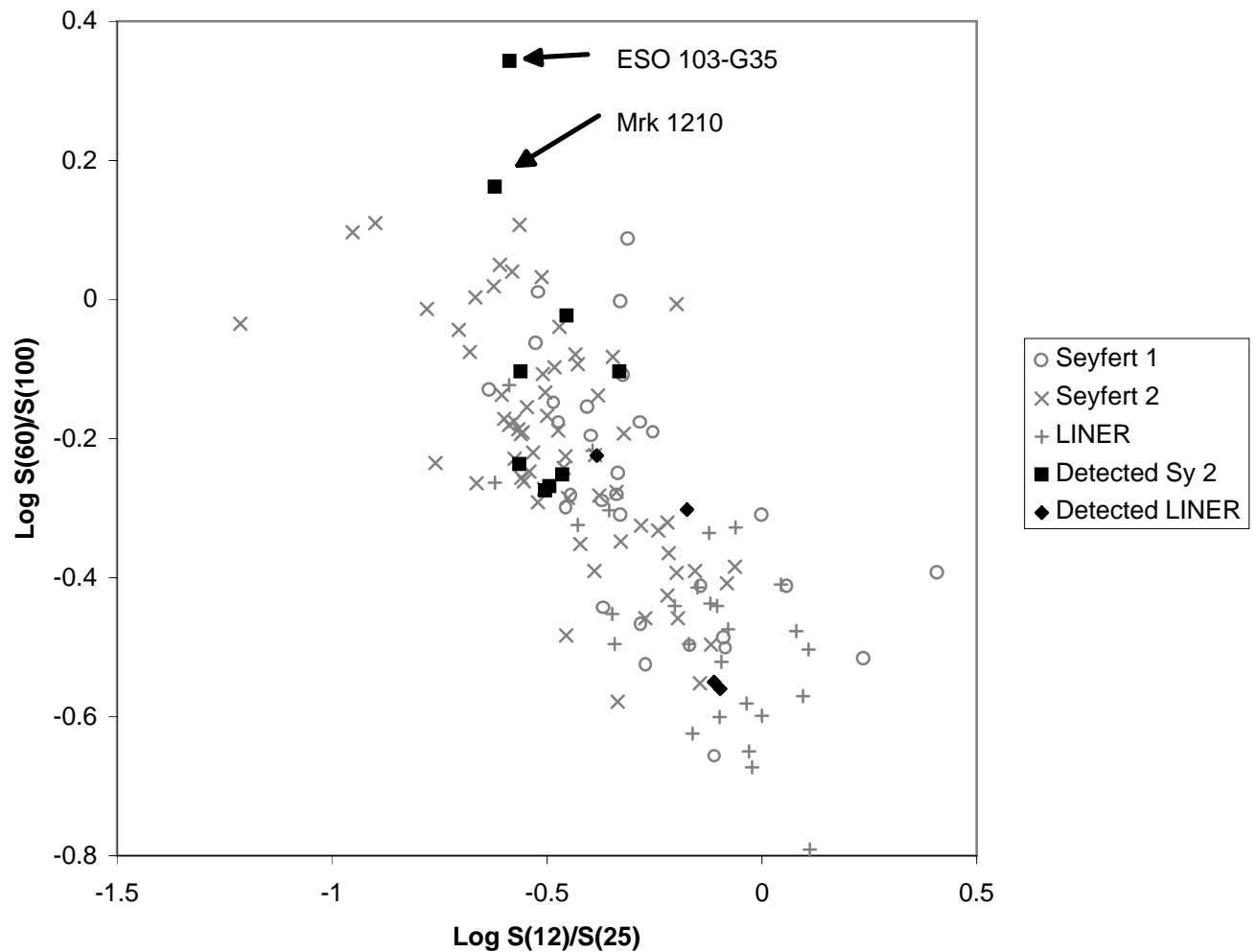
Power in the IRAS 100 Micron Band



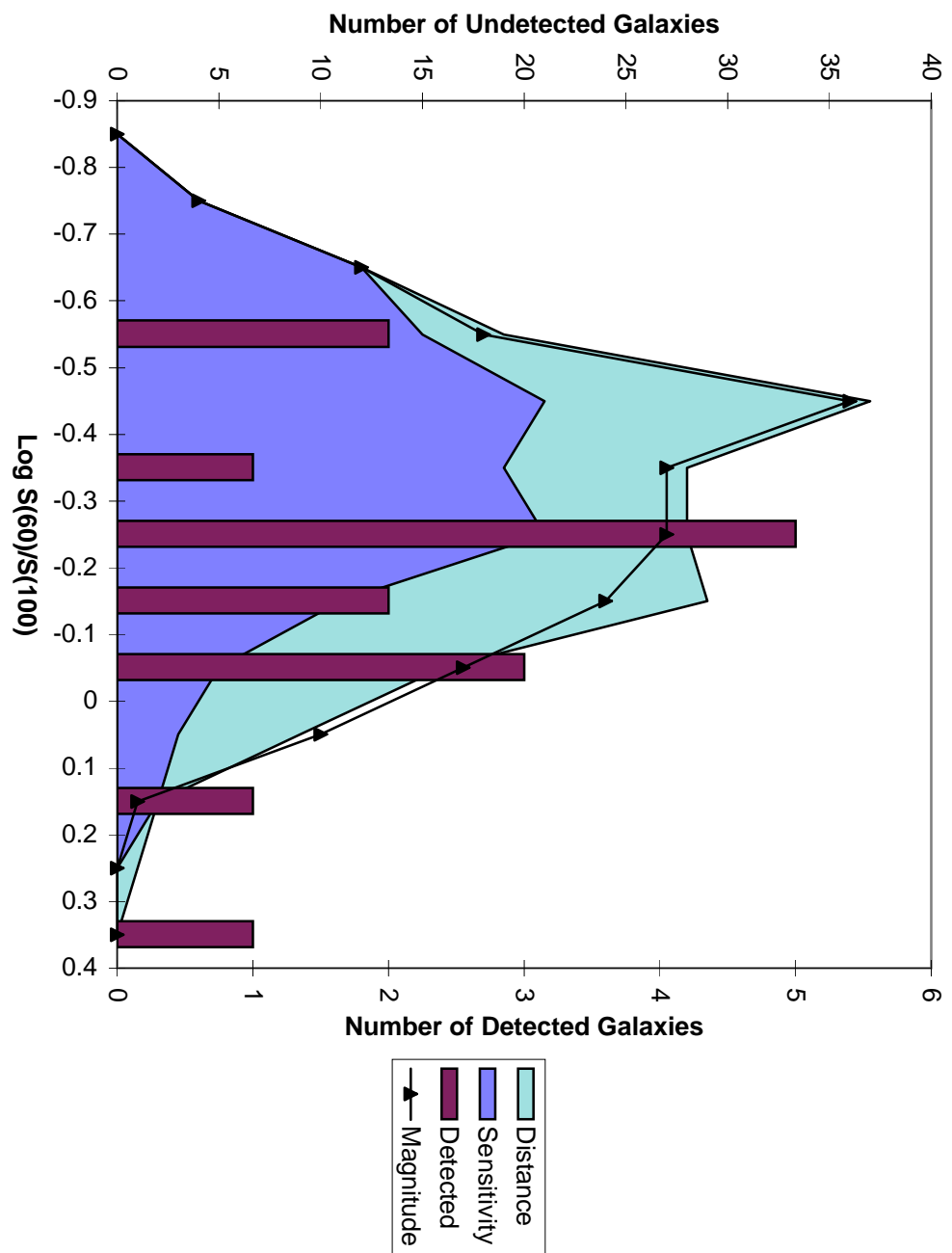
IRAS Flux-Flux Diagram



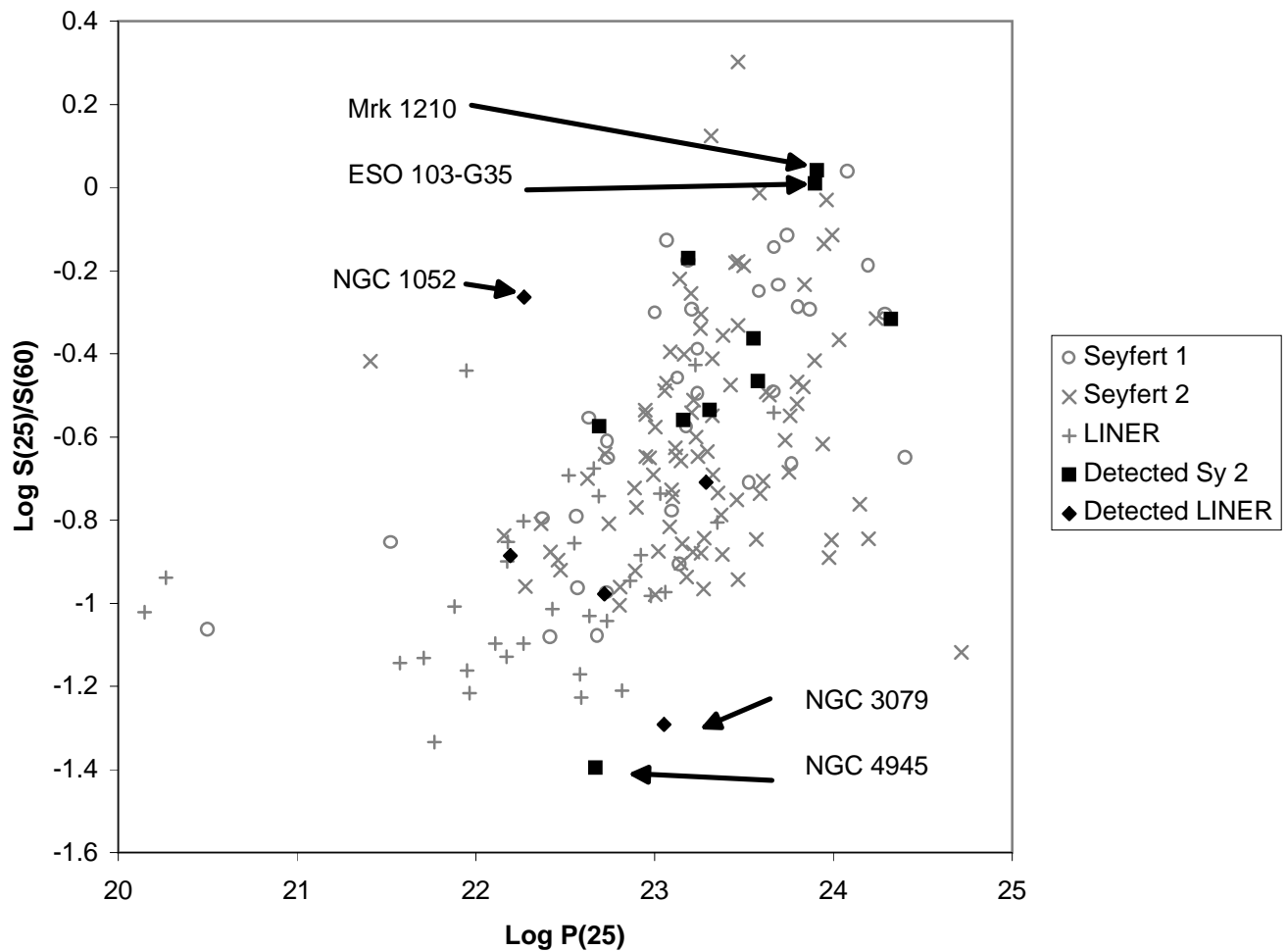
IRAS Color-Color Diagram



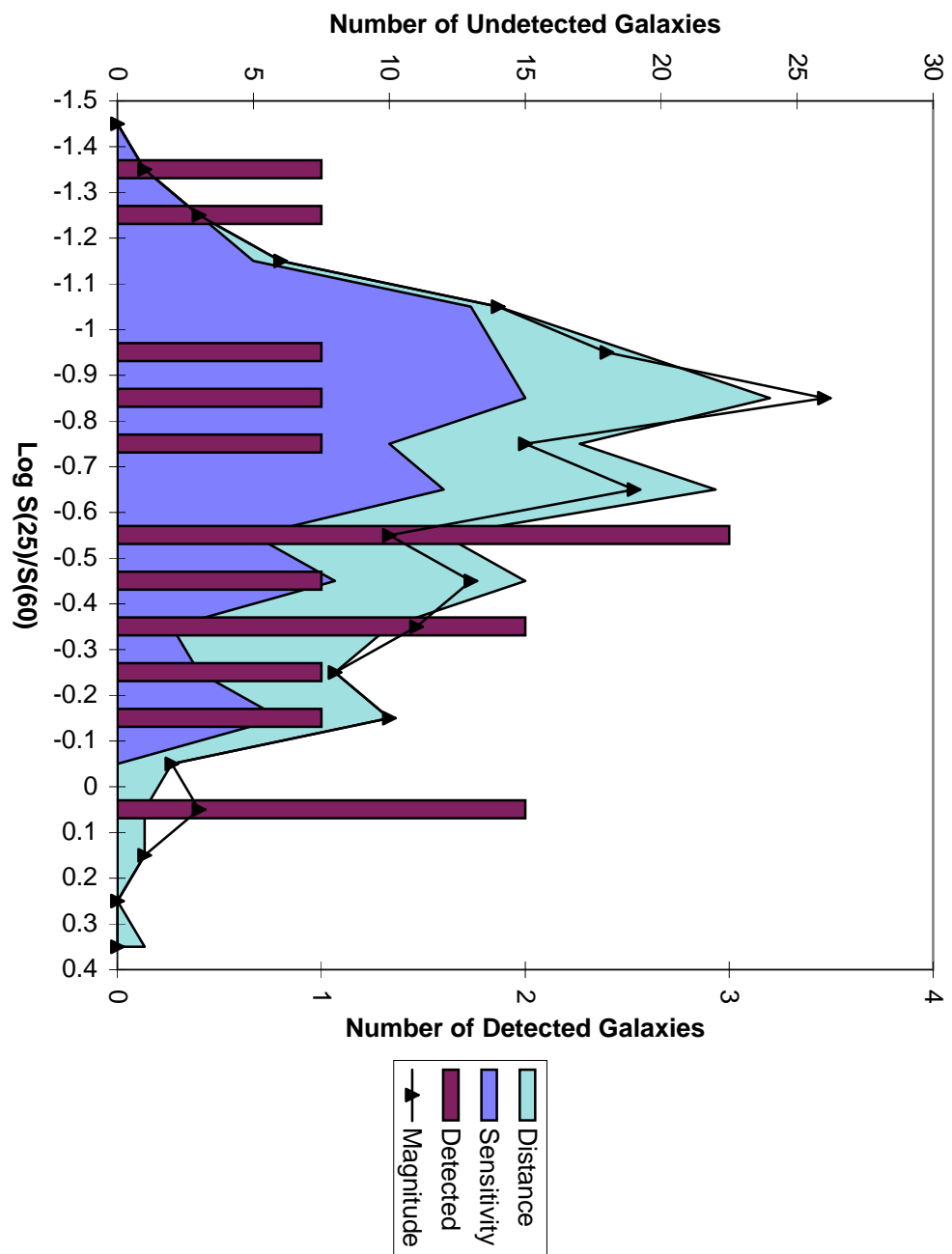
IRAS Flux Ratio $S(60)/S(100)$



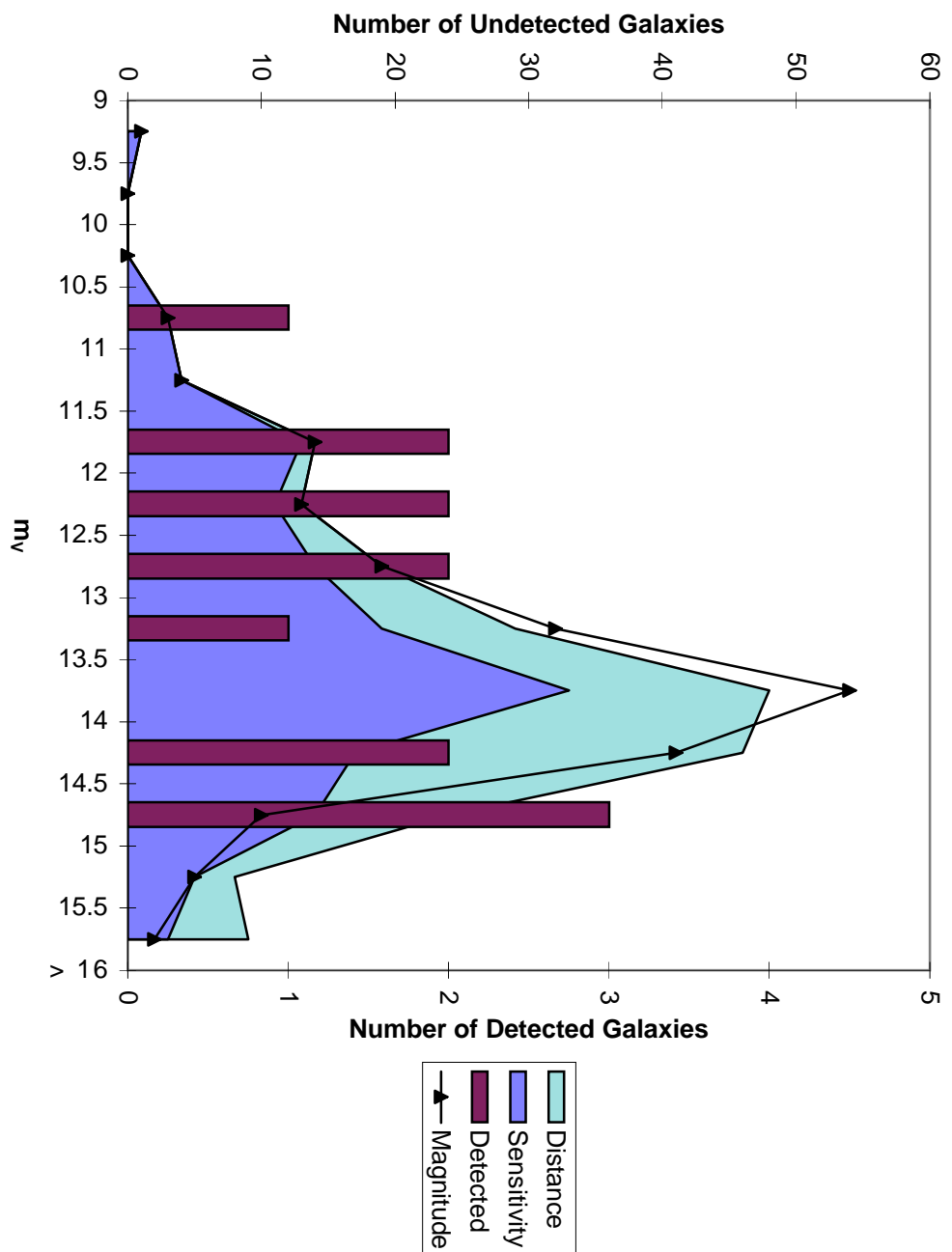
IRAS Color-Luminosity Diagram



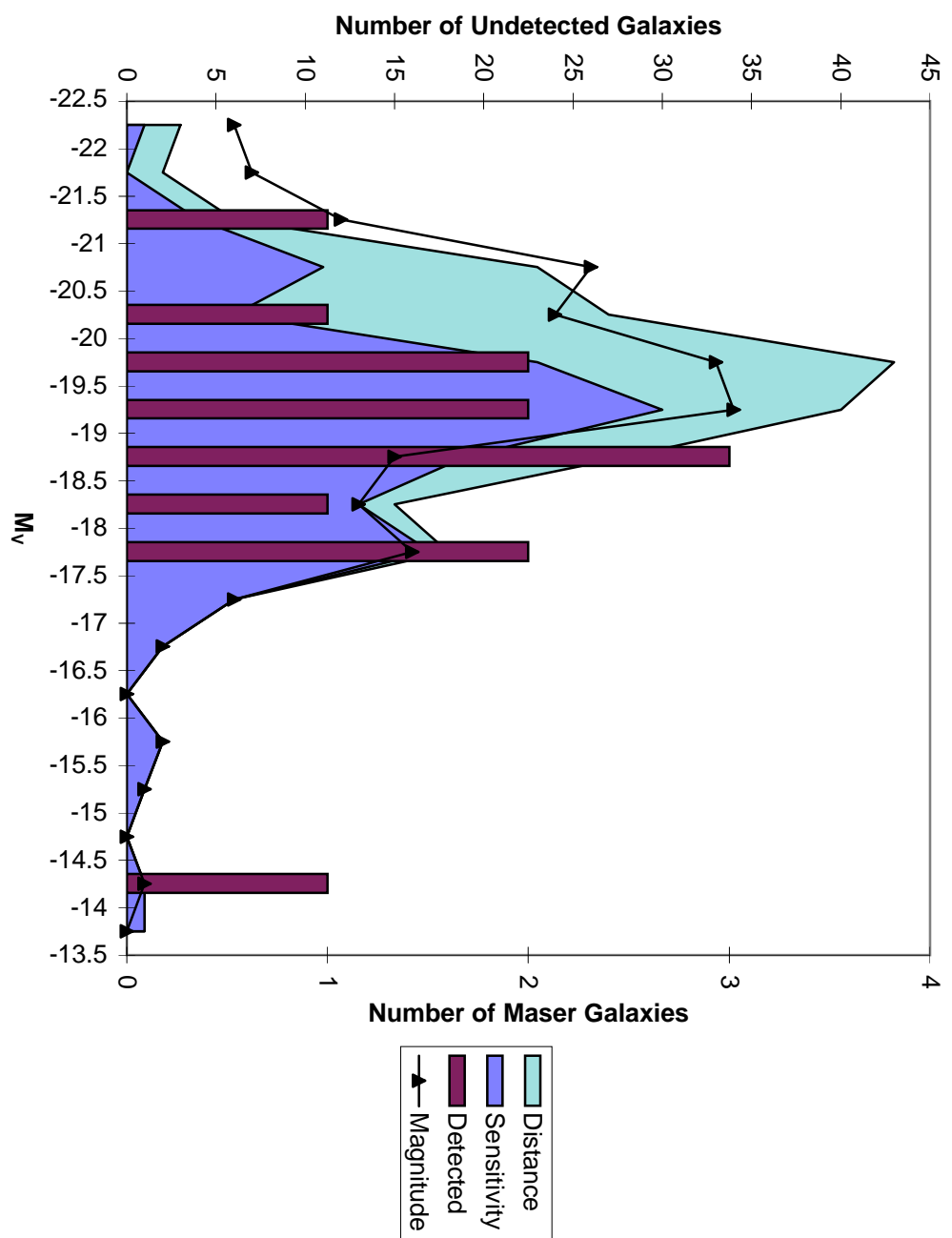
IRAS Flux Ratio $S(25)/S(60)$



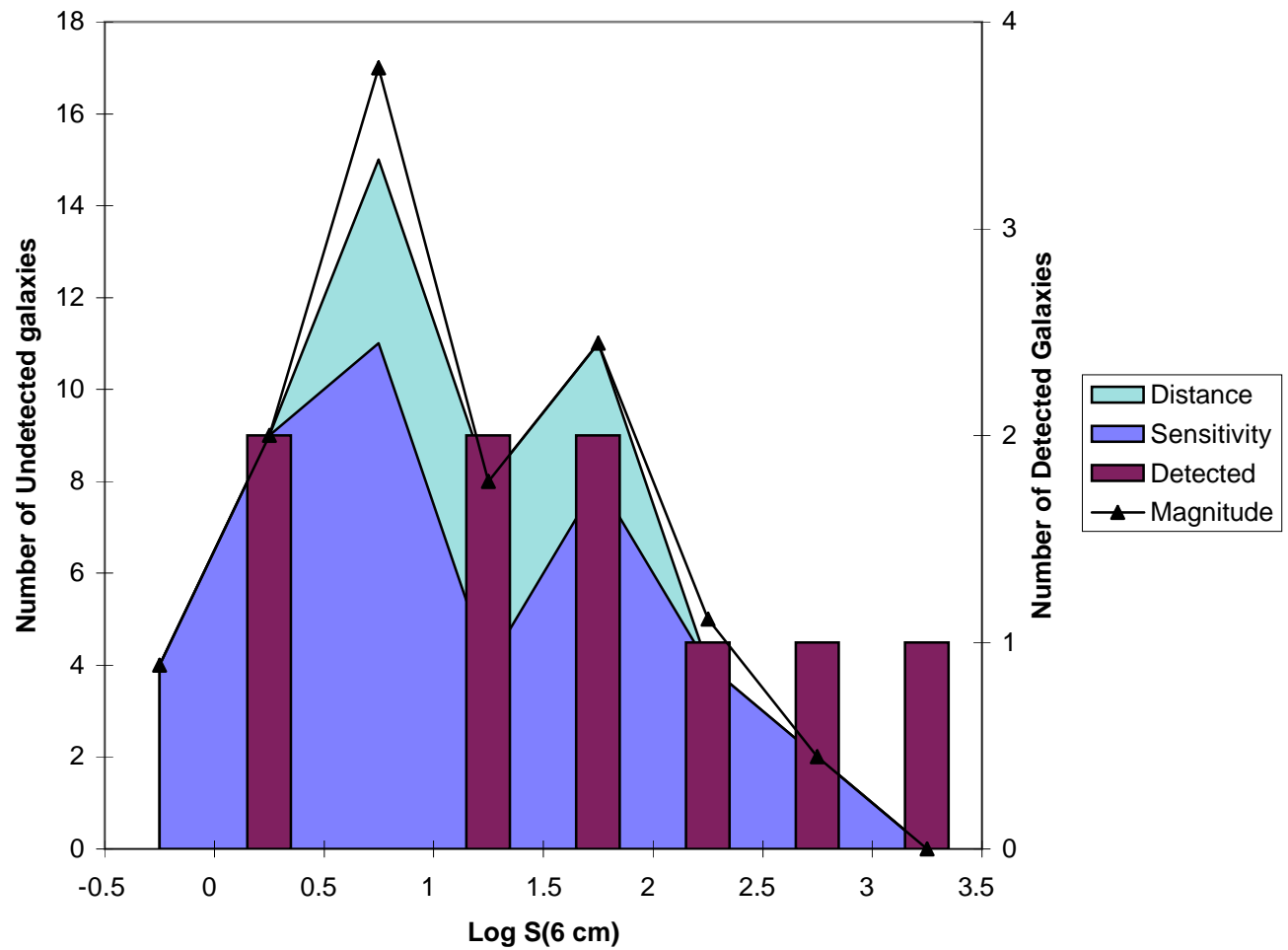
Nuclear V Magnitude

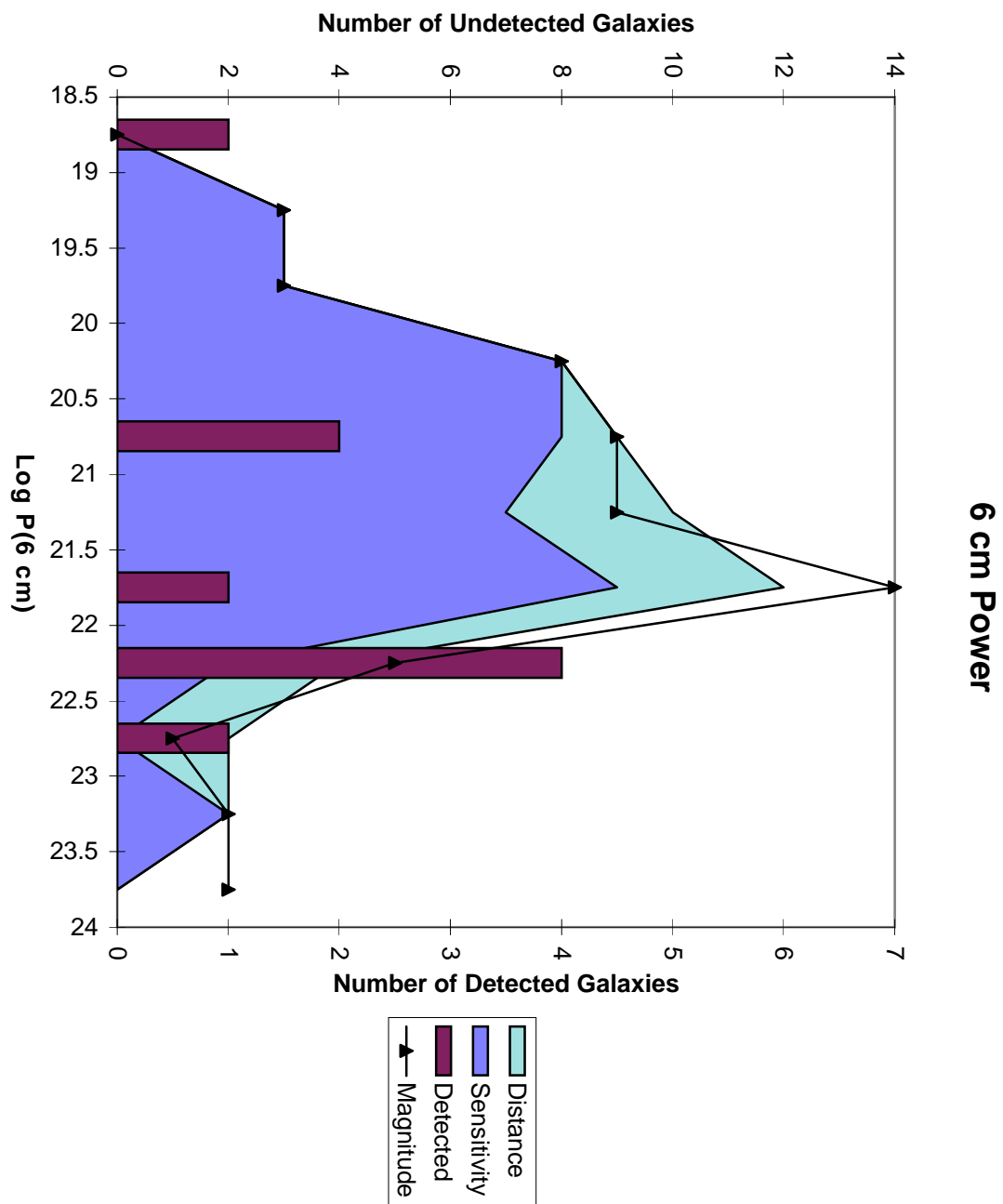


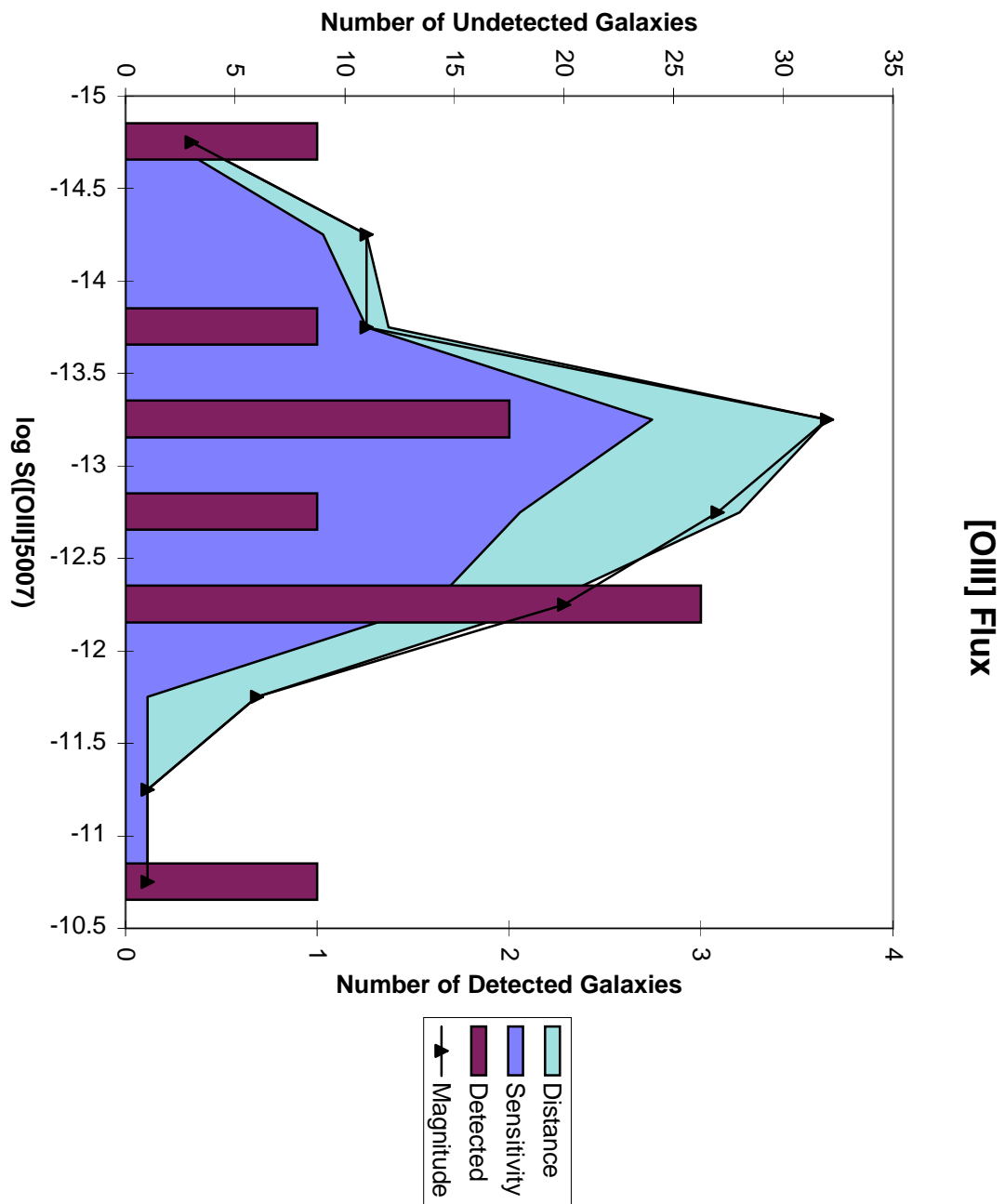
Absolute Nuclear V Magnitude



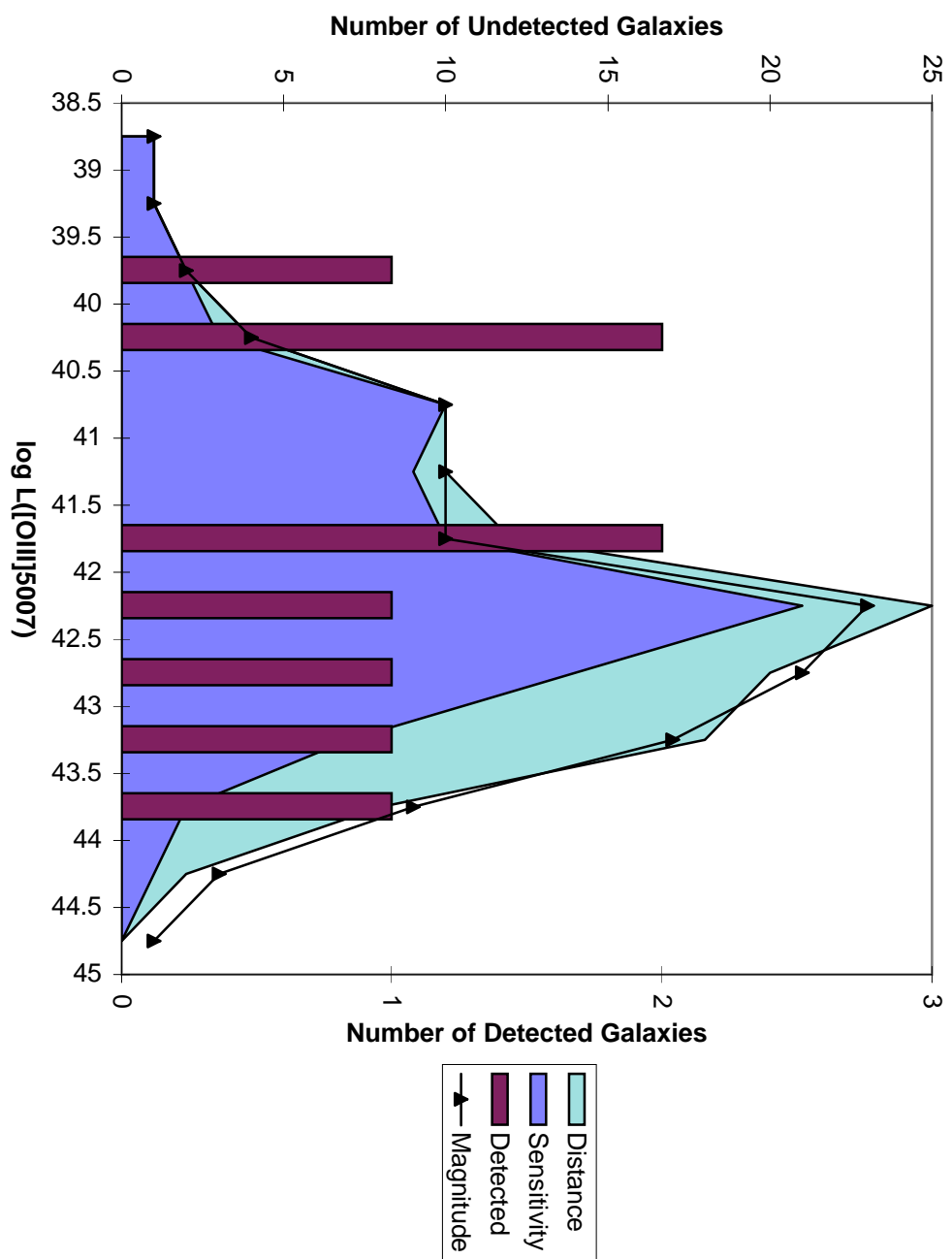
6 cm Flux



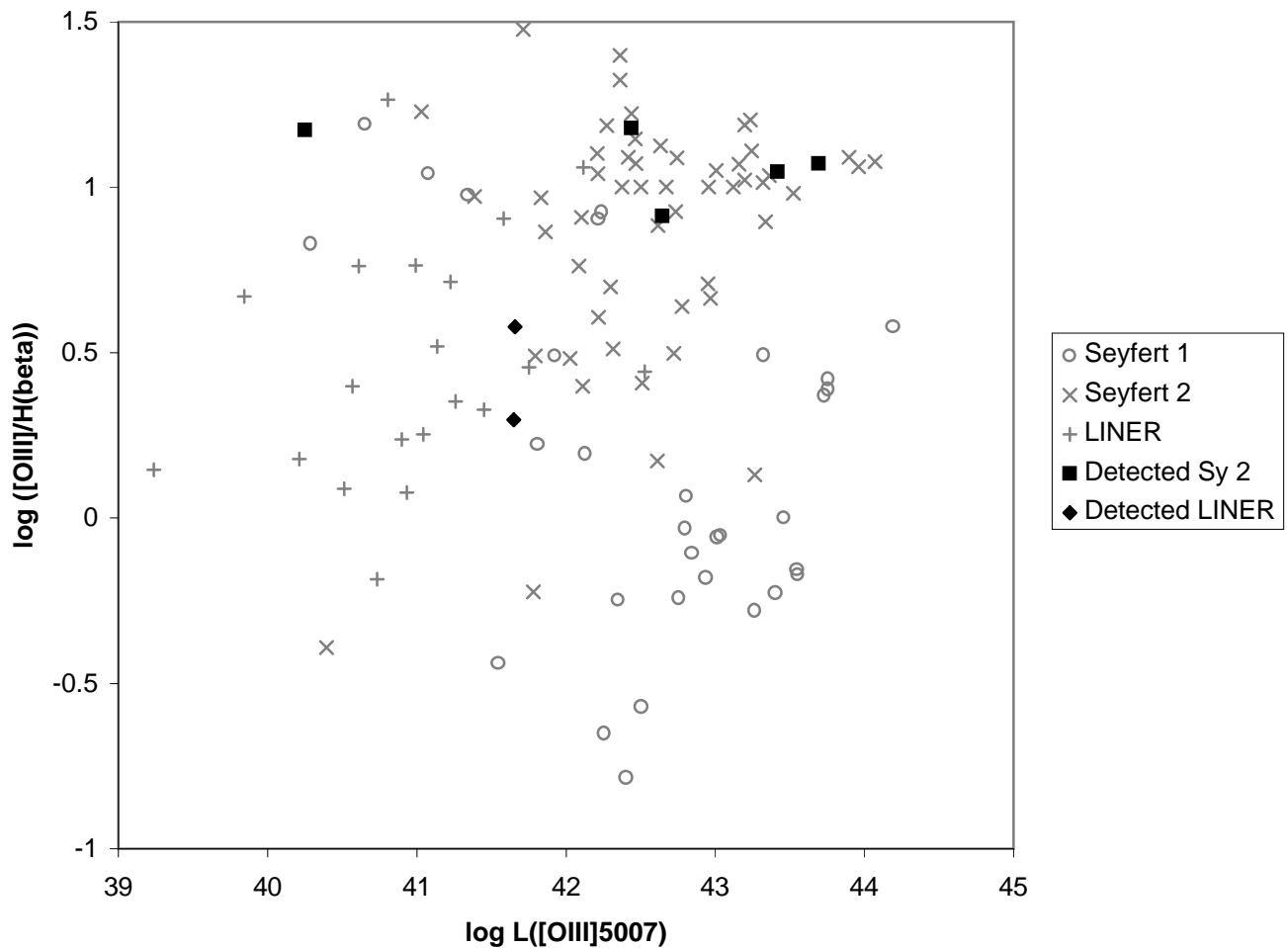




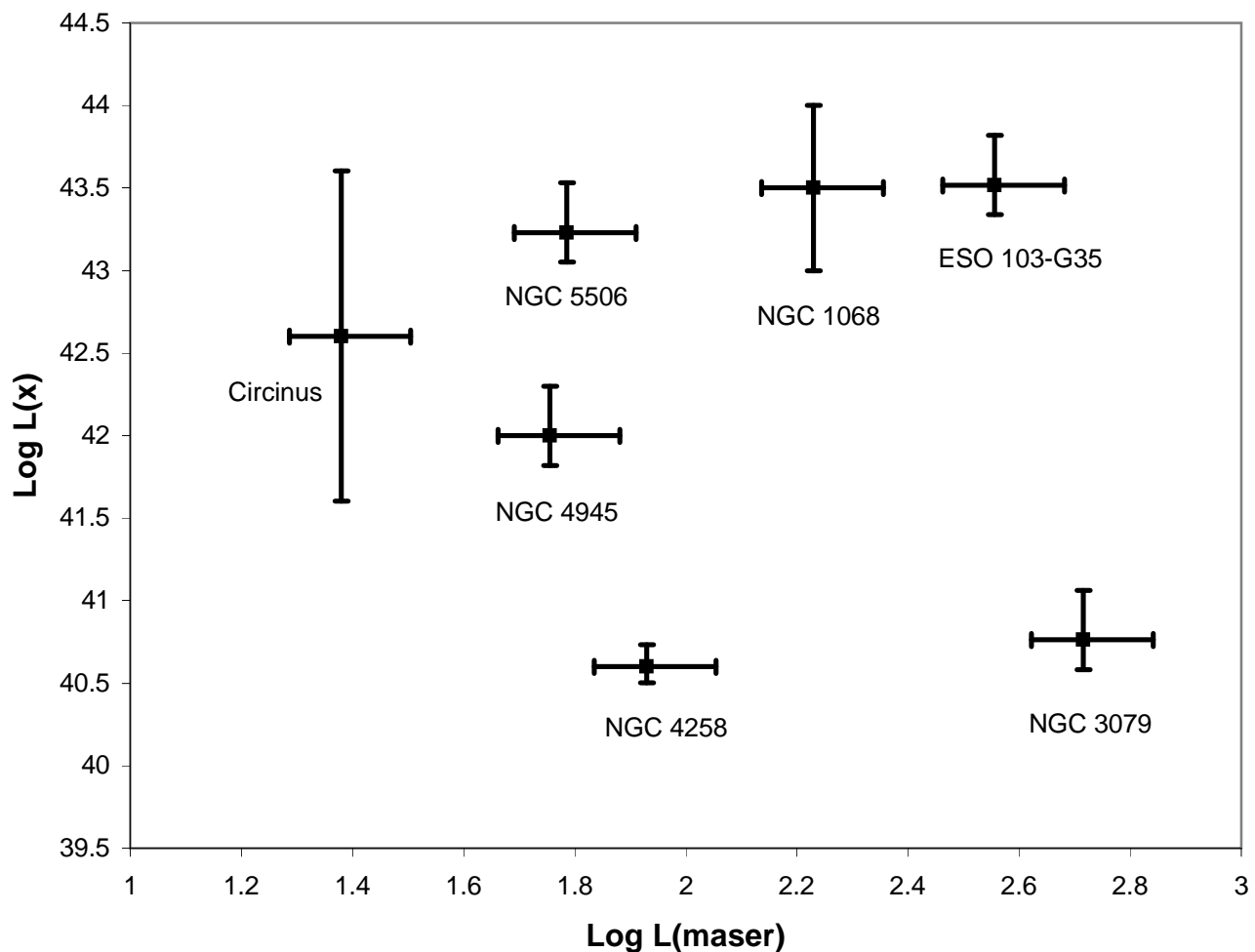
[OIII] Luminosity



[OIII]/H(beta) Ratio vs. [OIII] Luminosity



X-ray Luminosity vs. Maser Luminosity



X-ray Column Depth vs. Maser Luminosity

